The Dissertation Committee for Yumeng Tao Certifies that this is the approved version of the following Dissertation:

Evaluating the Site-Specific Applicability of One-Dimensional Seismic Ground Response Analysis

Committee:

Ellen M. Rathje, Supervisor

Brady R. Cox

Kenneth H. Stokoe II

Clark R. Wilson

Stephen P. Grand

Evaluating the Site-Specific Applicability of One-Dimensional Seismic Ground Response Analysis

by

Yumeng Tao

Dissertation

Presented to the Faculty of the Graduate School of

The University of Texas at Austin

in Partial Fulfillment

of the Requirements

for the Degree of

Doctor of Philosophy

The University of Texas at Austin

December 2018

Dedication

To my parents and grandparents, for their unconditional love and support

Acknowledgements

First and foremost, I would like to express my utmost gratitude to my advisor, Dr. Ellen M. Rathje. It has been an honor to be her student. She has taught and showed me, both consciously and subconsciously, how a good research is done. The enthusiasm she has for research was contagious and motivated me to keep seeking better answers in moments when I felt stuck. I greatly appreciate her contributions of time, brilliant ideas and funding to my Ph.D. research and providing me with a wealth of opportunities that make my grad school experience productive and stimulating.

I am also indebted to my committee members, Drs. Brady R. Cox, Kenneth H. Stokoe II, Clark R. Wilson and Stephen P. Grand for their support, valuable feedback and reviewing this dissertation. I would also like to thank all the faculty, staff and students of the Geotechnical Engineering Program at UT Austin, for creating such a fantastic atmosphere for education and platform for professional development

During my studies at UT Austin, various graduate students and friends in Austin have made contributions to my life, both professionally and personally and I would like to express my gratitude to them as well. Because of them, my grad school experience was a lot of fun and became a memorable and incredibly wonderful journey. I really enjoyed their company and cherish the friendship. I would also like to thank the professors and friends during my time at Tongji University, who continued to support and encourage me after I graduated from Tongji.

Finally, I would like to give my deepest gratitude to my parents, late grandparents and families. I would not get where I am today without them and I am truly grateful for their unconditional love, support, advice and belief in me, in all my life adventures.

Abstract

Evaluating the Site-Specific Applicability of One-Dimensional Seismic Ground Response Analysis

Yumeng Tao, Ph.D.

The University of Texas at Austin, 2018

Supervisor: Ellen M. Rathje

One-Dimensional (1D) seismic ground response analysis is the most commonly performed analysis in geotechnical earthquake engineering. However, previous studies have shown a troubling fact that only a small fraction of sites are modeled well by 1D analysis. The objectives of this research are to assess the site-specific suitability of 1D analysis by identifying the issues that hinder the performance 1D analysis and to develop approaches to better match the observed sites response.

The downhole array technique is used in this work to evaluate 1D analysis because it provides the most direct observations of how seismic waves are modified by the subsurface soil and rock. An important phenomenon in downhole array analysis is the potential presence of pseudo-resonances, which has not been effectively taken into account in previous studies and which affects the assessment of the accuracy of 1D analysis. The first

part of this research provides insights into the cause and effect of pseudo-resonances and an approach is outlined to distinguish true-resonances from pseudo-resonances.

The small-strain damping (D_{min}) is a key parameter in linear ground response analysis and using laboratory-measured values tend to over-predict the response because it does not account for wave scattering present in the field. The second part of this research focuses on methods of increasing the D_{min} values in the profiles to better match observed site response, with the site response evaluated in terms of different ground motion characteristics. Alternatively, the randomization of shear wave velocity profiles is also assessed to provide more insights into the variable seismic properties at a site. A hypothesis that links the level of increased damping to the level of spatial variability in materials implied by the geologic conditions is proposed.

To broaden the application of the 1D analysis, it is crucial to be able to identify sites that can be modeled accurately by 1D analysis. A taxonomy scheme is developed that classifies sites into different groups based on the similarity in their responses in terms of being modeled well by 1D analysis. This classification system is based on downhole array data but can be applied to non-downhole array sites. The taxonomy results presented in this study show that an increased portion of sites are suitable for 1D analysis.

Table of Contents

List of Tables xii

List of Figures xiii

Chapter 1: Introduction 1

1.1 Research Significance 1

1.2 Organization of Dissertation 2

Chapter 2: The influence of the down-going wave and Pseudo-resonances on Downhole Array Data 4

2.1 Introduction 5

2.2 Down-going Wave Effect in Downhole Data 7

2.3 The Influence of Boundary Conditions on Theoretical Transfer Functions 10

2.4 Pseudo-resonances vs. True-Resonances 17

2.4.1 Factors that Control the Presence of Pseudo-Resonances 17

2.4.2 Approaches to Identify Pseudo-Resonances and True-Resonances 20

2.5 Pseudo-Resonances and True-Resonances in Empirical Downhole Array Data 23

2.6 Conclusions 28

2.7 Data and Resources 30

2.8 Acknowledgements 30

2.9 Refences 30

Chapter 3: Insights into Modeling Small-Strain Site Response Derived from Downhole Array Data 35

3.1 Introduction 36

3.2 Assessment of Site Response 39

3.3 Description of Downhole Array Sites and Available Data 42

3.3.1 Garner Valley Downhole Array 42

3.3.2 EuroSeisTest Downhole Array 43

3.3.3 Treasure Island Downhole Array 44

3.3.4 Delaney Park Downhole Array 45

3.3.5 Characterization of Downhole Array Sites 46

3.4 Assessment of Site Response Predictions in the Frequency Domain 49

3.4.1 Quantification of Goodness-of-Fit 49

3.4.2 Transfer Functions and Amplification Factors 51

3.4.3 Influence of D_{min} multiplier on Transfer Functions and Amplification Factors 54

3.4.4 Role of HVSR Data to Evaluate Site Response Predictions 55

3.5 Alternative Assessments of Site Response Predictions 58

3.5.1 Time Domain Ground Motion Parameters 58

3.5.2 High Frequency Spectral Decay Parameter 61

3.5.3 Shear Wave Velocity Randomization 63

3.6 Discussion 67

3.7 Conclusions 72

3.8 Acknowledgements 73

3.9 References....73

Chapter 4: Taxonomy for Evaluating the Site-Specific Applicability of One-Dimensional Ground Response Analysis....84

4.1 Introduction....85

4.2 Distinguishing Pseudo-resonances from True-resonances....90

4.3 Data Selection and Analysis....93

4.3.1 Data Processing....95

4.3.2 Vs Profile Calibration using HVSR....97

4.4 Proposed Site Response Taxonomy....99

4.4.1 Group A: 1D Sites Dominated by True Resonances....100

4.4.2 Group B: 1D sites with Both Pseudo-Resonances and True-Resonances....105

4.4.3 Group C: 1D sites Dominated by Pseudo-Resonances....108

4.4.4 Group D: Non-1D Sites....111

4.5 Discussion....114

4.5.1 Frequencies of Site Amplification....114

4.5.2 Comparison of Vs Profile Characteristics....117

4.5.3 Taxonomy Results Compared to Previous Studies....119

4.6 Conclusions....122

4.7 Data and Resources....124

4.8 Acknowledgements....124

4.9 References....125

Chapter 5: Summary, Conclusions and Recommendations.....131

5.1 Summary and Conclusions 131

5.2 Recommendations for Future Work 136

Appendix.....138

References.....155

List of Tables

Table 3.1: Goodness of fit parameters for theoretical TF and AF using D_{min} 52

Table 3.2: Goodness of fit parameters for theoretical TF and AF using scaled D_{min} 55

Table 3.3: f_{site} estimated from different methods 56

Table 3.4: D_{min} multipliers derived from time domain ground motion parameters 60

Table 3.5: Goodness of fit parameters for theoretical TF and AF using *Vs* randomization 65

Table 4.1 Summary of Sites Studied.....94

Table 4.2 Comparison of Taxonomy with Thompson *et al*. (2012) 120

Table A1 Vs profile for IBRH13 (Satoh *et al*., 2014) 150

Table A2 Modified Vs profile for IBRH17 150

Table A3 Modified Vs profile for IBRH18 151

Table A4 Modified Vs profile for SZOH39 151

Table A5 Modified Vs profile for TKCH05 151

Table A6 Modified Vs profile for EHMH02 151

Table A7 Modified Vs profile for IWTH27 152

Table A8 Modified Vs profile for KOCH05.....152

Table A9 Modified Vs profile for OKYH07 152

Table A10 Integrated and Modified Vs profile for Delaney Park Downhole Array 153

Table A11 Integrated and Modified Vs profile for EuroSeisTest Downhole Array.....153

Table A12 Integrated and Modified Vs profile for Garner Valley Downhole Array 154

Table A13 Integrated and Modified Vs profile for Treasure Island Downhole Array 154

List of Figures

Figure 2.1 Empirical transfer functions (shown in gray) and theoretical transfer functions for outcrop and borehole boundary conditions for different depths at the Garner Valley Downhole Array (Bonilla et al., 2002). 9

Figure 2.2 Boundary conditions and wave amplitudes considered in one-dimensional site response analysis. 10

Figure 2.3. Site response predictions based on the within and outcrop boundary conditions for two hypothetical models A and B. Transfer functions (*TF*) are shown in the middle row. The amplitudes of the up-going $|A_2|$, down-going $|B_2|$, and total waves $|A_2+B_2|$ in layer 2 given $A_1 = B_1 = 1.0$ are shown in the bottom row.....14

Figure 2.4. Theoretical time series at the surface and base of Models A and B from Figure 3 for a sine wave with $f = f_{site} = 1$ Hz and $A_1 = B_1 = 1.0$ at the surface. Up-going, down-going, and total waves at the base sensor depth of 100 m shown for separately for the two models and for the (a) within and (b) outcrop boundary conditions. 16

Figure 2.5. Within and outcrop transfer functions for four, 100-m deep hypothetical *Vs* profiles with a velocity impedance contrast (IC). All *Vs* profiles have *Vs* = 200 m/s above the IC and *Vs* = 1000 m/s below the IC. Results are shown for the IC located at depths of (a) 5 m, (b) 30 m, (c) 60 m, and (d) 90 m. 19

Figure 2.6 First mode frequency ratio (f_1 Ratio = $f_{1,outcrop}/f_{1,within}$) vs. impedance contrast (IC) depth relative to the base sensor for different values of IC. 20

Figure 2.7 Theoretical H/V Spectral Ratio (*HVSR*) plotted together with outcrop and within TFs to identify the frequencies associated with true-resonance. Results shown for the same profiles as Figure 5 with the IC located at depths of (a) 5 m, (b) 30 m, (c) 60 m, and (d) 90 m. 22

Figure 2.8. Empirical and theoretical transfer functions, along with measured *Vs* profiles, for four Kik-net downhole array sites.....25

Figure 2.9 Theoretical and empirical *HVSR*, along with empirical transfer functions (*TF*), for the four KiK-net sites shown in Figure 2.8.....26

Figure 3.1: Elements of linear elastic site response analysis. 37

Figure 3.2: Modified regional geologic maps for downhole arrays analyzed (red triangle represents the location of downhole array): (a) Garner Valley (McCrea *et al*. 2012), (b) EuroSeisTest (Manakou *et al*. 2010), (c) Treasure Island (Wagner *et al*. 1991), and (d) Delaney Park (Combellick 1999). 45

Figure 3.3 Shear wave velocity and small strain damping ratio profiles for downhole array. 47

Figure 3.4: Empirical and theoretical TF and AF for different levels of D_{min}. Median empirical values are shown in dash and the +/-2σ_{ln} range of the data are shown in gray. 53

Figure 3.5: Empirical and theoretical HVSR along with empirical TF 57

Figure 3.6 Example assessment of D_{min} multipliers using time domain ground motion parameters. (a) Recorded surface acceleration-time series, (b) predicted acceleration-time series using D_{min}, (c) predicted acceleration-time series using $3.4xD_{min}$, (d) recorded acceleration time series and predicted acceleration time series for $3.4xD_{min}$, (e) recorded velocity time series and predicted velocity time series for $3.6xD_{min}$, and (f) Arias intensity for recorded motion and predicted motions with D_{min} and $3.1xD_{min}$. Results shown for Garner Valley motion.....59

Figure 3.7: Average empirical $\Delta\kappa$ and theoretical $\Delta\kappa$ for the four sites. 62

Figure 3.8: Profiles of σ_{lnVs} *Vs*. depth that provide the best-match with the empirical transfer function. 64

Figure 3.9: Empirical TF and AF compared with theoretical TF and AF computed for Monte Carlo simulations using *Vs* randomization and D_{min}. Median empirical values are shown in dash and the $+/-2\sigma_{ln}$ range of the data is shown in gray. 66

Figure 3.10: Comparison of D_{min} multipliers considered for different ground response characteristics for each site. 70

Figure 4.1. Example Sites for Evaluation of SH1D Assumption: IBRH13 and IWTH12 are adapted from Thompson *et al*., (2012); KSRH05 is adapted from Tao and Rathje (2019b).....88

Figure 4.2. The Influences of Size and Depth of Impedance Contrast (IC) on Pseudo-resonances. 92

Figure 4.3. Example Sites for Vs Profile Calibration Using HVSR. 98

Figure 4.4. Flow Chart Showing the Steps for Site Response Taxonomy.....100
Figure 4.5. Transfer function responses, *HVSR* responses, and *Vs* profiles for three example sites from Group A. 102
Figure 4.6. *Vs* Profiles for All Sites in Group A. 104
Figure 4.7. Transfer function responses, *HVSR* responses, and *Vs* profiles for two example sites from Groups B. 106
Figure 4.8. *Vs* Profiles for Sites in Groups B_1 and B_2 108
Figure 4.9. Transfer function responses, HVSR responses, and Vs profiles for one example site from Group C. 109
Figure 4.10. Vs profiles of Group C. 110
Figure 4.11. Transfer function responses, *HVSR* responses, and *Vs* profiles for three example sites from Group D. 112
Figure 4.12. *Vs* Profiles Group D. 114
Figure 4.13. Comparison of frequencies of site amplification derived from *HVSR*, theoretical TF, and empirical *TF* for Groups A, B_1 and B_2. 116
Figure 4.14. Comparison of Features of Shear Wave Velocity Profile across different taxonomy groups. 118
Figure A1. Group A_1: Plots for Delaney Park Downhole Array 138
Figure A2. Group A_1: Plots for EuroSeisTest Downhole Array 139
Figure A3. Group A_1: Plots for Garner Valley Downhole Array 139
Figure A4. Group A_1: Plots for HYGH10 139
Figure A5. Group A_1: Plots for Treasure Island Downhole Array 140
Figure A6. Group A_2: Plots for FKSH16 140

Figure A7. Group A_2: Plots for IBRH17 140
Figure A8. Group A_3: Plots for FKSH14.....141
Figure A9. Group A_3: Plots for FKSH19.....141
Figure A10. Group A_3: Plots for IBRH11 141
Figure A11. Group A_3: Plots for IBRH13 142
Figure A12. Group A_3: Plots for IWTH04.....142
Figure A13. Group A_3: Plots for KSRH10 142
Figure A14. Group B_1: Plots for IBRH18.....143
Figure A15. Group B_1: Plots for KSRH05.....143
Figure A16. Group B_1: Plots for KSRH07.....143
Figure A17. Group B_1: Plots for MYGH05.....144
Figure A18. Group B_1: Plots for SZOH39.....144
Figure A19. Group B_1: Plots for TKCH05 144
Figure A20. Group B_2: Plots for EHMH02 145
Figure A21. Group B_2: Plots for IWTH27.....145
Figure A22. Group B_2: Plots for KOCH05.....145
Figure A23. Group B_2: Plots for OKYH07.....146
Figure A24. Group B_2: Plots for OKYH14.....146
Figure A25. Group C: Plots for El Centro – Meloland Downhole Array.....146
Figure A26. Group C: Plots for La Cienega Downhole Array (100m) 147
Figure A27. Group C: Plots for La Cienega Downhole Array (252m) 147
Figure A28. Group C: Plots for NMRH04.....147
Figure A29. Group D_1: Plots for IWTH12.....148

Figure A30. Group D_2: Plots for SMNH02 148
Figure A31. Group D_2: Plots for HRSH03 148
Figure A32. Group D_3: Plots for KSRH06 149
Figure A33. Group D_3: Plots for NIGH14 149
Figure A34. Group D_3: Plots for NGNH18 149
Figure A35. Group D_3: Plots for IWTH24.....150

Chapter 1: Introduction

1.1 Research Significance

The proper evaluation of ground response under earthquake shaking is crucial in many aspects of geotechnical engineering and ground response analysis remains one of the most common types of analyses performed in engineering practice. Most ground response analyses incorporate the one-dimensional (1D) assumption, in which the soil and rock layers are assumed to extend infinitely in the horizontal directions and the site response is dominated by vertically propagating, horizontally polarized SH waves (SH1D assumption, Kramer 1996).

The accuracy of 1D ground response analysis has been assessed in many previous studies. It started initially utilizing surface array recordings at soil and nearby rock sites (e.g., Idriss, 1990; Boatwright *et al*., 1991; Rollins *et al*., 1994) and then was followed by the more popular approach of using vertical downhole arrays (e.g., Bonilla *et al*., 2002; Thompson *et al*, 2009, 2012; Zalachoris and Rathje, 2015). Downhole array analyses became popular because for the surface array method it is difficult to find an outcropping rock site sufficiently close to a soil site, and even if one is identified, the surface rock may have its own site amplification due to near-surface weathering that makes it not representative of the rock motion at the base of the soil column.

When using downhole array data, one critical assumption is the boundary condition at the depth of the base, downhole sensor. The within boundary condition assumes that both up-going and down-going waves are present at the base (Bonilla *et al*., 2002), which is standard practice when analyzing downhole arrays. The outcrop boundary condition assumes the depth of the base sensor is a free-surface and thus the up-going wave is fully reflected and represents the down-going wave. When using the within boundary condition, the destructive interference between the up-going and down-going waves may produce pseudo-resonances that do not represent the true

dynamic response of a site. Additionally, ground response analyses performed in engineering practice predominantly utilize surface recordings as input motions, analogous to the surface array method, and thus adopt the outcrop boundary condition.

Another important issue when evaluating 1D site response analysis is the appropriate level of damping that provides ground motion amplitudes that match the recordings. Damping profiles are commonly assigned based on laboratory measurements of material damping; however, laboratory testing cannot account for seismic wave scattering due to material heterogeneities in the field (Thompson *et al*, 2009) and thus using such values tends to over-predict the site response.

To improve the effective evaluation and broaden the application of 1D ground response analysis, the goal of this research can be summarized into three aspects: (1) to provide insights into the phenomenon of pseudo-resonances and develop approaches to distinguish pseudo-resonances from true-resonances so that the true response of a site can be the focus of site response evaluations; (2) to investigate methods that modify damping levels to take into account the seismic energy dissipated by wave scattering and better match the empirical site response; and (3) to develop a taxonomy that classifies sites based on the applicability of 1D analysis and the influence of pseudo-resonance, and that can be applied to non-downhole array sites commonly encountered in engineering practice.

1.2 ORGANIZATION OF DISSERTATION

Following this introduction in Chapter 1, this dissertation is organized into three main chapters (i.e., Chapters 2, 3 and 4) and each chapter is a self-contained journal article that includes an introduction, literature review on related topics, research methodology, research findings,

discussions and conclusions. The last chapter, Chapter 5, concludes the dissertation and provides thoughts and recommendations on future work.

Chapter 2 investigates the pseudo-resonance phenomenon in downhole array data. To elucidate the cause of pseudo-resonances, theoretical wave propagation analyses are performed. In an effort to investigate the factors that influence the presence of pseudo-resonances, a series of hypothetical *Vs* profiles are created that represent different realistic site conditions and site response analyses are carried out for these profiles. A proposed approach to distinguish pseudo-resonances from true-resonances is outlined and illustrated by demonstrating the application to four realistic sites.

Chapter 3 investigates methods to assign damping profiles to site response analysis. The main approach is based on scaling the small-strain damping (D_{min}) profiles predicted from empirical models to match the empirical site response at small strain (i.e., low intensity motions). Various site amplification and ground motion characteristics are considered when evaluating the match to the empirical data. Alternative approaches of matching the high frequency decay parameter, κ, and using shear wave velocity randomization are also investigated to provide more insights into modeling small strain site response.

Chapter 4 builds on the work in Chapters 2 and 3 and tackles the difficult issue of identifying sites that can be modeled accurately by 1D ground response analysis. A classification scheme is developed in this chapter that groups sites based on the quality of the fit with 1D analysis and the influence of pseudo-resonances on the response. The taxonomy scheme can be applied to any site (even non-downhole array sites), making it easily applicable to sites analyzed in engineering practice.

Chapter 2: The influence of the down-going wave and Pseudo-resonances on Downhole Array Data

Yumeng Tao[1], and Ellen Rathje[2]

ABSTRACT

Downhole array networks are being used more often to study seismic site response and to evaluate the accuracy of one-dimensional site response analysis. However, the boundary conditions for a downhole array are unique because the downhole recording may contain both the up-going and down-going waves, which can lead to the appearance of pseudo-resonances that are not representative of the true site resonances. The goal of a site response analysis is to account for the true dynamic response of a soil deposit; therefore, it is important when using downhole array data to evaluate site response techniques to distinguish pseudo-resonances from true-resonances. This paper describes the down-going wave effect and explains its role in the appearance of pseudo-resonances. It is demonstrated that the presence of a pseudo-resonance is controlled by the existence of a sizable impedance contrast in the soil profile and the location of that impedance contrast relative to the base sensor depth. An approach is outlined to distinguish pseudo-resonances from true resonances using the theoretical 1D transfer functions for within and outcrop boundary conditions, as well as the horizontal to vertical spectral ratio (*HVSR*). We advocate that when evaluating the accuracy of 1D site response analysis using downhole array data only the frequencies associated with true-resonances be taken into account.

[1] Graduate Research Assistant, Department of Civil, Architectural, and Environmental Engineering, University of Texas, Austin, TX 78712

[2] Janet S. Cockrell Centennial Chair in Engineering, Department of Civil, Architectural, and Environmental Engineering, University of Texas, Austin, TX 78712

Key words: Site response, down-going wave effect, pseudo-resonances

2.1 INTRODUCTION

As observed in many previous earthquakes, local soil conditions play a significant role in modifying the characteristics of seismic shaking and they can influence the earthquake damage patterns over small distances (e.g., Borcherdt, 1970; Bradley and Cubrinovski, 2011). Therefore, accurately predicting the site amplification associated with local soil conditions is a critical part of the seismic design process.

One-dimensional (1D) site response analysis, which involves the propagation of seismic waves from a competent rock layer at depth through the overlying soil materials, is the most common approach used to compute site amplification (Kramer 1996). This analysis assumes a 1D layered system in which all the layer boundaries extend infinitely in the horizontal direction and the soil response is predominantly controlled by vertically propagating, horizontally polarized shear waves. To perform a 1D site response analysis, the shear wave velocity (Vs) profile and damping ratio (D) profile are needed to represent the site conditions. Soil nonlinearity can be taken into account through an iterative, equivalent-linear (EQL) approach in which the *Vs* and D are assigned to each layer based on induced shear strains and the nonlinear shear modulus reduction and damping curves. If the induced shear strains are small (i.e., less than about 10^{-3}%), only the small-strain *Vs* and D profiles are needed and a simple linear elastic analysis is performed.

The accuracy of 1D site response analysis has been evaluated in many studies, initially using surface arrays of nearby surface recordings on soil and rock (e.g., Idriss, 1990; Boatwright *et al*., 1991; Rollins *et al*., 1994). This approach uses the nearby outcropping rock recording as input into the site response analysis, propagates that motion through 1D soil column, and compares

the computed soil surface response with the recorded motion. Because it can be difficult to find soil and rock sites sufficiently close to one another for this analysis, it has become more common to use vertical downhole arrays to evaluate 1D site response analysis. A vertical downhole array consists of at least one pair of sensors, with one installed at the surface and one (or more) at depth within the ground. The main difference between the empirical site amplification implied by surface arrays and downhole arrays is the reference condition (Steidl *et al*., 1996; Thompson *et al*., 2009). For surface arrays the site amplification is defined as the ratio of the motions recorded at the outcropping soil surface and at outcropping rock, while for downhole arrays the site amplification is the ratio of the motions recorded at the outcropping soil surface and at the base sensor within the ground.

A critical assumption of the surface array method is that the reference rock motion at the surface is equivalent to the motion at bedrock below the soil layers and that there is no site effect at the reference rock site after the free-surface effect is removed (Steidl *et al*., 1996). However, it is often difficult to find a nearby rock site and, even when one is identified, the surface rock may be fractured or weathered and have its own site amplification. Abercrombie (1997) showed that even a stiff granite site displays site effects that need to be taken into account, and Steidl *et al*. (1996) showed that ignoring this site response at the reference rock site will result in an underestimation of the site amplification at a soil site. Other researchers have also reported that estimates of site amplification from the surface array method are influenced by the choice of the reference rock site (Yu and Haines, 2003; Malagnini *et al*., 2004; Cadet *et al*., 2010).

An important advantage of the downhole array method is that it provides the most direct observation of how the materials between two depths modify the seismic waves. With the increase

in availability of downhole array data, many researchers have focused on the downhole array method to evaluate one-dimensional site response analysis (e.g., Thompson *et al.*, 2009, 2012; Kaklamanos *et al.*, 2015; Zalachoris and Rathje, 2015; Tao and Rathje, 2019). The site response simulations used in these studies utilize the within boundary condition at the depth of the base sensor, which accounts for the presence of both the up-going and down-going waves and is the appropriate boundary condition for a point within the subsurface. However, the destructive interference between the up-going and down-going waves can result in the appearance of pseudo-resonances that do not represent the true dynamic response of the site. Additionally, almost all site response analyses performed in engineering practice utilize recorded surface motions as the input motion (analogous to the surface array method) and thus use an outcrop boundary condition. This outcrop boundary condition does not include the effects of the down-going wave and thus no pseudo-resonances are present.

The goal of this study is to closely examine the influence of the down-going wave effect on site response predictions for downhole arrays and the impact of this effect on pseudo-resonances and true-resonances. To best elucidate these issues, we perform theoretical wave propagation analyses utilizing hypothetical velocity profiles that model different profile characteristics. The insights from the hypothetical profiles are used to interpret downhole array data from selected downhole array sites in Japan and to develop an approach to distinguish pseudo-resonances from true-resonances in downhole array data.

2.2 Down-going Wave Effect in Downhole Data

The subsurface motion recorded at a downhole sensor includes the effects of both incident up-going waves and reflected down-going waves. The up-going and down-going waves interfere

with each other, affecting the characteristics of motion recorded at the downhole sensor. This phenomenon is commonly referred to as the down-going wave effect. Shearer and Orcutt (1987) used a simple plane wave model of a homogeneous, un-damped half-space to illustrate the timing of the up-going and down-going pulses and the resulting nodes (i.e., zero amplitudes) in the Fourier Amplitude Spectra (*FAS*) of the total motion at different depths. The pattern of nodal frequencies is related to the depth and the difference in time arrivals of the up-going and down-going pulses at each depth. Because of the small *FAS* amplitudes at the nodal frequencies at depth, the ratio of the surface *FAS* to *FAS* at depth displays peaks at these frequencies. Other researchers (e.g., Mehta *et al*., 2007; Parolai *et al*., 2009; Oth *et al*., 2011) have investigated the up-going and down-going wave pulses associated with recordings at different depths within a downhole array. Similar to the theoretical results from Shearer and Orcutt (1987), the up-going wave pulse arrives at the downhole sensor before it arrives at the surface, and the down-going wave pulse arrives later due to the travel time through the upper layers. The down-going wave pulse can be observed at depth, but the pulse tends to be weaker than the up-going wave pulse.

Bonilla *et al.* (2002) analyzed earthquake events recorded at the Garner Valley Downhole Array, computing the observed and theoretical *FAS* transfer functions for recordings at depths between 6 m and 500 m. They considered a theoretical Borehole response, which is the same as the within boundary condition including both up-going and down-going waves, and a theoretical Outcrop response that includes only the up-going wave at the base sensor. Figure 2.1 shows their

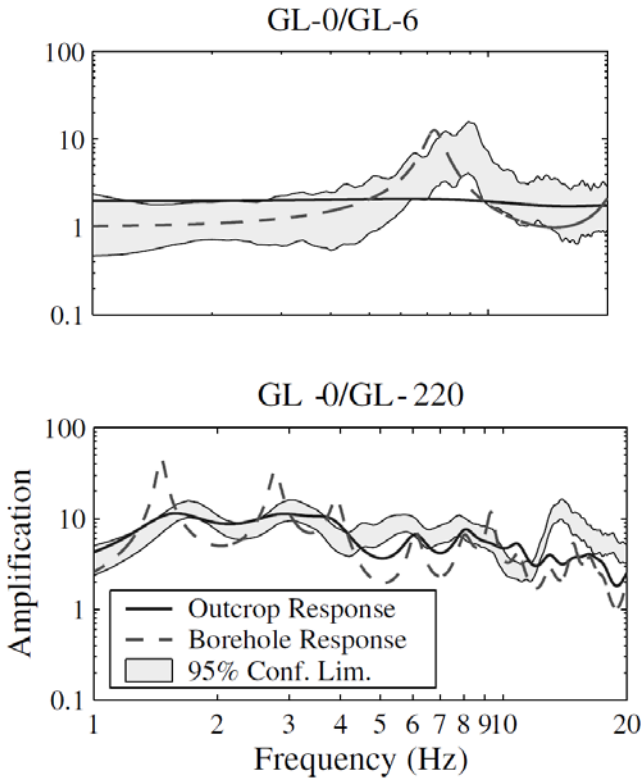

Figure 2.1 Empirical transfer functions (shown in gray) and theoretical transfer functions for outcrop and borehole boundary conditions for different depths at the Garner Valley Downhole Array (Bonilla et al., 2002).

results for the Surface to 6 m and Surface to 220 m transfer functions. At 6 m, the Borehole response matches the observed response well, while the Outcrop response is flat. Between the surface and 6 m, the material is alluvium with a shear wave velocity of about 200 m/s; thus the outcrop response is flat and the borehole response is dominated by the down-going wave effect with a peak at about 9 Hz. At 220 m, the Borehole and Outcrop responses have peaks at similar frequencies, but the peaks in the Outcrop response are much smaller and better match the empirical transfer function. Bonilla *et al.* (2002) concluded that the interference between the up-going and down-going waves produces pseudo-resonant peaks in the empirical transfer function at shallow depth, but these effects are minimized at larger depths.

2.3 The Influence of Boundary Conditions on Theoretical Transfer Functions

The transfer functions used to propagate SH waves through a one-dimensional soil profile can be formulated for two types of boundary conditions at the base: within and outcrop. Figure 2.2 shows a schematic commonly used to explain these boundary conditions. A layered soil profile with up-going waves (A_i) and down-going waves (B_i) in each layer is underlain by a rock half

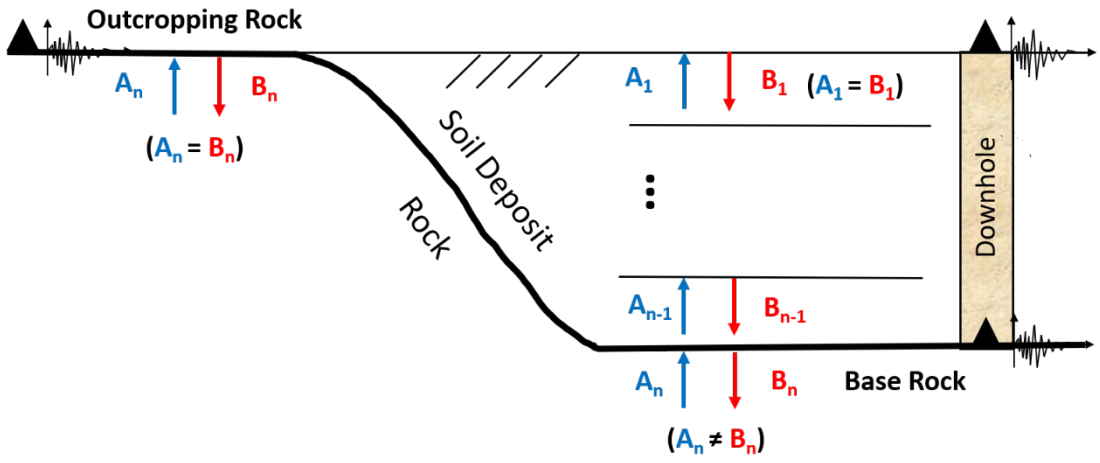

Figure 2.2 Boundary conditions and wave amplitudes considered in one-dimensional site response analysis.

space. The rock half space is within the subsurface profile and thus both up-going and down-going waves are present in the rock half space. Input motions used in site response analyses in practice are almost always recorded at the ground surface on outcropping rock, and at this location the up-going and down-going waves are the same ($A_n = B_n$) because of the free surface effect. However, when considering a downhole array, the input motion is recorded within the subsurface profile and thus $A_n \neq B_n$.

The schematic in Figure 2.2 can be simplified into a two-layer system with the second layer representing the half space, either within the subsurface profile or as an adjacent outcropping layer.

For each frequency, we define the up-going wave in layer *i* as A_i and the down-going wave as B_i. Following the nomenclature in Kramer (1996), the displacements in each layer for harmonic motion can be expressed as:

$$u_1(z_1, t) = (A_1 e^{ik_1^* z_1} + B_1 e^{-ik_1^* z_1}) \cdot e^{i\omega t} \quad (2.1)$$

$$u_2(z_2, t) = (A_2 e^{ik_2^* z_2} + B_2 e^{-ik_2^* z_2}) \cdot e^{i\omega t} \quad (2.2)$$

where ω is angular frequency, t is time, z_i is the depth below the top of layer i, and k_i^* is the complex wave number in layer i ($k^* = \omega / Vs^* = \omega / [\ Vs \cdot (1 + iD) \cdot k\ ]$, where D = equivalent viscous damping ratio).

For any outcropping layer at a free surface, the up-going wave is fully reflected and thus $A_i = B_i$. For all subsurface layers the up-going and down-going waves are not the same and thus $A_i \neq B_i$. When analyzing downhole array data it is important to properly model the down-going wave for the within boundary condition, and when analyzing site response using outcropping rock motions it is important to properly model the free surface outcropping boundary condition. The transfer functions for each boundary condition are derived below.

The compatibility of displacements and continuity of stress at the layer interface lead to (Kramer, 1996):

$$A_2 = \frac{1}{2} A_1 [(1 + \alpha_{12}^*) e^{ik_1^* H_1} + (1 - \alpha_{12}^*) e^{-ik_1^* H_1}] \quad (2.3)$$

$$B_2 = \frac{1}{2} A_1 [(1 - \alpha_{12}^*) e^{ik_1^* H_1} + (1 + \alpha_{12}^*) e^{-ik_1^* H_1}] \quad (2.4)$$

where α_{12}^* represents the complex impedance ratio (i.e., $\alpha_{12}^* = \frac{\rho_1 Vs_1^*}{\rho_2 Vs_2^*}$) and H_1 represents the thickness of layer 1. Eqs (2.3) and (2.4) can be substituted into eq (2.2) to compute the amplitude of the wave at the top of layer 2 (i.e., $z_2 = 0$) as a function of A_1 and B_1:

$$A_2 + B_2 = A_1(e^{ik_1^* H_1} + e^{-ik_1^* H_1}) \tag{2.5}$$

However, if layer 2 is outcropping with $B_2 = A_2$, then the amplitude at the top of layer 2 become:

$$2A_2 = A_1[(1 + \alpha_{12}^*)e^{ik_1^* H_1} + (1 - \alpha_{12}^*)e^{-ik_1^* H_1}] \tag{2.6}$$

The outcrop boundary condition for layer 2 represents the case where input motions are applied to the analysis that were recorded at the ground surface (i.e., at an outcrop) and thus do not have any down-going waves present. Finally, the wave amplitudes at the ground surface (i.e., $z_1 = 0$ is simply $2A_1$ due to the free surface effect.

A transfer function (*TF*) is defined as the ratio between the wave amplitudes at two locations. For the geometry in Figure 2.2 the *TF* is computed as the ratio of the wave amplitudes at the ground surface and the top of layer 2. The *TF* can be computed for the within boundary condition (TF_{within}), which includes the down-going wave, or for the outcrop boundary condition ($TF_{outcrop}$), which does not. The resulting *TF* can be expressed using the previously defined wave amplitudes as:

$$TF_{within} = \frac{2A_1}{A_2 + B_2} = \frac{2A_1}{A_1(e^{ik_1^* H_1} + e^{-ik_1^* H_1})} = \frac{2}{e^{ik_1^* H_1} + e^{-ik_1^* H_1}} \tag{2.7}$$

$$TF_{outcrop} = \frac{2A_1}{2A_2} = \frac{2A_1}{A_1[(1+\alpha_{12}^*)e^{ik_1^* H_1} + (1-\alpha_{12}^*)e^{-ik_1^* H_1}]} = \frac{2}{(1+\alpha_{12}^*)e^{ik_1^* H_1} + (1-\alpha_{12}^*)e^{-ik_1^* H_1}} \tag{2.8}$$

Note the important difference in the two transfer functions: TF_{within} is solely related to the properties of layer 1, while $TF_{outcrop}$ is a function of the properties of both layers through the inclusion of the complex impedance ratio (α_{12}^{*}). The derivation above is focused on only two layers, but it is easily extended to a multi-layer system using the recursive expressions for A_i and B_i (Kramer, 1996) and defining the transfer functions from the base layer within the half-space. For the multi-layer system, the observations above still hold: TF_{within} is only a function of the properties of the materials above the base layer and $TF_{outcrop}$ is a function of the properties both above and below the layer.

To better understand the site amplification predicted by the within and outcrop boundary conditions, consider two simplified systems (Models A and B) shown in Figure 2.3. Model A represents two layers with the same shear wave velocity (Vs) equal to 400 m/s, while Model B represents the same *Vs* = 400 m/s layer at the surface but underlain by a *Vs* = 1000 m/s layer. The first layer is 100 m thick, resulting in a natural site frequency (f_{site}) equal to 1 Hz for the material found above 100 m. All layers have a damping ratio of 2%. Both models are analyzed for the outcrop boundary condition at the base ($A_2 = B_2$) and for the within boundary condition ($A_2 \neq B_2$). These boundary conditions are schematically shown in Figure 2.3, along with TF_{within} and $TF_{outcrop}$ for each model. TF_{within} is the same for both models because, as noted earlier, TF_{within} only depends on the properties of the first layer and both models have the same properties in the first layer. $TF_{outcrop}$ is significantly different for the two models, with Model A displaying a flat response and Model B displaying peaks at similar frequencies as TF_{within} but with smoother and smaller peaks. The transfer functions for Model A are similar to the transfer functions shown in Figure 2.1 at 6 m depth for Garner Valley. The characteristics of the different transfer functions in Figure 2.3 can

be traced back to the characteristics of the waves at the base of each model and for each boundary condition.

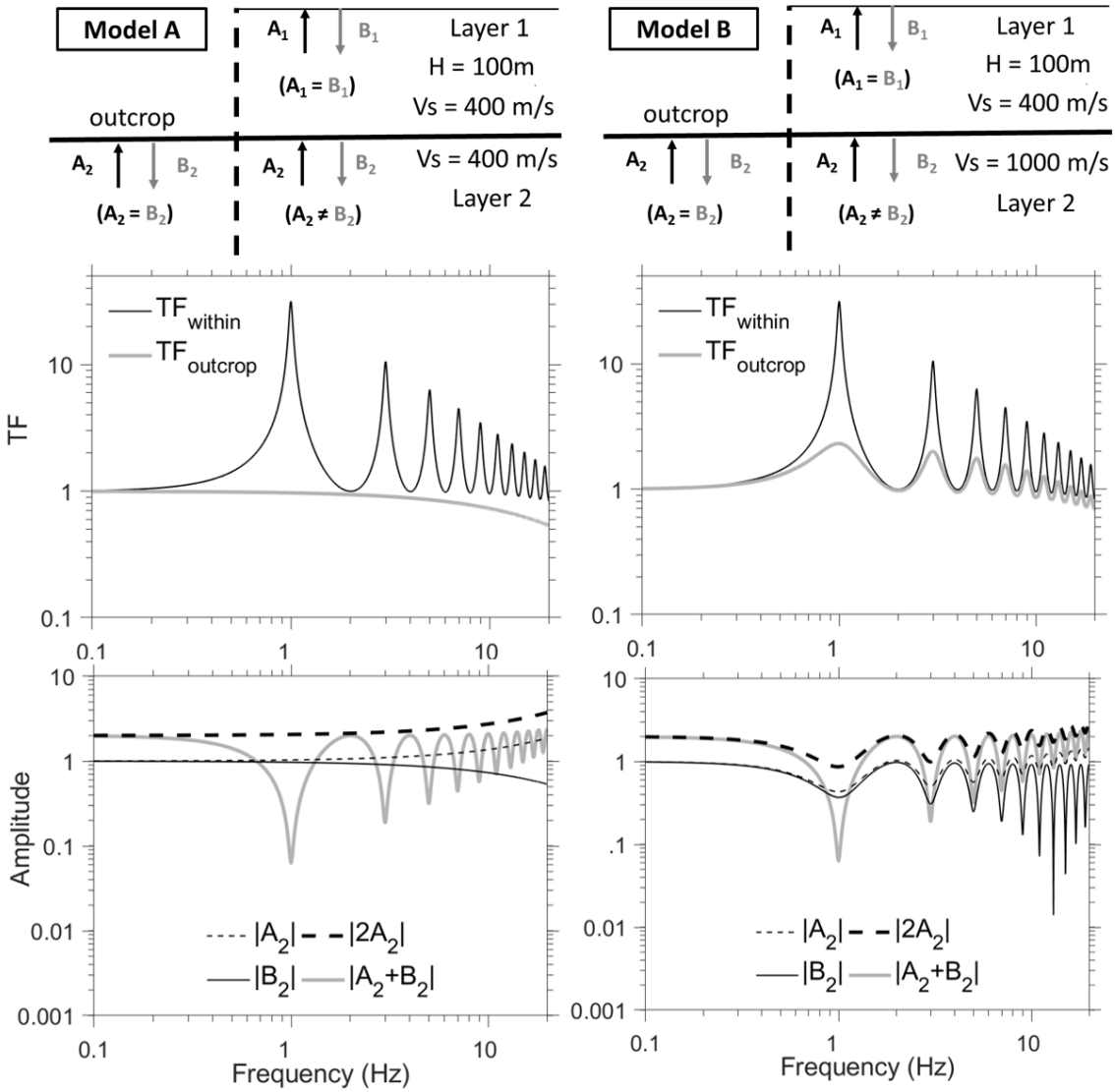

Figure 2.3. Site response predictions based on the within and outcrop boundary conditions for two hypothetical models A and B. Transfer functions (*TF*) are shown in the middle row. The amplitudes of the up-going $|A_2|$, down-going $|B_2|$, and total waves $|A_2+B_2|$ in layer 2 given $A_1 = B_1 = 1.0$ are shown in the bottom row.

The amplitudes A_2, B_2, $2A_2$ and $A_2 + B_2$ are shown in Figure 2.3 for each model for $A_1 = B_1 = 1$. Note that these are the components incorporated in the transfer functions (eqs 2.7 and 2.8). For Model A with $\alpha_{12}^* = 1$, $|A_2|$ and $|B_2|$ are flat and very similar to one another because there is no impedance contrast to change the wave amplitudes. $|B_2|$ is smaller than $|A_2|$, particularly at higher frequencies, due to the damping effects on the down-going wave during its travel up and then down through layer 1. For Model B with $\alpha_{12}^* \neq 1$, again $|A_2|$ and $|B_2|$ are very similar but in this case the amplitudes are not flat, but rather show smaller amplitudes at f_{site} and at higher mode frequencies due to the resonances that occur above the impedance contrast. Interestingly, $|A_2 + B_2|$ for the two models are the same despite the fact that $|A_2|$ and $|B_2|$ are different. An important characteristic of $|A_2 + B_2|$ is the very small amplitudes that occur at f_{site} and at higher mode frequencies, which lead directly to the very large peaks in TF_{within}. These small amplitudes are caused by the destructive interference of the up-going and down-going waves (Steidl *et al.*, 1996), as illustrated in Figure 2.4.

Figure 2.4 shows the response of Models A and B for a $f = 1$ Hz wave that arrives at the surface at $t = 2$ s with $A_1 = B_1 = 1$. Note that $f = f_{site}$ in this case. For the within boundary condition for both models (Figure 2.4a), the up-going wave is observed 0.25 s before it arrives at the surface due to the travel time through layer 1 and the down-going wave is observed 0.25 s after it arrives at the surface, again due to the travel time through layer 1. The resulting 0.5 s delay between the up-going and down-going waves results in the two waves being one-half cycle (i.e., 180°) out of phase, and when summed together $A_2 + B_2$ is very small (~ 0.06). Note that $A_2 + B_2$ is not zero because A_2 and B_2 do not have the exact same amplitude due to the effects of damping. The resulting TF_{within} at 1 Hz is equal to $2A_1/(A_2 + B_2) = 2/0.06 = 33.3$. The same behavior is observed

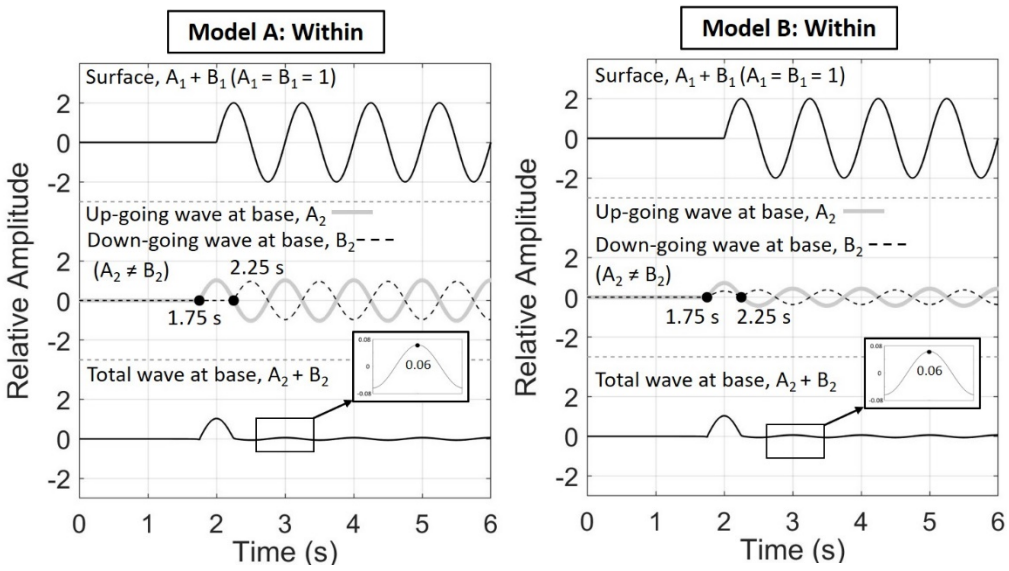

(a)

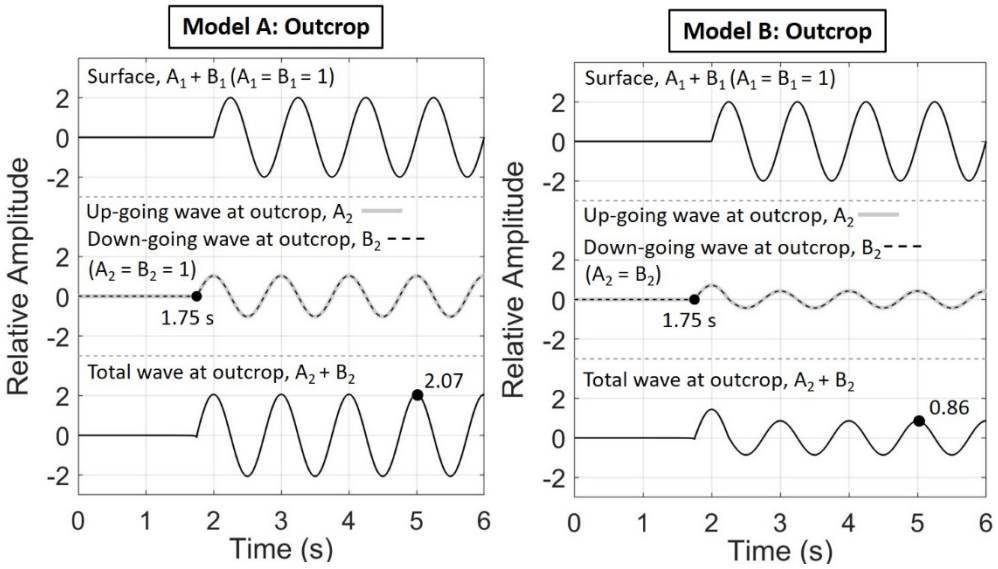

(b)

Figure 2.4. Theoretical time series at the surface and base of Models A and B from Figure 3 for a sine wave with $f = f_{site}$ = 1 Hz and $A_1 = B_1$ = 1.0 at the surface. Up-going, down-going, and total waves at the base sensor depth of 100 m shown for separately for the two models and for the (a) within and (b) outcrop boundary conditions.

for both models, although the amplitudes of A_2 and B_2 are different. This destructive interference occurs at $f = f_{site}$ because the two-way travel time of 0.5 s is equal to one-half cycle of the 1 Hz

wave. Similar destructive interference occurs at the higher mode frequencies where the two-wave travel time is equal to 3/2, 5/2, etc. cycles of the wave. For the outcrop boundary condition shown in Figure 2.4b, the up-going and down-going waves are the same in layer 2 (i.e., $A_2 = B_2$) and thus there is no destructive interference. For Model A, the total wave amplitudes $2A_2 = 2.07$ and with $2A_1 = 2.0$ the resulting $TF_{outcrop} = 2\ A_2 / 2A_1 = 2/2.07 = \sim 1.0$. For Model B, $2A_2$ is smaller (i.e., $2A_2 = 0.86$) due to the larger velocity in layer 2 and the resulting $TF_{outcrop}$ is greater than 1 ($TF_{outcrop} = 2/0.86 = 2.32$).

The responses shown in Figures 2.3 and 2.4 demonstrate the important influence of an impedance contrast on the outcrop and within transfer functions. For sites with an impedance contrast at the base, the within boundary condition simply changes the amplitude of the *TF* at the site frequencies relative to the outcrop *TF*. For sites without an impedance contrast, the within boundary condition displays large peaks simply due to the destructive interference of the up-going and down-going waves. These peaks can be considered pseudo-resonances (Bonilla *et al*., 2002) because they do not appear in the outcrop *TF* and the frequencies at which they occur are related only to the two-way travel time of the wave through the overlying material.

2.4 PSEUDO-RESONANCES VS. TRUE-RESONANCES

2.4.1 Factors that Control the Presence of Pseudo-Resonances

The example in the previous section demonstrated the importance of an impedance contrast in the *Vs* profile on the presence of pseudo-resonances in the within transfer function. To further investigate the relationship between impedance contrasts (IC) and pseudo-resonances, a series of hypothetical *Vs* profiles are created that represent different depths to the IC for a downhole array

with the base sensor at 100 m depth. The profiles consist of a surface layer with *Vs* = 200 m/s underlain by a layer with *Vs* = 1,000 m/s, representing an IC of 5. The thickness of the first layer is modeled separately as 5 m, 30 m, 60 m, and 90 m, representing 5%, 30%, 60%, and 90% of the distance to the base sensor. The theoretical TF_{within} and $TF_{outcrop}$ between the surface and the base sensor depth of 100 m are computed accordingly for each *Vs* profile.

For the case with IC at 5 m depth (Figure 2.5a), $TF_{outcrop}$ shows a single peak at 10 Hz representing the resonant frequency of the top layer (i.e., $Vs / 4 \cdot H$ = 200 (m/s) / 4·5 (m) = 10 Hz) even though the transfer function represents the full depth of 100 m. TF_{within} shows 5 peaks, with the first peak at ~2.5 Hz representing the pseudo-resonance of the full 100 m profile and the other peaks representing a combination of pseudo and true resonances. In general, the alignment of a peak in TF_{within} and $TF_{outcrop}$ means the peak is a true resonance, and if the peak is only present in TF_{within} then it represents a pseudo-resonance. For the case with the IC at 30 m (Figure 2.5b), the first peaks in $TF_{outcrop}$ and TF_{within} occur at relatively similar frequencies (~1.5 to 1.7 Hz) indicating it is a true resonance, but TF_{within} contains additional peaks at higher frequencies (e.g., ~ 3.5 Hz) that represent pseudo-resonances. As the IC continues deeper (60 m and 90 m in Figures 5c and d), most of the peaks in the two transfer functions are aligned, which indicates that all peaks are true resonances. Thus, as the depth of the IC approaches the depth of the base sensor the peaks become predominantly true resonances but when the IC is shallow relative to the base sensor depth the peaks represent a combination of pseudo and true resonances.

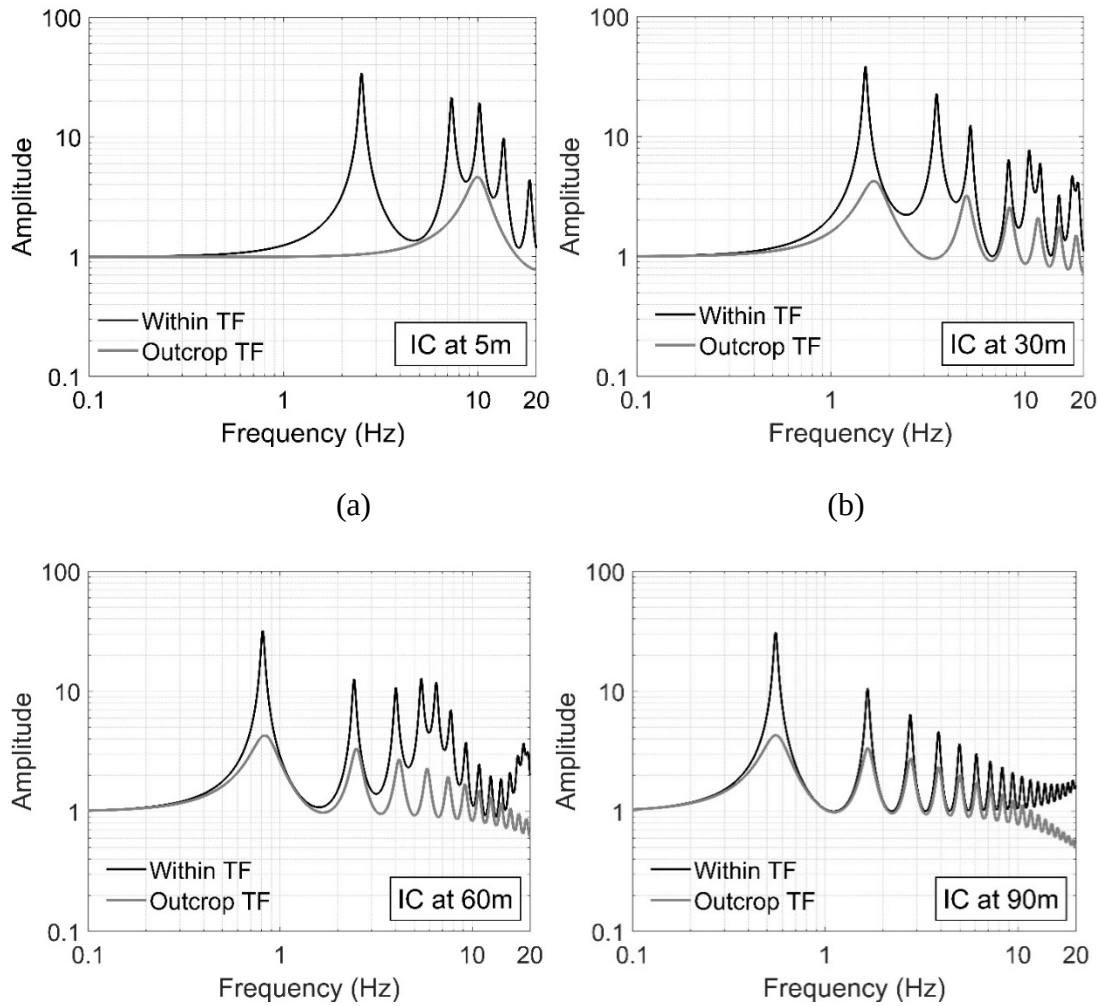

Figure 2.5. Within and outcrop transfer functions for four, 100-m deep hypothetical *Vs* profiles with a velocity impedance contrast (IC). All *Vs* profiles have *Vs* = 200 m/s above the IC and *Vs* = 1000 m/s below the IC. Results are shown for the IC located at depths of (a) 5 m, (b) 30 m, (c) 60 m, and (d) 90 m.

The size of the IC also influences the presence of pseudo-resonances. To quantify this influence, we define the f_1 Ratio as the ratio between the frequency of the first peak from the within and outcrop *TF* (i.e., f_1 Ratio = $f_{1,outcrop} / f_{1,within}$). When the f_1 Ratio is close to one the peaks align and the first peak in TF_{within} is considered a true-resonance, although there may be pseudo-resonances at higher frequencies. When the f_1 Ratio is greater than one, $f_{1,outcrop}$ is greater than $f_{1,within}$,

which indicates that the first peak in TF_{within} is affected by a pseudo-resonance. Figure 2.6 plots the f_1 Ratio vs. the IC depth normalized by the base sensor depth for IC values of 2 through 10. For each IC, the f_1 Ratio increases as the relative IC depth decreases, and for each IC depth, the f_1 Ratio increases as the IC decreases. Thus, a large IC (~10) at a shallow depth will be less affected by pseudo-resonances than a smaller IC (~3) at the same depth.

2.4.2 Approaches to Identify Pseudo-Resonances and True-Resonances

Figure 2.6 helps elucidate the *Vs* profile characteristics that lead to pseudo-resonances in the within transfer function, but the results shown are based on simple, 2-layer *Vs* profiles where it is easy to identify an IC. Real *Vs* profiles are rarely that simple and it can be challenging to identify the dominant IC that influences the presence of pseudo-resonances. Therefore alternative approaches are needed to identify pseudo-resonances and true-resonances that are present in a within transfer function.

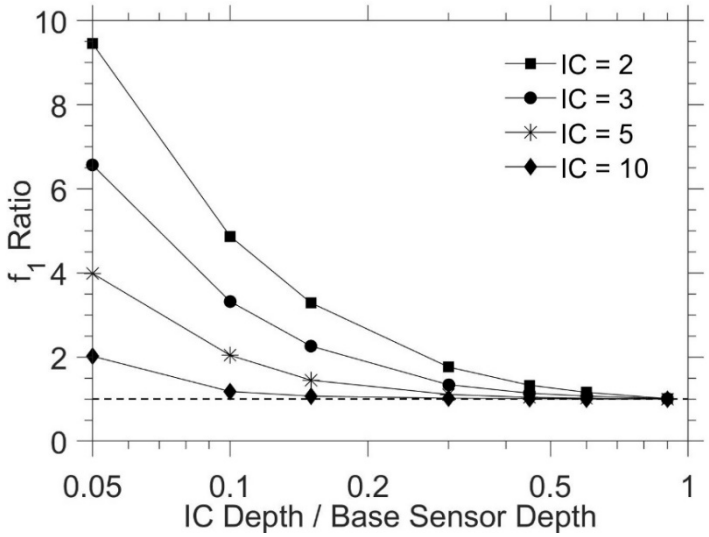

Figure 2.6 First mode frequency ratio (f_1 Ratio = $f_{1,outcrop}/f_{1,within}$) vs. impedance contrast (IC) depth relative to the base sensor for different values of IC.

Comparing TF_{within} with $TF_{outcrop}$ plays an important role in distinguishing true-resonances and pseudo-resonances, as shown in Figure 2.5. If the frequency of a peak in TF_{within} aligns with a peak in $TF_{outcrop}$, then the peak is a true resonance. If the peak does not align with a peak in $TF_{outcrop}$, then it is a pseudo-resonance. Another approach to identify a true resonant frequency involves the horizontal to vertical spectral ratio (*HVSR*), which is attractive in this case because its measurement is completely independent of the theoretical *TF* calculation based on the measured *Vs* profile. The *HVSR* is defined as the ratio of the horizontal to vertical Fourier Amplitude Spectra of a recording at the ground surface. Using ambient noise or small earthquake recordings, it has been shown that *HVSR* can successfully identify the fundamental resonant frequency of a soil deposit (e.g., Lermo and Chávez-García, 1994; Seekins *et al.*, 1996; Bard *et al*., 1997; Haghshenas *et al*., 2008), particularly for sites with a strong impedance contrast (Rodriguez and Midorikawa, 2002; Bard *et al*., 2005). Guidelines of implementing the *HVSR* technique have been developed by Bard *et al*. (2005).

To demonstrate the use of *HVSR* for the hypothetical *Vs* profiles used to generate Figure 2.5, theoretical *HVSR* are computed using the HV-INV program by Piña-Flores *et al.* (2014) and García-Jerez *et al*. (2016). This program computes the *HVSR* for a given site using diffuse wavefield theory (Sánchez-Sesma e*t al.*, 2011) given the *Vs* profile, the compression wave velocity (V_p) profile, and the density profile. For the *Vs* profiles used in Figure 2.5, the V_p profile was generated using a Poisson's ratio of 0.33 and the density was taken as 1800 kg/m^3. The resulting theoretical *HVSR* are shown along with the TF_{within} and $TF_{outcrop}$ in Figure 2.7. The peak in the theoretical *HVSR* for each site corresponds with the first mode site frequency in the outcrop transfer function, confirming that the peak in $TF_{outcrop}$ is a true resonance and any lower frequency peaks present in

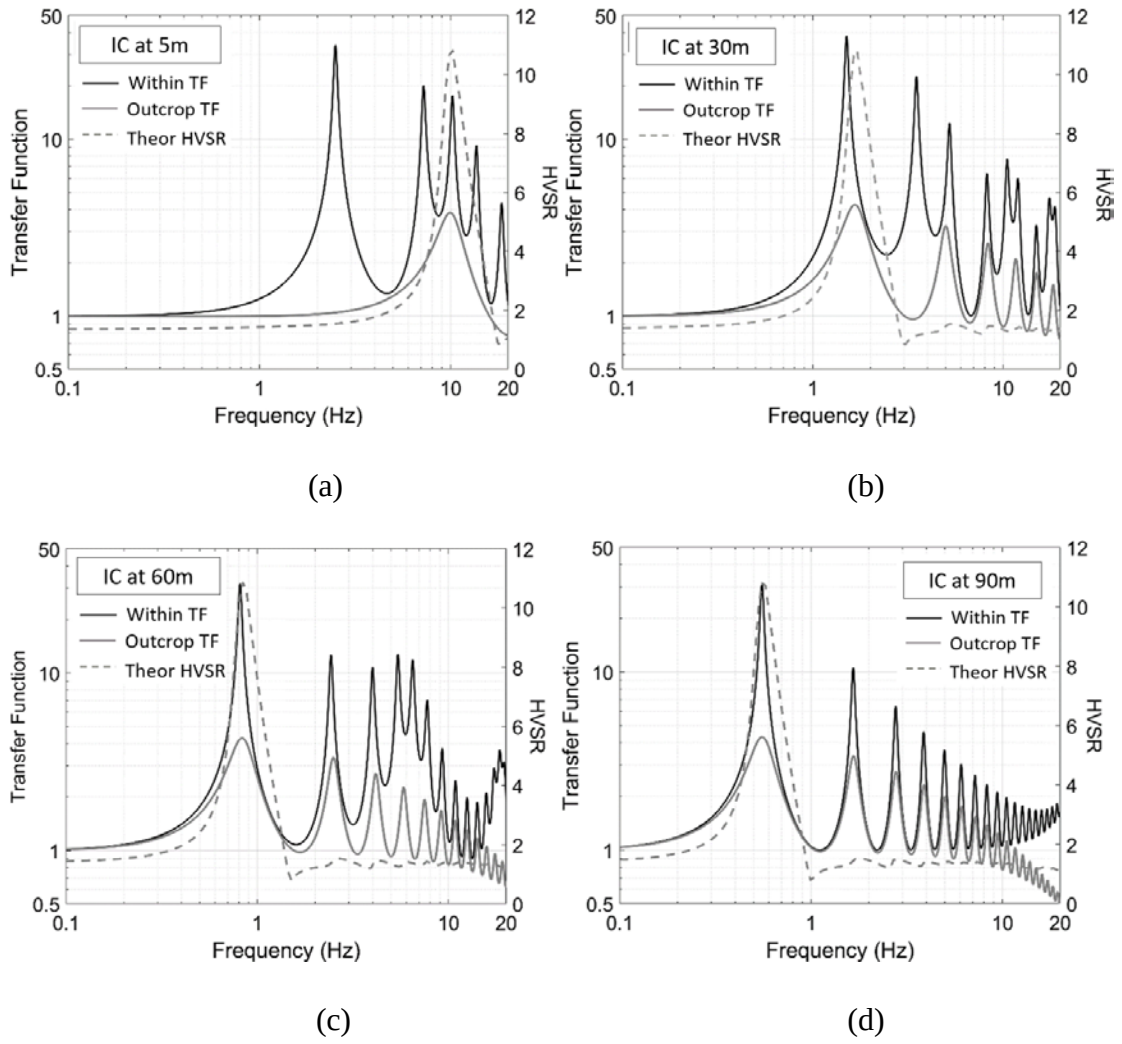

Figure 2.7 Theoretical H/V Spectral Ratio (*HVSR*) plotted together with outcrop and within TFs to identify the frequencies associated with true-resonance. Results shown for the same profiles as Figure 5 with the IC located at depths of (a) 5 m, (b) 30 m, (c) 60 m, and (d) 90 m.

TF_{within} are pseudo-resonances. This is most clearly observed in the case with the IC at 5 m where a pseudo-resonance occurs at 2.5 Hz and the true-resonance occurs at 10 Hz. Generally, the theoretical *HVSR* only captures the first mode frequency, although empirical *HVSR* from field recording may be able to capture some higher modes. Nonetheless, the results in Figure 2.7 demonstrate that the *HVSR* can provide an independent check of the true resonances of a site, that can supplement observations of the peaks from the within and outcrop transfer functions.

2.5 Pseudo-Resonances and True-Resonances in Empirical Downhole Array Data

To demonstrate the approaches outlined above to distinguish pseudo-resonances from true resonances using TF_{within}, $TF_{outcrop}$, and *HVSR* for real sites, we consider four downhole arrays from the Kiban Kyoshin (KiK-net) strong-motion network in Japan (Aoi *et al*., 2004). These sites are HYGH10, FKSH14, KSRH05, and KOCH05. The theoretical, linear-elastic transfer functions (both within and outcrop) are computed for each site for the reported *Vs* profile and an assumed small-strain damping profile from Darendeli (2001) based on confining pressure. Low-intensity earthquake motions are used to compute the empirical *TF* for comparison with the theoretical *TF*. The small-strain response (i.e., maximum shear strain < 0.01% - 0.1%, Kaklamanos *et al*., 2015) is confirmed by computing the induced maximum shear strain (γ_{max}) from linear elastic 1D site response analysis and ensuring that the γ_{max} profile consistently stays below 0.01%. Additionally, the empirical H/V spectra ratio (*HVSR*) is computed from the surface recordings at each site and the theoretical *HVSR* is computed from the Vs, V_P, and density profiles. The empirical and theoretical *HVSR* are compared with the empirical *TF* to confirm the identification of the true-resonances of each site.

Figure 2.8 displays the transfer functions and *Vs* profiles for the four sites, while Figure 2.9 displays the *HVSR*. Consider first HYGH10, a site in which TF_{within} and $TF_{outcrop}$ have peaks at similar frequencies and these peaks coincide with the peaks in the empirical *TF* (Figure 2.8a). This alignment indicates all peaks are true resonances, and the first mode frequency at about 1.4 Hz is further confirmed by the peaks at similar frequencies in the empirical and theoretical *HVSR* (Figure 2.9a). Based on these observations, the empirical *TF* for HYGH10 is dominated by true-resonances. The absence of any pseudo-resonances at this site is due to the fact that an impedance

contrast is found in the *Vs* profile at a depth of about 80 m, which is close to the base sensor depth of 100 m.

For site FKSH14, the lowest frequency peaks in TF_{within} and $TF_{outcrop}$ occur at similar frequencies (~ 1.2 to 1.3 Hz), but there are some differences in the higher mode peaks (Figure 2.8b). For example, TF_{within} displays peaks at 3.0 Hz and 4.2 Hz, but $TF_{outcrop}$ only displays one peak at about 3.9 Hz. These differences between TF_{within} and $TF_{outcrop}$ are similar to those shown in Figure 2.5b for a theoretical site with an IC at 30 m depth (i.e., ~30% of the base sensor depth), and in fact FKSH14 has an IC at a depth approximately 35% of the base sensor depth. The empirical *HVSR* for FKSH14 (Figure 2.9b) indicates a first mode frequency of about 1.0 to 1.2 Hz, in general agreement with the empirical *TF*. Based on these observations, the empirical *TF* for FKSH14 is dominated by true-resonances but is slightly affected by a pseudo-resonance at around 3 Hz.

Site KSRH05 displays a distinctly different empirical *TF*, with very small amplitude peaks at frequencies less than 6 Hz, and a large amplitude peak at a frequency of 9.8 Hz (Figure 2.8c). TF_{within} displays very strong peaks that align with the small amplitude peaks in the empirical *TF*, but $TF_{outcrop}$ displays an almost flat response at frequencies less than 6 Hz. Both TF_{within} and $TF_{outcrop}$ show an increase in amplitudes around 10 Hz, but only $TF_{outcrop}$ displays its largest peak at around 10 Hz. These differences in TF_{within} and $TF_{outcrop}$ are similar to those shown in Figure 2.5a for a hypothetical site with a shallow IC at 5% of the base sensor depth, and KSRH05 has a very shallow IC at 1.2% of the base sensor depth. The empirical and theoretical *HVSR* (Figure 2.9c) confirm that the first mode frequency of the site is close to 9-10 Hz. Thus, the assessment for

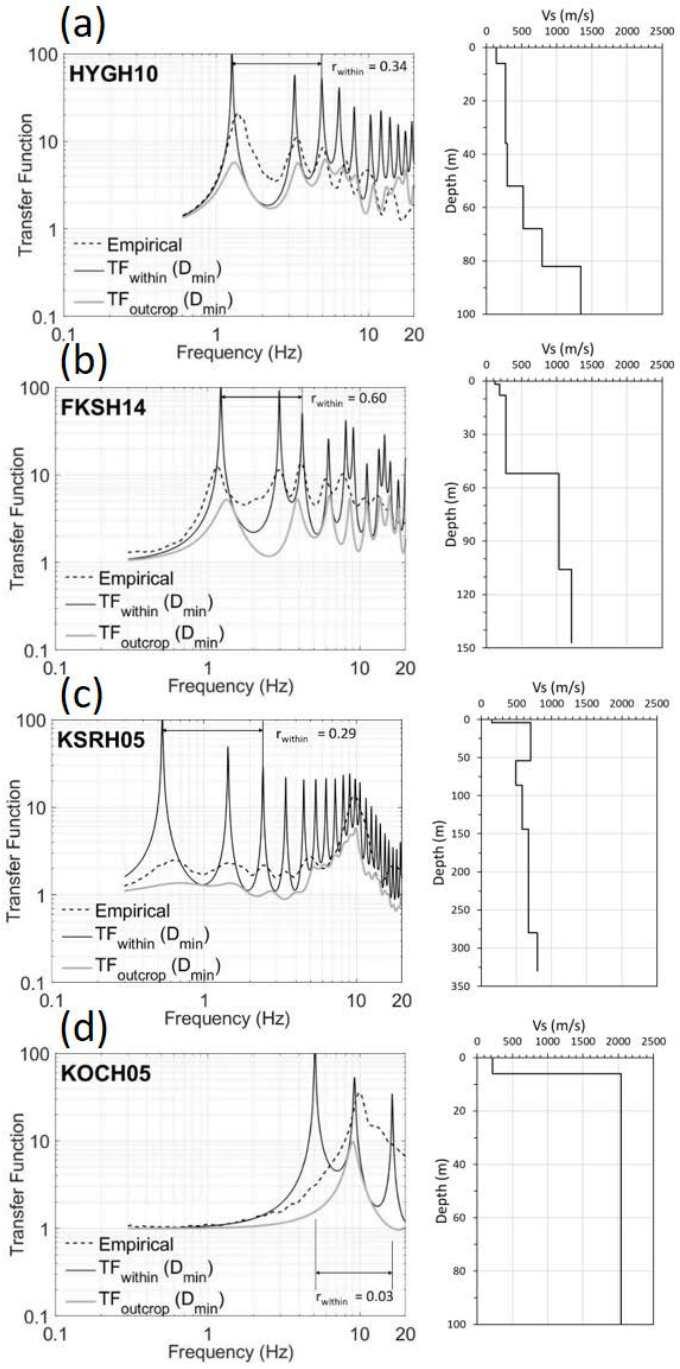

Figure 2.8. Empirical and theoretical transfer functions, along with measured *Vs* profiles, for four Kik-net downhole array sites.

KSRH05 is that the true-resonance at the site is at 10 Hz, and all lower frequency peaks in the empirical *TF* and TF_{within} represent pseudo-resonances.

Finally, site KOCH05 (Figure 2.9d) displays an empirical *TF* with a single, large amplitude

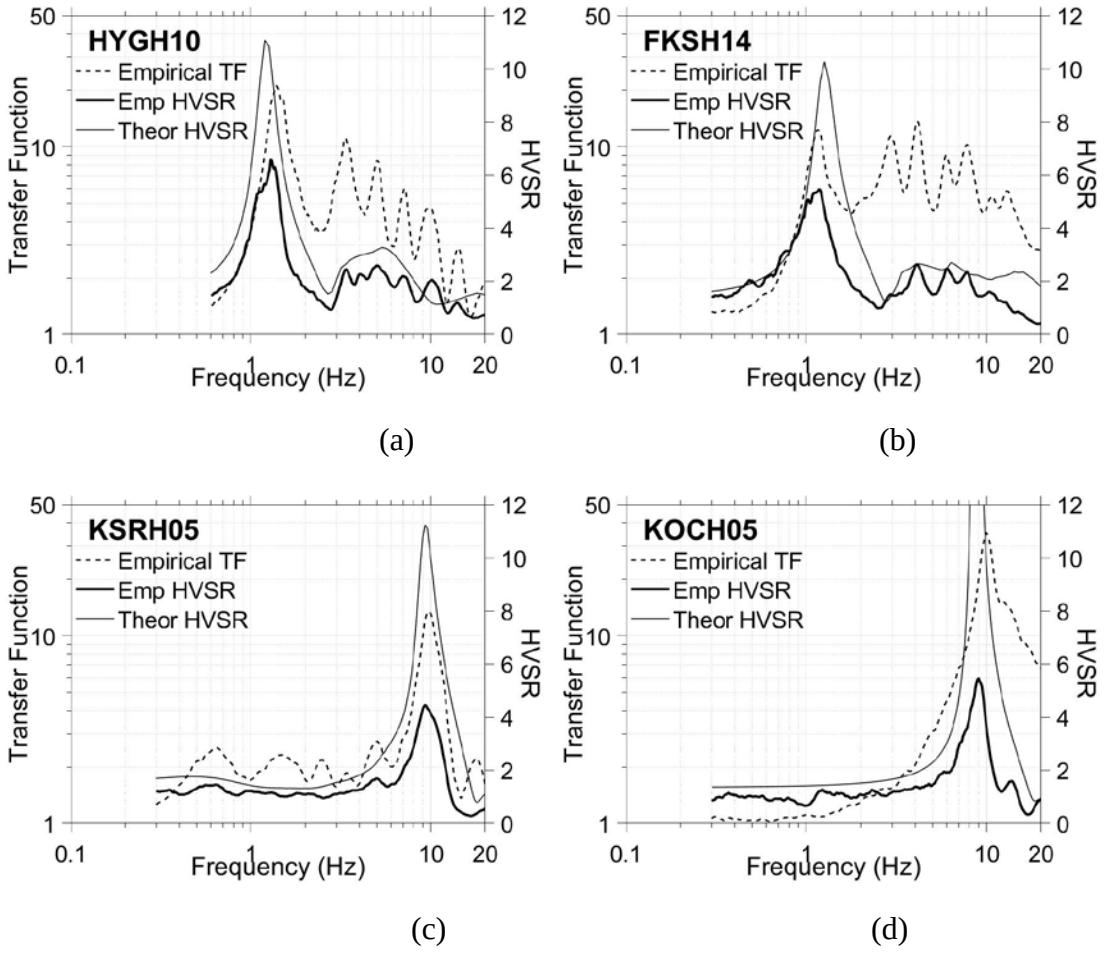

Figure 2.9 Theoretical and empirical *HVSR*, along with empirical transfer functions (*TF*), for the four KiK-net sites shown in Figure 2.8.

peak at about 10 Hz. TF_{within} displays peaks at 5 Hz, 9 Hz, and 16 Hz, while $TF_{outcrop}$ only shows a peak at about 9 Hz. This site has a shallow impedance contrast at about 6% of the base sensor depth, and thus is very similar to the hypothetical site from Figure 2.5a. Similar to KSRH05, the

empirical and theoretical *HVSR* (Figure 2.9d) for KOCH05 confirm a first mode frequency for the site close to 9-10 Hz. All lower frequency peaks are considered pseudo-resonances for KOCH05.

Although sites KSRH05 and KOCH05 both have shallow impedance contrasts with true-resonances of about 9-10 Hz, their empirical *TF* differ somewhat at lower frequencies. For KSRH05 the empirical *TF* displays very weak peaks at the pseudo-resonances, but for KOCH05 the empirical *TF* displays no peaks associated with the pseudo-resonances. This difference may be caused by differences in the characteristics of the material below the impedance contrast. For KSRH05 the average shear wave velocity is about 600 m/s below the impedance contrast, while for KOCH05 it is about 2000 m/s. The larger *Vs* below the IC for KOCH05 may result in the down-going wave being trapped in the low velocity surface layer, avoiding any destructive interference with the up-going wave and resulting in no pseudo-resonances in the empirical *TF*. It appears that this effect is less pronounced when the *Vs* below the IC is smaller.

It is important to note that most studies that have used downhole array data to evaluate the accuracy of one-dimensional site response analysis (e.g., Thompson *et al.*, 2012; Zalachoris and Rathje, 2015) have used the within boundary condition for their simulations, because this is the proper boundary condition from a theoretical perspective. However, as discussed above, for some sites the response predicted using the within boundary condition is dominated by pseudo-resonances, which may not be representative of the true site response that is of main interest in a forward analysis.

Because of the complexities associated with the specification of the boundary conditions for analyses of downhole arrays, quantitative measures of the goodness-of-fit between empirical and theoretical *TF* may not always accurately assess the ability of 1D site response to match the

empirical *TF* from a downhole array. For example, a Pearson correlation coefficient, *r*, greater than 0.6 was used by Thompson *et al*. (2012) as the threshold to represent a good alignment of the peaks in the empirical *TF* and the theoretical TF_{within}. The values of *r* are computed between the first and third peaks in TF_{within} (r_{within}) for the four example sites in Figure 2.8. Interestingly, only site FKSH14 meets the Thompson *et al*. (2012) criteria of 0.6. Although qualitatively HYGH10 displays a good match between the empirical *TF* and TF_{within}, its r_{within} value is only 0.34. This small value does not accurately reflect the match in Figure 2.8a, illustrating an issue with using only quantitative measures to compare empirical and theoretical *TF*. Sites KSRH05 and KOCH05 are both dominated by pseudo-resonances at frequencies less than about 5 Hz, and thus their r_{within} values are significantly smaller than 0.6. Nonetheless, it is clear that $TF_{outcrop}$, which would be used in a forward analysis, would accurately capture the true-resonances at higher frequencies for these sites.

These examples demonstrate the problems with only considering the within *TF* for down-hole array analyses and using quantitative measures of the goodness-of-fit between empirical and theoretical *TF*. As a result, when evaluating site response methods using downhole array data, we advocate that the within *TF*, the outcrop *TF*, and the empirical *HVSR* spectra be examined together to identify the true-resonances at a site, and that the fit of a theoretical *TF* to an empirical *TF* be assessed, qualitatively, over the frequency range associated with the true-resonances.

2.6 CONCLUSIONS

Downhole arrays have gained popularity within the research community to investigate the accuracy of one-dimensional site response analysis. However, the presence of the down-going

wave in the recorded downhole wavefield introduces a complexity in modeling site response that can influence the assessment of the accuracy of 1D site response analysis.

The destructive interference between the up-going and down-going waves results in diminished wave amplitudes at the downhole sensor at frequencies related to the two-way travel time between the downhole and surface sensors. These diminished wave amplitudes can either increase the amplitude of the transfer function at the site's true resonant frequencies or they can generate pseudo-resonances that are associated only with the depth of the base sensor. These pseudo-resonances do not reflect the true resonant frequencies of amplification that would be predicted in a forward site response analysis using an outcrop boundary condition. Pseudo-resonances occur for downhole array sites with little to no impedance contrast or for sites with an impedance contrast that is closer to the surface.

The within boundary condition for site response analysis incorporates the effects of the down-going wave and is used to analyze downhole array data. However, most site response analyses performed in engineering practice utilize the outcrop boundary condition because a downhole sensor is not available. Thus, when using downhole array data to assess the accuracy of 1D site response analysis it is important to focus on the true-resonances of the site that would be modeled by the outcrop *TF*. To distinguish true-resonances from pseudo-resonances, it is recommended to consider the within *TF*, the outcrop *TF*, and the empirical *HVSR* spectra. All peaks in the outcrop *TF* are true-resonances, while peaks that are present in the within *TF* but not present in the outcrop *TF* are considered pseudo-resonances. The peaks in the empirical *HVSR* spectra represent true resonances and these peaks should align with the true-resonances present in the within and outcrop *TF*. After identifying the true-resonances for a site, the comparison of the empirical and theoretical

TF for a downhole array site should be focused over the frequencies associated with the true-resonances.

2.7 Data and Resources

Downhole array data (seismograms and boring log data) used in this study were obtained from the KiK-net strong motion network (http://www.kyoshin.bosai.go.jp/, last accessed July, 2018).

2.8 Acknowledgements

This study was supported by the U.S. Nuclear Regulatory Commission (NRC) under grant NRC-HQ-60-15-C-0005. This support is gratefully acknowledged.

2.9 Refences

Abercrombie, R. E. (1997). Near-surface attenuation and site effects from comparison of surface and deep borehole recordings. *Bull. Seism. Soc. Am*, *87*(3), 731-744.

Aoi, S., Kunugi, T., and Fujiwara, H., (2004). Strong-Motion Seismograph Network Operated by NIED: K-NET and KiK-net, *Journal of Japan Association for Earthquake Engineering*. 4 (3), 65-74.

Bard P-Y, Duval AM, Lebrun B, Lachet C, Riepl J, Hatzfeld D. (1997). Reliability of the H/V technique for site effect measurement: an experimental assessment. *Proc.,17th International conference on soil dynamics and earthquake engineering,* Istanbul, 19–24 July 1997

Bard, P. Y., SESAME-Team, (2005). Guidelines for the implementation of the H/V spectral ratio technique on ambient vibrations measurements, processing and interpretation. *SESAME European Research Project EVG1-CT-2000-00026*.

Bonilla, L. F., Steidl, J. H., Gariel, J. C., & Archuleta, R. J. (2002). Borehole response studies at the Garner Valley downhole array, southern California. *Bull. Seism. Soc. Am*, *92*(8), 3165-3179.

Bonilla, L. F., Steidl, J. H., Lindley, G. T., Tumarkin, A. G., & Archuleta, R. J. (1997). Site amplification in the San Fernando Valley, California: variability of site-effect estimation using the S-wave, coda, and H/V methods. *Bull. Seism. Soc. Am*, *87*(3), 710-730.

Borcherdt, R. D. (1970). Effects of local geology on ground motion near San Francisco Bay. *Bull. Seism. Soc. Am*, *60*(1), 29-61.

Bradley, B. A., and Cubrinovski, M. (2011). Near-source strong ground motions observed in the 22 February 2011 Christchurch earthquake. *Seismol Res Lett*, *82*(6), 853-865.

Cadet, H., Bard, P. Y., & Rodriguez-Marek, A. (2010). Defining a Standard Rock Site: Propositions Based on the KiK-net Database Defining a Standard Rock Site: Propositions Based on the KiK-net Database. *Bull. Seism. Soc. Am*, *100*(1), 172-195.

Darendeli, M. B. (2001). Development of a new family of normalized modulus reduction and material damping curves. *Ph.D. Dissertation, University of Texas at Austin*, 296-298.

García-Jerez, A., Piña-Flores, J., Sánchez-Sesma, F. J., Luzón, F., & Perton, M. (2016). A computer code for forward calculation and inversion of the H/V spectral ratio under the diffuse field assumption. *Computers & Geosciences*, 97, 67-78.

Haghshenas, E., Bard, P. Y., Theodulidis, N., and SESAME WP04 Team. (2008). Empirical evaluation of microtremor H/V spectral ratio. *Bulletin of Earthquake Engineering*, 6(1), 75-108.

Idriss, I. M. (1990). Response of soft soil sites during earthquakes. In *Proc. HB Seed Memorial Symp.* (Vol. 2, pp. 273-289).

Kaklamanos, J., Baise, L. G., Thompson, E. M., and Dorfmann, L. (2015). Comparison of 1D linear, equivalent-linear, and nonlinear site response models at six KiK-net validation sites. *Soil Dynam Earthquake Eng*, 69, 207-219.

Kramer, S. L. (1996). *Geotechnical Earthquake Engineering*, Prentice-Hall, New Jersey, pp. 255

Lermo, J., and Chávez-García, F. J. (1994). "Are microtremors useful in site response evaluation?" *Bull. Seism. Soc. Am*, 84(5), 1350-1364.

Malagnini, L., Mayeda, K., Akinci, A., & Bragato, P. L. (2004). Estimating absolute site effects. *Bull. Seism. Soc. Am*, *94*(4), 1343-1352.

Mehta, K., Snieder, R., & Graizer, V. (2007). Extraction of near-surface properties for a lossy layered medium using the propagator matrix. *Geophysical Journal International*, *169*(1), 271-280.

Oth, A., Parolai, S., & Bindi, D. (2011). Spectral analysis of K-NET and KiK-net data in Japan, Part I: Database compilation and peculiarities. *Bull. Seism. Soc. Am*, *101*(2), 652-666.

Parolai, S., Ansal, A., Kurtulus, A., Strollo, A., Wang, R., & Zschau, J. (2009). The Ataköy vertical array (Turkey): insights into seismic wave propagation in the shallow-most crustal layers by waveform deconvolution. *Geophysical Journal International*, *178*(3), 1649-1662.

Piña-Flores, J., García-Jerez, A., Luzón, F., Perton, M., and Sánchez-Sesma, F. J. (2014). "Inversion of H/V ratio in layered systems." *American Geophysical Union, Fall Meeting 2014*, San Francisco, CA, abstract id. S12A-07.

Rodriguez, V. H., and Midorikawa, S. (2002). Applicability of the H/V spectral ratio of microtremors in assessing site effects on seismic motion. *Earthquake Engineering and Structural Dynamics*, 31(2), 261-279.

Rollins, K. M., Hryciw, R. D., Shewbridge, S. E., McHood, M. D., & Homolka, M. (1994). Ground response on Treasure Island in The Loma Prieta, California, Earthquake of October 17, 1989 – Strong Ground Motion R. D. Borcherdt (Editor). *US Geol. Surv. Prof. Pap, 1551-A*.

Sánchez-Sesma, Francisco J., Miguel Rodríguez, Ursula Iturrarán-Viveros, Francisco Luzón, Michel Campillo, Ludovic Margerin, Antonio García-Jerez, Martha Suarez, Miguel A. Santoyo, and Alejandro Rodríguez-Castellanos. (2011). A theory for microtremor H/V spectral ratio: application for a layered medium. *Geophysical Journal International* 186, no. 1 (2011): 221-225.

Seekins, L. C., Wennerberg, L., Margheriti, L., and Liu, H. P. (1996). Site amplification at five locations in San Francisco, California: A comparison of S waves, codas, and microtremors. *Bull. Seism. Soc. Am*, 86(3), 627-635.

Shearer, P. M., & Orcutt, J. A. (1987). Surface and near-surface effects on seismic waves—theory and borehole seismometer results. *Bull. Seism. Soc. Am*, *77*(4), 1168-1196.

Steidl, J. H., Tumarkin A.G., and Archuleta R.J. (1996) What is a reference site? *Bull. Seism. Soc. Am*, 86.6: 1733-1748.

Tao, Y., Rathje, E. M. (2019). Insights into Modeling Small-Strain Site Response Derived from Downhole Array Data. *Journal of Geotechnical and Geoenvironmental Engineering*. (second-round review).

Thompson, E., L. Baise, R. Kayen, and B. Guzina. (2009). Impediments to Predicting Site Response: Seismic Property Estimation and Modeling Simplifications. *Bull. Seism. Soc. Am*, 99(5), 2927-2949

Thompson, E., L. Baise, Y. Tanaka, and R. Kayen. (2012). A Taxonomy of Site Response Complexity. *Soil Dynam Earthquake Eng*, 41, 32-43

Yu, J., and Haines, J. (2003). The choice of reference sites for seismic ground amplification analyses: Case study at Parkway, New Zealand. *Bull. Seism. Soc. Am*, *93*(2), 713-723.

Chapter 3: Insights into Modeling Small-Strain Site Response Derived from Downhole Array Data

Yumeng Tao[3], M. ASCE, and Ellen Rathje[4], F. ASCE[5]

ABSTRACT

The small strain damping ratio (D_{min}) is a key parameter in site response models and using values from laboratory tests tends to over-predict the site response because laboratory tests cannot capture the wave scattering effects that are present in the field. In this study, earthquake motions from four downhole array sites are used to investigate the increase in D_{min}, as quantified by the D_{min} multiplier applied to the laboratory based D_{min}, required to match the site response. Empirical observations from the downhole array data are compared with theoretical results from linear-viscoelastic, one-dimensional site response analysis. Different measures of ground response are considered when evaluating the site response: the acceleration transfer function (TF), the spectral acceleration amplification factor (AF), the surface motion PGA, PGV, and Arias Intensity (Ia), and the change in the high frequency spectral decay parameter ($\Delta\kappa$) between the downhole and surface sensors. We recommend that the D_{min} multiplier for a site be selected to best match the Ia rather than the TF. Across the four sites, the required D_{min} multiplier varies from 1.5 to 5.5. It is hypothesized that the magnitude of the D_{min} multiplier may be related to the geologic depositional environment of the site, with larger D_{min} multipliers associated with more spatially variable geologic

---

[3]Graduate Research Assistant, Department of Civil, Architectural, and Environmental Engineering, University of Texas, Austin, TX 78712

[4] Janet S. Cockrell Centennial Chair in Engineering, Department of Civil, Architectural, and Environmental Engineering, University of Texas, Austin, TX 78712

[5] This chapter was accepted as a journal paper *by Journal of Geotechnical and Geoenvironmental Engineering* and expected to be published in 2019. Both authors contributed equally to the paper.

conditions. These conditions have more variation in shear wave velocity across a site that leads to more wave scattering and larger D_{min} multipliers.

Keywords: Site Response, damping, wave scattering

3.1 INTRODUCTION

Site response analysis involves the propagation of seismic waves through the near-surface geo-materials, generally from a layer of competent rock through the overlying soil materials, with the goal of predicting site amplification and earthquake shaking at the ground surface. Site response analysis is one of the most commonly performed types of analysis in geotechnical earthquake engineering because proper evaluation of ground response is crucial to many aspects of earthquake engineering.

Most site response analyses incorporate a one-dimensional (1D) model of the subsurface, which assumes that all soil and rock layers extend infinitely in the horizontal direction and that the soil response is predominantly controlled by vertically propagating, horizontally polarized shear waves (SH1D assumption; Kramer 1996). 1D site response analysis often is performed in the frequency domain, where the shear wave velocity (*Vs*) and damping ratio (D) profiles are used to compute the acceleration transfer function for the site (Figure 3.1). The transfer function is derived from the closed form solution to the 1D wave equation for linear viscoelastic material response. Soil nonlinearity can be taken into account through equivalent-linear (EQL) analysis, an iterative procedure that assigns linear elastic properties to each layer based on the induced strains in the layer and the assigned shear modulus reduction curve (G/G_{max}) and material damping ratio (D) curve for the layer. Alternatively, fully nonlinear site response analysis can be performed, which directly models the nonlinear stress-strain response of the soil. However, if the induced shear

strains are small (i.e., peak shear strain less than about 0.01% or corresponding PGA less than 0.1 to 0.3 g, Kaklamanos *et al*., 2015), linear-elastic analysis is appropriate and only the *Vs* profile and small-strain damping ratio (D_{min}) profile are needed to perform an analysis.

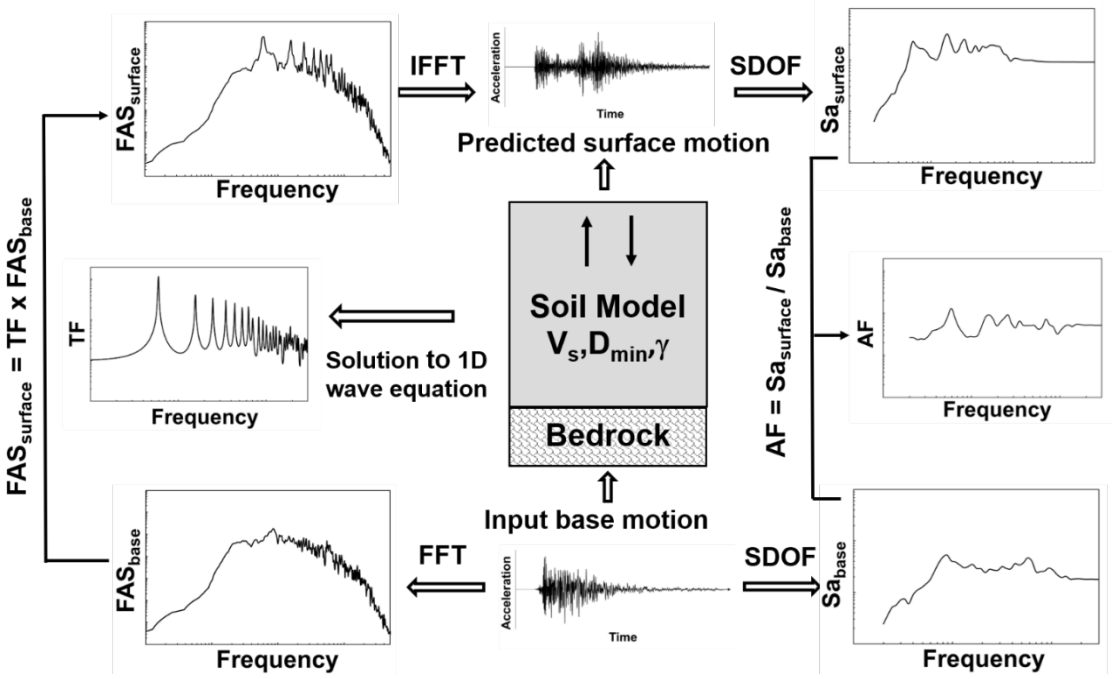

Figure 3.1: Elements of linear elastic site response analysis.

Previous studies have shown that the effectiveness of 1D site response analysis is affected by several factors: the applicability of the SH1D assumption to the site (e.g., Zalachoris and Rathje, 2015; Thompson *et al.*, 2009) and the accuracy of the characterization of the properties of site (i.e., *Vs* and damping ratio profile). For sites where the SH1D assumption is applicable, which is usually indicated by good agreement between the resonant peak frequencies from empirical and theoretical ground responses, the key is then to properly evaluate the damping ratio profile such that the amplitudes of the responses match. The damping ratio profile commonly is specified based on laboratory measurements; however, laboratory measurements only capture material damping and

cannot capture other energy dissipation mechanisms encountered in the field (i.e., wave scattering). While the energy of propagating seismic waves is conserved, the attenuation can be perceived as the redistribution of seismic energy (Stein and Wysession, 2003). Seismic wave scattering is thus essentially a modification of the propagating seismic waves due to soil heterogeneities (Thompson *et al*., 2009).

Observations of seismic site response from downhole arrays provide valuable information regarding the appropriate level of small-strain damping, and this information can be used to supplement laboratory characterization. A variety of downhole studies have recommended that the damping ratio profile derived from laboratory tests be increased to account for wave scattering effects that cannot be captured by laboratory test. Some studies recommended D_{min} values between 3 and 5% should be used (e.g., Tsai and Hashash, 2009; Elgamal *et al*., 2001), while others recommend that 1% to 4% be added to laboratory-based D_{min} profiles (Yee *et al*., 2013) or that the laboratory-based D_{min} profiles be increased by a factor between 2 and 5 (Zalachoris and Rathje, 2015). Based on a review of the literature, Stewart *et al.* (2014) recommended that additional damping greater than the laboratory-measured D_{min} be considered as an epistemic uncertainty in site response analysis and a range of additional D_{min} from 0% and 5% to be added to the laboratory-based D_{min} profile.

Another approach to model the effects of wave scattering in 1D site response analysis is through the randomization of shear wave velocity profiles within a Monte Carlo simulation of the 1D response. This approach averages the 1D ground response for a large number of statistically generated shear wave velocity profiles. Although each 1D analysis assumes laterally homogeneous soil layers, the combined response of multiple *Vs* realizations accounts for the additional attenuation from the wave scattering generated by spatial variability in *Vs* (e.g., Nour *et al*., 2003). There

are various approaches to generate the *Vs* realizations, but most studies use the statistical models developed by Toro *et al.* (1992) and Toro (1995). These models use a baseline *Vs* profile from field measurements, along with estimates of the standard deviation of ln*Vs* (σ_{lnVs}) and the inter-layer correlation coefficient, to generate the *Vs* profiles. More recently, researchers have proposed using the multiple *Vs* profiles generated from geophysical surface wave characterizations in lieu of statistical *Vs* profiles (Griffiths *et al.*, 2016).

The goal of this study is to investigate the ability of 1D site response analysis to accurately predict ground response and the effects of wave scattering. Low-intensity recordings (i.e., peak ground accelerations < 0.1g) from four, well-characterized downhole arrays are used: Garner Valley (GV) in California, EuroSeisTest (EST) in Greece, Treasure Island (TI) in California, and Delaney Park (DP) in Alaska. The ability of 1D site response analysis to capture the observed ground response is assessed using various measures of ground shaking. Two approaches are considered to capture the effects of wave scattering: (1) increasing the level of small-strain damping within the subsurface layers and (2) statistically varying the shear wave velocity profiles within a Monte Carlo simulation. The increased level of damping and the level of *Vs* variability (σ_{lnVs}) required to match the recorded responses for each of the downhole array site is compared among the different measures of ground shaking and the different sites, and the results are interpreted within the context of the local geology.

3.2 Assessment of Site Response

This study considers various measures of the ground response to evaluate the ability of 1D analysis to accurately capture the observed site response at downhole arrays. Specifically, we consider transfer functions (TF), response spectral amplification factors (AF), H/V spectral ratios

(HVSR), amplification of various ground motion parameters computed in the time domain (i.e., peak ground acceleration, peak ground velocity, Arias intensity), and the high frequency spectral decay parameter (κ_o). These different approaches are described below.

Given the soil properties (*Vs* and D_{min} profiles) at a site, the theoretical TF for the ground response is derived from solving the 1D wave equation (Figure 3.1). The theoretical TF is expressed as the Fourier Amplitude Spectrum (FAS) of the surface motion divided by the FAS of the input motion. The theoretical amplification factor (AF) is defined as the computed surface pseudo-acceleration response spectrum (Sa) divided by the Sa of the input motion. To compute the theoretical AF, the site response analysis is performed using the theoretical TF to compute the surface acceleration-time history and the theoretical AF is computed from the response spectra of the computed surface motion and recorded input motion (Figure 3.1).

Although the theoretical TF and AF display peaks at the same frequencies, it is important to note the differences in their shapes (Figure 3.1). Each frequency in a transfer function is independent, and therefore, the transfer function is characterized by sharp, narrow peaks. Amplification factors exhibit much broader peaks because they are computed from response spectra, which represent the responses of single-degree-of-freedom (SDOF) oscillators of different natural frequencies subjected to an earthquake motion. Because the response of a SDOF oscillator is influenced by a range of frequencies, the theoretical AF peaks are not as sharp or narrow as the theoretical TF (Bora *et al*., 2016).

An important issue when analyzing downhole array data is the appropriate boundary conditions at the borehole sensor. Generally, the wavefield at any point in the soil deposit consists of an up-going (incident) and a down-going (reflected) seismic wave. The standard practice when analyzing downhole array data is to assume that the effects of both waves are present at the

borehole sensor (e.g., Zalachoris and Rathje, 2015; Bonilla *et al.*, 2002), which is commonly referred to as the "within" boundary condition, although others have investigated alternative boundary conditions (e.g., up-going only, Thompson *et al.*, 2009 or outcrop, Bonilla *et al.*, 2002). The assumed boundary condition can significantly affect the peak amplitudes of the theoretical TF and the resulting theoretical AF. The "within" boundary condition is used in this study.

To assess the accuracy of 1D analysis, the theoretical TF and AF are compared with empirical transfer functions and amplification factors that are computed directly from the recorded motions at the surface and borehole sensors. For the empirical TF, the FAS of the two motions are computed and the ratio is obtained at each frequency. For the empirical AF, the response spectra of the two motions are computed and the ratio is obtained at each frequency. Other ground motion parameters can be used to evaluate the 1D response, such as peak ground acceleration (PGA), peak ground velocity (PGV), or Arias Intensity (Ia). In these cases, the predicted surface time-history is obtained by propagating the base recording through the 1D soil model, the ground motion parameters are computed from the predicted surface motion, and these values are compared with those from the recorded surface motion. These ground motion parameters provide an alternative approach to assess the predicted ground response in terms of a broader range of frequencies, as PGA represents high frequencies, PGV represents intermediate frequencies, and Arias intensity accounts for the intensity, frequency content, and duration of a motion (Kramer, 1996).

The H/V spectral ratio (HVSR) technique is another method that can be used to investigate the accuracy of a site response model and is particularly useful when a downhole recording is not available. The HVSR, defined as the ratio between the horizontal and vertical components of the FAS at surface, was first introduced by Nogshi and Igarashi (1971), and further developed by Nakamura (1989, 2000). A large number of studies have shown that the H/V technique can

successfully identify the fundamental resonant frequency of a soil deposit (e.g., Lermo and Chávez-García, 1994; Seekins *et al.*, 1996; Bard *et al*., 1997; Haghshenas *et al*., 2008). The application of HVSR has been particularly successful for sites where there is strong impedance contrast (Rodriguez and Midorikawa, 2002; Bard *et al*., 2005). Guidelines of implementing the HVSR technique have been developed by Bard *et al*. (2005).

Finally, the site-specific high frequency spectral decay parameter, κ_0, has been widely used in engineering seismology to model the high frequency FAS shape of earthquake motions. The parameter κ_0 can be related to the shear wave velocity and damping ratio profile at a site, and thus the change in κ_0 derived from the surface and downhole recordings can provide additional constraint on the small strain damping ratio profile for a site.

3.3 Description of Downhole Array Sites and Available Data

The four downhole array sites used in this study were selected to span a range of geographic and geologic conditions. Importantly, an initial evaluation of the recordings at these sites indicated that the empirical site response generally matched the 1D assumption in terms of the locations of the modal frequencies, as discussed later. For each site, the regional geology and subsurface soil conditions are described below, along with the characteristics of the downhole array and the available ground motions. Note that for each motion for each site, the induced shear strain profile was computed by site response analysis and used to confirm that the strains were less than 0.01% and therefore linear elastic analysis was appropriate.

3.3.1 Garner Valley Downhole Array

The Garner Valley Downhole Array (GV) site was installed in 1989 in a narrow valley within the Peninsular Range in southern California (Figure 3.2a). The valley is about 4 km at its

widest and 10 km long, and is surrounded by mountains that rise about 1700 m above the valley (Bonilla *et al.*, 2002) and consist of granite and Tertiary fanglomerates (Hill, 1981; Bedrossian *et al*., 2012). The valley is an ancient lake bed that consists of soft alluvial deposits underlain by rock. The upper 18–25 m of the site consists of soil types ranging from silty sand, sand, clayey sand and silty gravel, and there is a large layer of decomposed granite that extends from 25 to 87 m. At 87 m the contact with hard competent bedrock (i.e., granodiorite) is reached (Bonilla *et al*., 2002).

The strong motion sensors currently available at GV are located at depths of 0, 15, 22, 50, and 150 m. For this study, only the 0 m and 150 m sensors were used. Earthquake motions with PGA at the ground surface between 0.001g and 0.01 g were initially selected, and after applying a signal to noise ratio (SNR) > 3 criterion, 50 events (i.e., 100 horizontal motions) were finally used in the analyses.

3.3.2 EuroSeisTest Downhole Array

The EuroSeisTest (EST) permanent network was established in 1993 in the Mygdonian basin in northern Greece. The Mygdonian basin is a sediment-filled graben about 50 km long and 5.5 km wide with the center of the valley as deep as 200 m (Figure 3.2b). The valley is covered mainly by a lower unit of Neogene sediments consisting of conglomerates, sandstones, silt sands and red-beds, and an upper unit of Quaternary sediments consisting of sands, silts, and clays (Manakou *et al*., 2010).

The strong motion sensors currently available at TST are located at depths of 0, 18, 40, 73, 136 and 196 m. For this study, only the 0 m and 196 m sensors were used. Motions with larger PGA (i.e., 0.001 g to 0.05 g) were used at this site to obtain enough high-quality motions from the

196 m sensor. Applying a SNR > 3 criterion across a frequency range that extended down to 0.32 Hz (to capture the 0.7 Hz first mode frequency of the site), resulted in 7 events (i.e., 14 motions) available for analysis.

3.3.3 Treasure Island Downhole Array

The Treasure Island Downhole Array (TI) site was installed in 1993 on Treasure Island, located in San Francisco Bay, California (Baise *et al*., 2003). Treasure Island is a 400-acre man-made hydraulic fill island built on Yerba Buena shoal (Figure 3.2c), a sandbar immediately north-west of the rock outcrop on Yerba Buena Island in San Francisco Bay (Rollins *et al*., 1994), and underlain by San Francisco Bay Mud (Lee, 1969).

The subsurface near the TI downhole array site is horizontally stratified, as indicated by geological cross-sections at various locations near the site (Papadopulos and Eliahu, 2009). The top 15 m is the sandy hydraulic fill, which is underlain by a layer of compressible Young San Francisco Bay Mud about 15 m thick. The remaining part of the profile includes silty sand, Old San Francisco Bay Mud, and a transition zone of sands, gravels, and clay. The bedrock is located at approximately 91 m depth and consists of shale and sandstone of the Franciscan Formation (Gibbs, 1994).

The strong motion sensors currently available at TI are located at depths of 0, 7, 16, 31, 44 and 122 m. For this study, only the 0 m and 122 m sensors were used. The PGA range was extended from 0.001g to 0.1g to identify motions because the PGA of the majority of the surface recordings exceed 0.01g. After the SNR > 3 criterion was applied, 5 events (i.e., 10 motions) were available for analysis.

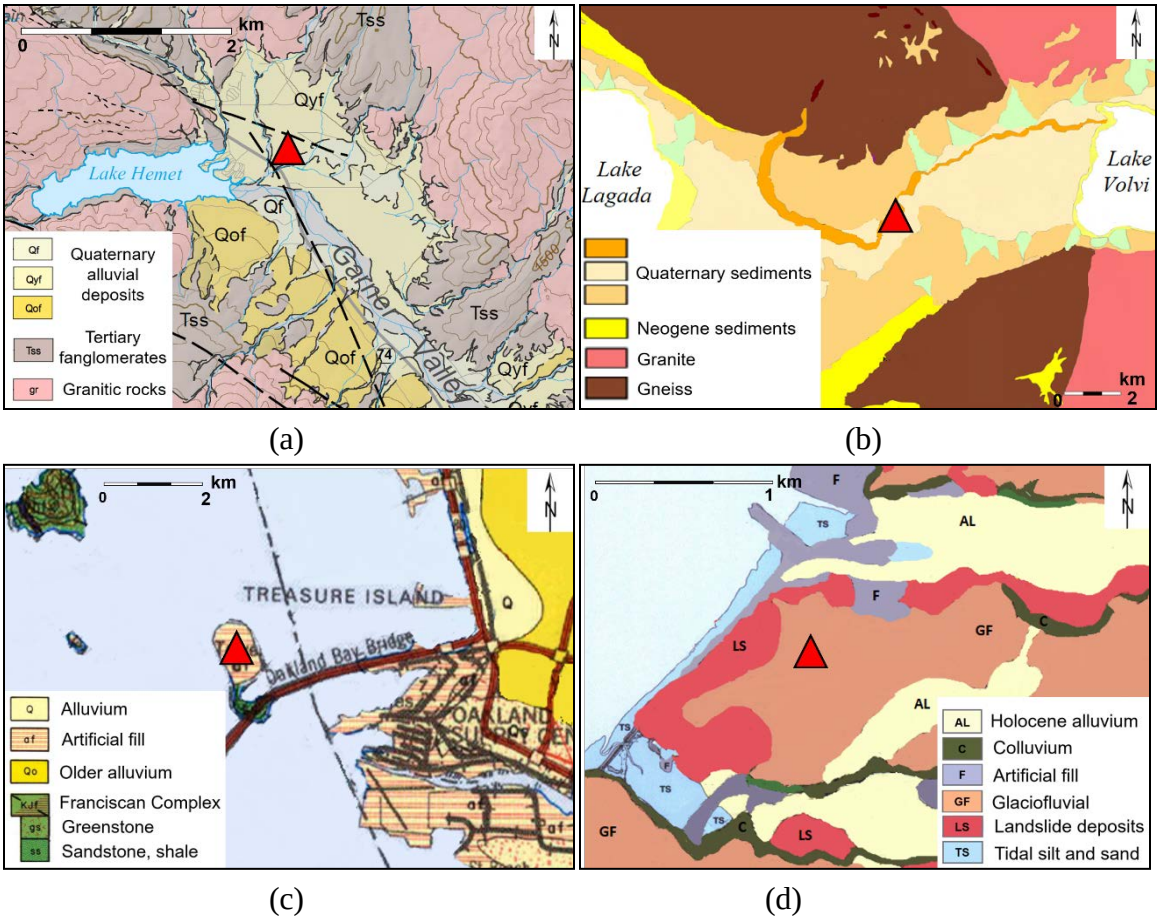

Figure 3.2: Modified regional geologic maps for downhole arrays analyzed (red triangle represents the location of downhole array): (a) Garner Valley (McCrea *et al*. 2012), (b) Euro-SeisTest (Manakou *et al*. 2010), (c) Treasure Island (Wagner *et al*. 1991), and (d) Delaney Park (Combellick 1999).

3.3.4 Delaney Park Downhole Array

The Delaney Park Downhole Array (DP) was deployed in 2004 in downtown Anchorage, Alaska. Downtown Anchorage is adjacent to the sea on a triangular lowland that extends west from the Chugach Mountains (Figure 3.2d). Lying above the bedrock are thick Tertiary sediments that in turn are overlain by Quaternary deposits of clay, silt, sand and gravel derived from the glacial advances in the Pleistocene (Badal *et al*., 2004).

The western part of downtown Anchorage is mainly underlain by the famous Bootlegger Cove Formation which constitutes an important part of the Quaternary deposits consisting of glacio-estuarine/lacustrine silt and clay (Updike *et al*., 1988). At the Delaney Park site, the first 18 m is glacial outwash, which is followed by about 30 m of Bootlegger Cove clay above glacial till. Three geological cross-sections near the site (Combellick, 1999) show similar soil layering but also indicates significant differences in layer thicknesses within small distances (i.e., ~ 300 m), especially in the north-south direction. Across this zone, the glacial outwash deposits vary from 10 to 15 m thick, the thickness of the Bootlegger Cove clay varies from 60 to 85 m, and the depth to the glacial till varies from 70 to 100 m.

The strong motion sensors currently available at Delaney Park are located at depths of 0, 4.6, 10.7, 18.3, 30.5, 45.4 and 61 m. For this study, only the 0 m and 61 m sensors were used. Again, larger PGA intensities were considered (0.001g to 0.05g) in this case because the downhole array has significant background noise due to its location in an urban environment. After the SNR > 3 criterion was applied, 6 events (i.e., 12 motions) were available for analysis.

3.3.5 Characterization of Downhole Array Sites

Site response analyses require shear wave velocity and damping ratio profiles. For each site, these shear wave velocity profiles were developed from available site-specific data, and the damping ratio profiles were developed from the empirical relationship of Darendeli (2001) as a function of confining pressure and plasticity index. These profiles are shown in Figure 3.3 and each site is discussed below.

Various researchers have measured shear wave velocities at Garner Valley. Downhole measurements were performed by Gibbs (1989), PS suspension logging was performed by

Agbabian Associates (1994 ,1996), and SASW was performed by Stokoe *et al.* (2004). Figure 3.3 shows the shear wave velocity profile for Garner Valley used in this study. The original shear wave velocity model is a modified version of the PS logging and downhole profiles, with the shear

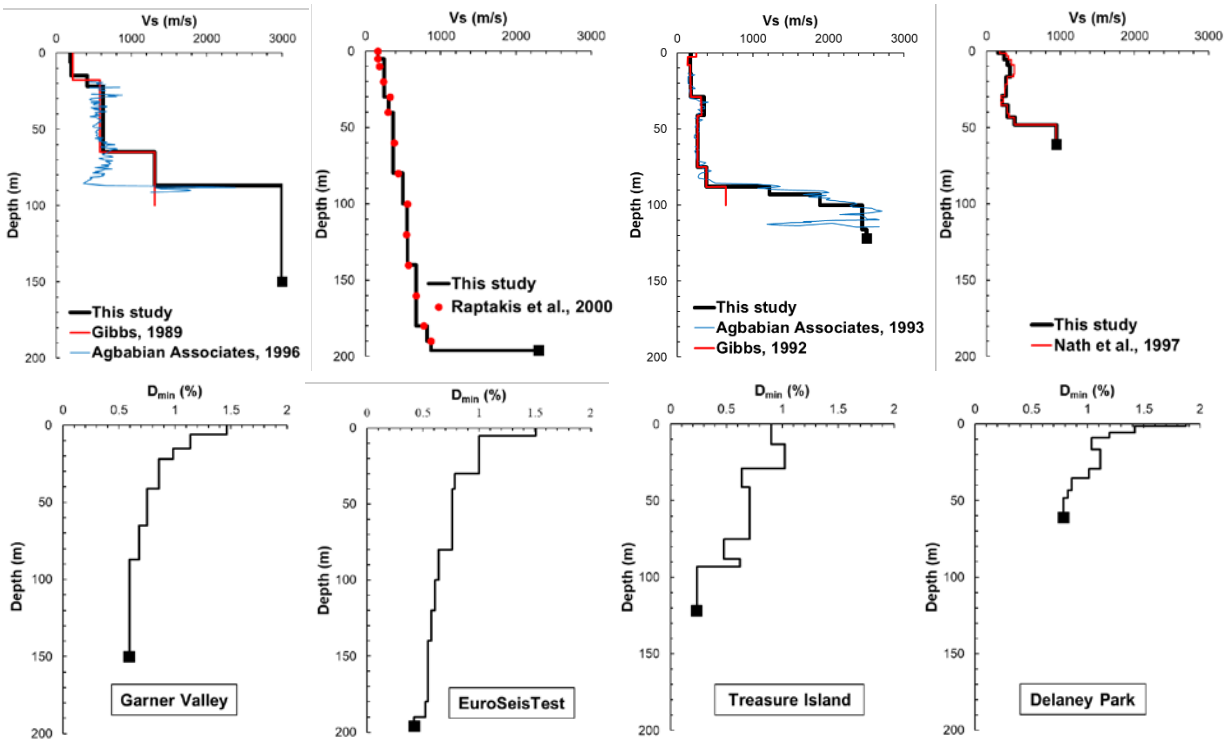

Figure 3.3 Shear wave velocity and small strain damping ratio profiles for downhole array.

wave velocity of the layer between 87 and 150 m increased from 1700 m/s to 3000 m/s to provide a better match with the first mode resonant frequency of the empirical TF. This increased velocity is supported by the shear wave velocity measurements at two nearby sites (Keenwild and Pinon Flat) where the outcropping granite has a shear wave velocity of between 2700 and 3000 m/s. The shear wave velocity profile used in this study is also consistent with recent measurements by Teague *et al.* (2018) using a joint inversion of surface wave dispersion data and HVSR. The

damping ratio profile at the site is based on the in-situ confining stress and assumed constant plasticity index of 15 (Figure 3.3).

The detailed shear wave velocity profile at the EuroSeisTest site (Figure 3.3) was measured by surface wave inversion (Raptakis *et al.*, 2000). The shear wave velocity gradually increases from about 200 m/s at the surface to about 750 m/s below 150 m. The underlying bedrock consists of gneiss with *Vs* = 2000 m/s and is encountered at 196 m. The damping ratio profile at the site (Figure 3.3) is based on the in-situ confining stress and assumed plasticity indices between 0 to 20, depending on the soil type indicated in Raptakis *et al.* (2000).

Shear wave velocity profiles at Treasure Island have been measured by several researchers. Downhole measurements were performed by Gibbs *et al.* (1992) and PS suspension logging was performed by Agbabian Associates (1993). The shear wave profile used in this study (Figure 3.3) represents an average of the available data, as presented in Grazier *et al.* (2011). The damping ratio profile at the site (Figure 3.3) is based on the in-situ confining stress and an assumed plasticity index of 0 for most sandy layers and of ~ 25 for clay layers.

The shear wave model for Delaney Park is a slightly modified version of a velocity model presented in Nath *et al.* (1997) based on downhole measurements at a nearby site about 200 m away (Kalkan *et al.* 2017). The damping ratio profile at the site (Figure 3.3) is assigned from the Darendeli (2001) empirical model based on the confining stress and assumed plasticity index ranging from 10 to 30.

Across the four sites, all have strong impedance contrasts close to the bottom of the downhole array, although they occur at different depths. The damping ratio profiles indicate 1 to 1.5% damping at the surface and about 0.5% at depth. These profiles are similar across the sites because they are all based on the Darendeli (2001) empirical model. It is also important to contrast the

different geologic settings for the four downhole arrays (Figure 3.2) as these conditions will influence the level of variability at the sites. Considering the depositional processes at work at the different sites, it is likely that the Delaney Park site is most laterally variable due to the influence of the glacial processes and Treasure Island is likely the least variable due to its location in a large estuary environment.

3.4 Assessment of Site Response Predictions in the Frequency Domain

For this study the empirical TF and AF for a motion are only plotted over the frequency range in which the SNR is larger than 3.0 for both the surface and base motions. After identifying this frequency range for a motion, the following processing steps were applied: removal of mean, application of a fifth-order Butterworth, time-domain, acausal filter over the defined frequency range, and baseline correction. The empirical TFs are smoothed in the frequency domain using a log-scale rectangular window as described by Goulet *et al.* (2014). Across all the motions analyzed, the empirical data are represented by its median and the $+/-2\sigma_{ln}$ range of the data in the same manner as Thompson *et al.* (2009).

3.4.1 Quantification of Goodness-of-Fit

Various parameters have been proposed to judge the goodness-of-fit between model predictions and observed data. In general, all goodness-of-fit parameters have positive and negative attributes in terms of their ability to accurately quantify model performance (Legates and McCabe 1999) and thus the use of multiple parameters offers the best assessment of model performance. The Pearson correlation coefficient, r, has been used to quantify how well the peaks align in theoretical and empirical TFs and $r > 0.6$ has been proposed as the threshold to indicate good fit of the modal frequencies (Thompson *et al.*, 2012).

Legates and McCabe (1999) note that *r* has the limitations of being overly influenced by extremes in the data and they identify alternative parameters to judge model fit. The index of agreement (d_j) is defined over *N* values of frequency as:

$$d_j = 1.0 - \frac{\sum_{i=1}^{N}|Emp_i - Theor_i|^j}{\sum_{i=1}^{N}(|Emp_i - \overline{Emp}| + |Theor_i - \overline{Emp}|)^j} \quad (3.1)$$

where Emp_i is the observed empirical TF or AF at frequency *i*, $Theor_i$ is the theoretical predictions of TF or AF at frequency *i*, and $\overline{Emp}$ represents the mean of the observed empirical TF or AF across all frequencies considered. Legates and McCabe (1999) recommend using *j* = 1 because it does not overly weight large differences in the data. The index of agreement takes on values between 0 and 1, with values closer to 1 representing superior model performance. This parameter represents the degree to which the predictions are error free, assuming that the mean of the observations ($\overline{Emp}$) is error free (Willmott, 1981). The last goodness-of-fit parameter considered is the root mean square error (*RMSE*), which can be used to judge the average difference between the theoretical predictions and empirical observations. *RMSE* and can be computed in logarithmic space as:

$$RMSE = \sqrt{\frac{1}{N}\sum_{i=1}^{N}[\ln(Theor_i) - \ln(Emp_i)]^2} \quad (3.2)$$

In (3.2), the natural logarithm is used because it is assumed that the TF and AF follow a log-normal distribution (Thompson *et al.*, 2012). It is important to note the frequency range over which the various parameters are computed. Thompson *et al.* (2012) recommend using the frequencies between the first and fourth mode in the theoretical TF and this frequency range is used here.

$$r = \frac{\sum_{i=1}^{N}(Emp_i(f) - \overline{Emp})(Theor_i(f) - \overline{Theor})}{\sqrt{\sum_{i=1}^{N}(Emp_i(f) - \overline{Emp})^2}\sqrt{\sum_{i=1}^{N}(Theor_i(f) - \overline{Theor})^2}} \quad (3.3)$$

3.4.2 Transfer Functions and Amplification Factors

The theoretical TF and AF from linear-elastic analysis are compared with the median of the empirical transfer functions and amplification factors from the recordings in Figure 3.4. The $+/-2\sigma_{ln}$ range of the data is shown in gray. The locations of the peaks in the theoretical TF and AF depend on the assumed soil model (i.e., *Vs* profile and layer thickness) and the amplitudes of the peaks are mainly controlled by the damping ratio profile. The locations of the peaks in the theoretical TF and AF generally agree with the locations of the peaks from the empirical data, although the heights of the peaks and the width of the theoretical and empirical curves differ. The differences are more significant for the TFs than for the AFs. The theoretical TFs generally having very large (amplitudes ~ 80 to 100) and narrow peaks at the first mode, while the empirical TFs display smaller amplitude peaks that are less sharp. The theoretical TFs also tend to have deeper troughs than the empirical TF. Treasure Island and Delaney Park display deep troughs similar to the theoretical TF, but Garner Valley and EuroSeisTest do not. The theoretical and empirical AFs display relatively similar shapes with each other, although the amplitudes are somewhat different.

The values for *r*, the index of agreement (d_1), and *RMSE* for the four sites for both TFs and AFs computed with the D_{min} profile are listed in Table 3.3.1 along with the frequency range over which these parameters are computed for each site. The parameters in Table 3.3.1 generally indicate that the site that is best fit by its 1D theoretical model is Treasure Island (i.e., largest *r* and d_1, smallest *RMSE*), while the site with the poorest fit is Garner Valley. The difference in the computed goodness-of-fit parameters for these two sites is driven predominantly by the flatter troughs in the empirical TF for Garner Valley. All the parameters indicate better agreement in terms of AF than in terms of TF, due to the fact that the peaks and troughs of the AF curves are not as large as for the TFs. The lack of strong peaks (i.e., amplitudes ~ 80 to 100) and troughs in the theoretical

AF is due to the fact that the spectral acceleration at a given frequency is influenced by a range of frequencies.

Table 3.1: Goodness of fit parameters for theoretical TF and AF using D_{min}

Site	Frequency range, Hz	Transfer Function			Amplification Factor		
		r	d_1	*RMSE*	*r*	d_1	*RMSE*
GV	1.95 - 9.02	0.38	0.32	0.80	0.41	0.36	0.29
EST	0.71 - 3.88	0.44	0.39	0.79	0.86	0.58	0.30
TI	0.81 - 4.77	0.70	0.59	0.66	0.94	0.65	0.21
DP	1.39 - 9.45	0.54	0.46	0.59	0.81	0.42	0.46

Interestingly, using the $r > 0.6$ threshold of Thompson *et al.* (2012) for TF, only the Treasure Island site would be considered modeled well by 1D analysis. However, visual examination arguably indicates that all four sites are modeled well across the first four modal frequencies. The *r* parameter does not adequately reflect this agreement due to the significant differences in peak amplitudes between the theoretical and empirical data for Garner Valley, EuroSeisTest, and Delaney Park.

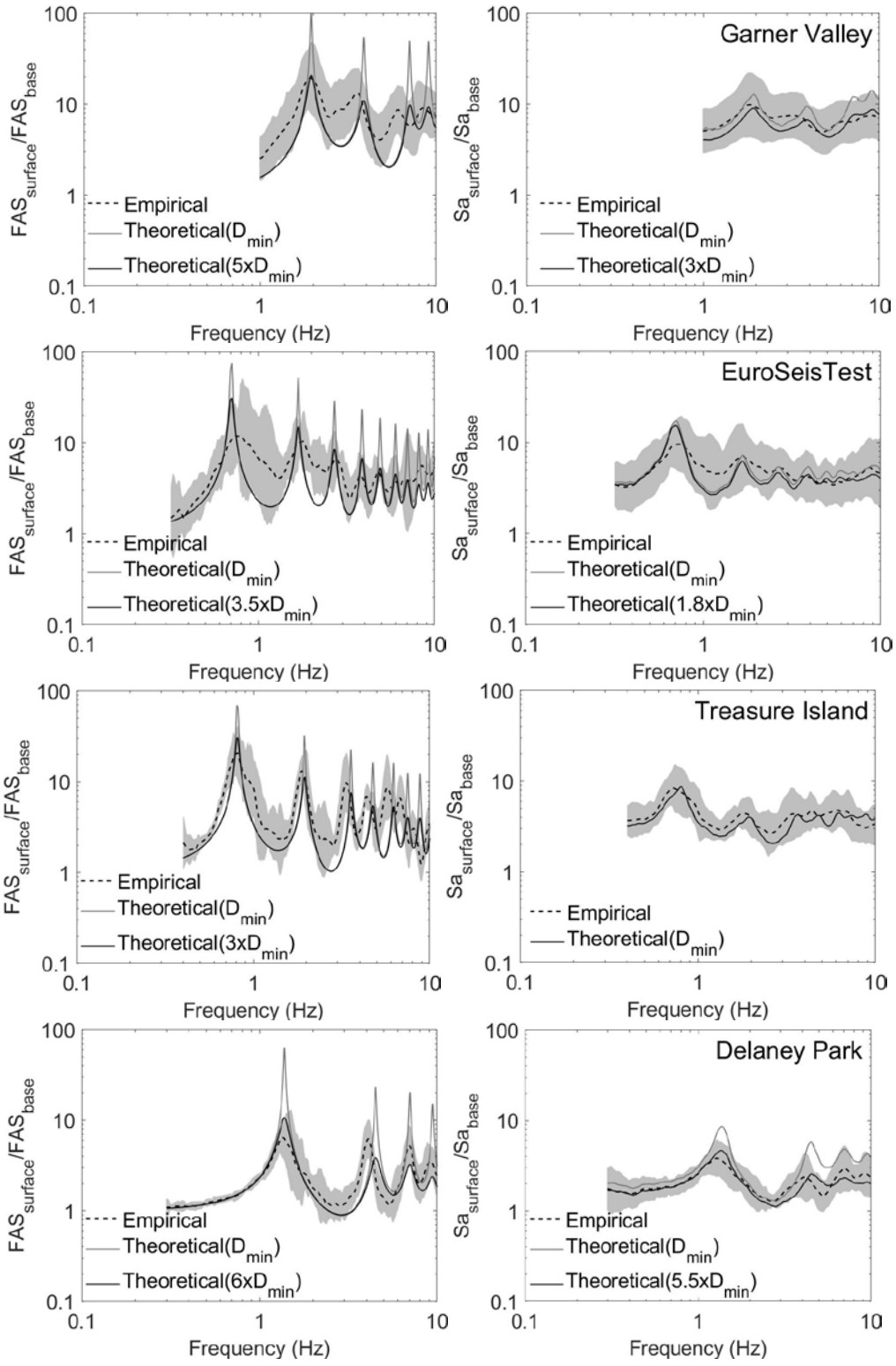

Figure 3.4: Empirical and theoretical TF and AF for different levels of D_{min}. Median empirical values are shown in dash and the +/-2σ_{ln} range of the data are shown in gray.

3.4.3 Influence of D_{min} multiplier on Transfer Functions and Amplification Factors

To provide a better match between the theoretical and empirical responses, a scale factor for the original D_{min} profiles (called the D_{min} multiplier) is applied to the entire depth of each site to reduce the peaks in the theoretical responses. As noted earlier, many researchers have recommended the need to increase the level of D_{min} to better match downhole array data. The D_{min} multiplier is selected for each site to maximize the *r* and d_1 parameters without overdamping the higher modes (i.e., in some cases a slightly smaller D_{min} multiplier was chosen to better match the higher modes while maintaining similar, but slightly smaller, *r* or d_1 values). Separate D_{min} multipliers are developed for the TF and AF for each site. The resulting D_{min} multipliers and associated *r*, d_1, and *RMSE* are listed in Table 3.3.2, and the resulting changes in TF and AF for these D_{min} multipliers are shown in Figure 3.4. Across the four sites, the D_{min} multipliers that provide the best fit to the empirical TFs are between 3 and 6. The larger damping values increase *r* and d_1, and decrease *RMSE*, for each site, with *r* affected more significantly due to its sensitivity to large values (i.e. TF peaks). The d_1 and *RMSE* values are not changed as significantly because although the larger damping values reduce the peaks in the theoretical TF, they do not change the shape of the peaks and they do not change the depths of the troughs (Figure 3.4).

The D_{min} multipliers that provide the best fit to the empirical AFs are smaller (between 1 and 5.5) than those needed to fit the empirical TFs (Table 3.2). The theoretical AFs in Figure 3.4 display smaller and broader peaks than the theoretical TFs, which, as noted earlier, is due to the different responses that AF and TF represent. The *RMSE* values computed for the theoretical AFs are much smaller than for the TFs, indicating that 1D site response analyses can capture response spectral amplification more accurately than transfer functions.

Comparing across the four sites, Delaney Park requires the largest D_{min} multipliers (~ 5.5 to 6) while Treasure Island requires the smallest (~1-3). Garner Valley and EuroSeisTest require intermediate D_{min} multipliers between ~2 to 5.

Table 3.2: Goodness of fit parameters for theoretical TF and AF using scaled D_{min}

		Transfer Function				Amplification Factor			
Site	Frequency range, Hz	D_{min} Multiplier	*r*	d_1	*RMSE*	D_{min} Multiplier	*r*	d_1	*RMSE*
GV	1.95 - 9.02	5	0.65	0.45	0.68	3	0.57	0.48	0.20
EST	0.71 - 3.88	3.5	0.63	0.47	0.73	1.8	0.87	0.54	0.34
TI	0.81 - 4.77	3.0	0.82	0.66	0.64	1.0	0.94	0.65	0.21
DP	1.39 - 9.45	6.0	0.67	0.62	0.42	5.5	0.81	0.63	0.19

3.4.4 Role of HVSR Data to Evaluate Site Response Predictions

The empirical data in Figure 3.4 allow researchers to evaluate whether sites are captured well by the 1D assumption. However, for sites that do not have a downhole sensor it is difficult to confirm that a 1D model will capture the site response. HVSR can provide important information to evaluate this issue when a downhole sensor is not available at a site. HVSR computed using the vertical and horizontal surface recordings of earthquake shaking for each of the downhole array sites are shown in Figure 3.5. Also shown in Figure 3.5 are the theoretical HVSR and the median empirical TF from Figure 3.4. The theoretical HVSR is computed from the *Vs* profiles using the HV-INV program developed by Piña-Flores *et al.* in 2014, which is based on an assumed diffuse wavefield (Sánchez-Sesma *et al.*, 2011). The empirical HVSR data for all four sites show clear first peaks that can be identified as the fundamental mode of each site using the criteria of Bard *et al.* (2005).

The clear peaks in the empirical HVSR in Figure 3.5 are a result of the large impedance contrasts present in the shear wave velocity profiles at each site (Figure 3.3). The locations of the first mode peaks from the theoretical HVSR agree well with those from the empirical HVSR and empirical TF, indicating that the shear wave velocity profiles estimated for these sites are consistent with the empirical site response.

The first mode frequency for each site (f_{site}) estimated from the theoretical and empirical HVSR, as well as the empirical TF, are listed in Table 3.3. For Garner Valley, EuroSeisTest and

Table 3.3: f_{site} estimated from different methods

Site	Site Frequency (Hz)			HVSR (Empirical *Vs.* Theoretical)	
	Empirical HVSR	Theoretical HVSR	Empirical TF	r	Frequency range (Hz)
GV	1.93	1.92	1.96	0.86	1.0 - 6.4
EST	0.69	0.69	0.76	0.65	0.3 - 1.4
TI	0.75	0.74	0.81	0.78	0.4 - 1.8
DP	1.11	1.44	1.34	0.45	0.3 - 2.5

Treasure Island, the estimates of f_{site} from the theoretical HVSR agree very well with the values from the empirical HVSR, with $r > 0.6$ between the empirical and theoretical HVSR. There is also general agreement with the f_{site} from the empirical TF. For Delaney Park there are some discrepancies, with f_{site} from the theoretical HVSR about 30% larger than f_{site} from the empirical HVSR and $r = 0.45$. Nonetheless, f_{site} from the theoretical HVSR agrees well with the value from the empirical TF, which indicates that the f_{site} from the empirical HVSR at Delaney Park may be questionable.

The results in Figure 3.5 demonstrate that empirical and theoretical HVSR data can provide an assessment of the consistency of the shear wave velocity profiles in terms of the f_{site} when there is not a downhole data available.

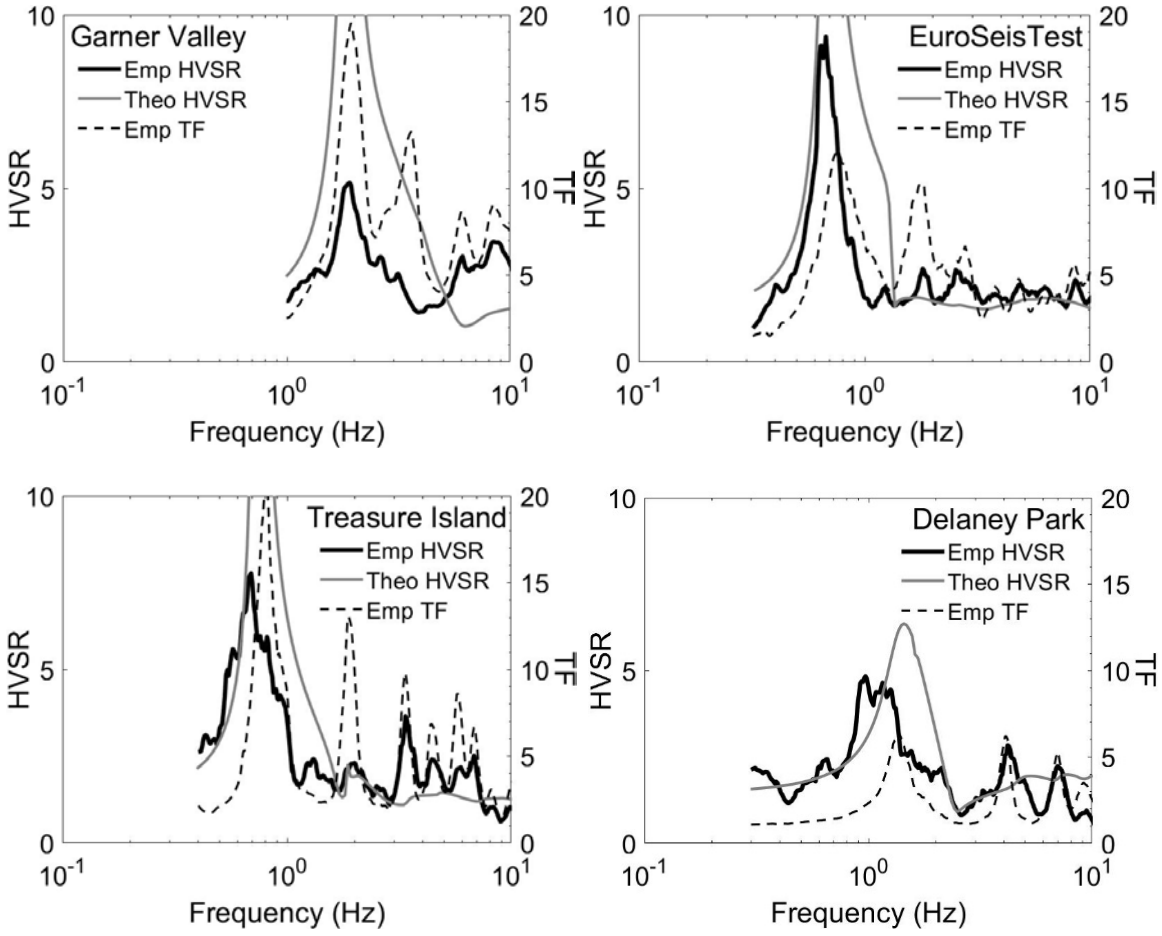

Figure 3.5: Empirical and theoretical HVSR along with empirical TF

3.5 Alternative Assessments of Site Response Predictions

3.5.1 Time Domain Ground Motion Parameters

The accuracy of 1D site response analysis can also be evaluated by comparing various ground motion parameters of the surface time series from the empirical and theoretical responses. Figure 3.6 illustrates an example from Garner Valley of the comparison between the predicted and recorded time series at the ground surface. Figure 3.6a shows the recorded surface motion and Figure 3.6b shows the predicted surface motion using the original D_{min} profile. There is an 58% overprediction in PGA when using the D_{min} profile, but the prediction is improved when using a D_{min} multiplier of 3.4 (Figure 3.6c). The agreement with the recording is further demonstrated for the shear window of the acceleration-time history (t ~ 10 - 13 s) in Figure 3.6d and of the velocity-time history and PGV in Figure 3.6e. Here the similarity in the detailed waveforms is noted. Using a D_{min} multiplier of 3.1, the predicted Arias intensity (Ia) is also in good agreement with the recorded (Figure 3.6f). The predicted Ia using the original D_{min} profile is 3 times larger than recorded. For the recording shown in Figure 3.6, similar D_{min} multipliers worked well for PGA, PGV, and Ia, but that is not always the case.

It is more complex to assess the D_{min} multiplier to match a time domain ground motion parameter than to match a TF or AF. The required D_{min} multiplier to match the recorded surface motion is different for each motion and requires a computation of the surface motion for each possible D_{min} multiplier. Garner Valley has a relatively large number of motions, so a subset of 16 motions were used to obtain the D_{min} multipliers for time domain parameters. For each site, the computed D_{min} multiplier for each motion and each ground motion parameter were averaged

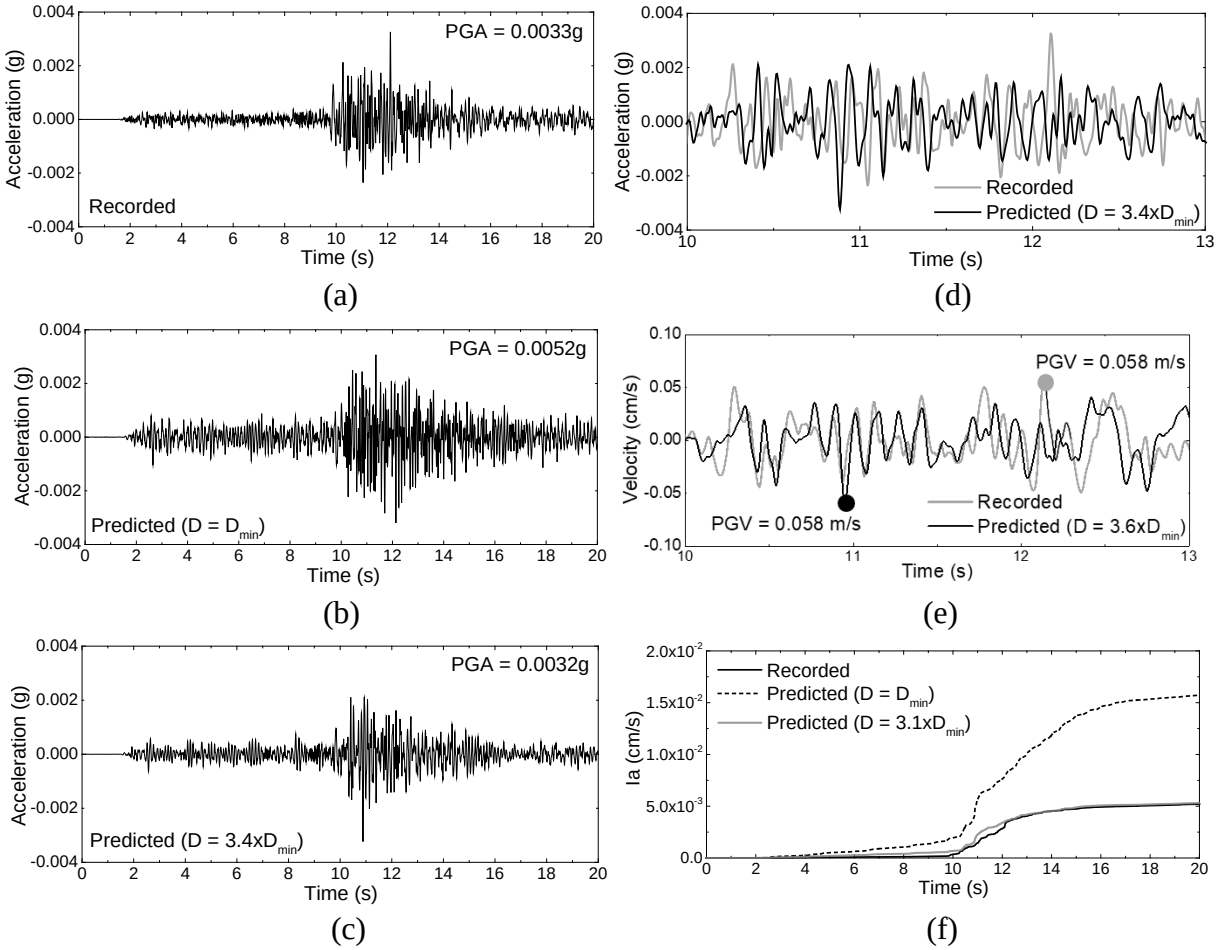

Figure 3.6 Example assessment of D_{min} multipliers using time domain ground motion parameters. (a) Recorded surface acceleration-time series, (b) predicted acceleration-time series using D_{min}, (c) predicted acceleration-time series using $3.4xD_{min}$, (d) recorded acceleration time series and predicted acceleration time series for $3.4xD_{min}$, (e) recorded velocity time series and predicted velocity time series for $3.6xD_{min}$, and (f) Arias intensity for recorded motion and predicted motions with D_{min} and $3.1xD_{min}$. Results shown for Garner Valley motion.

and the results are summarized in Table 3.4. Across the sites, Delaney Park requires the largest D_{min} multiplier from 2.6 ~ 6.2, while Garner Valley and EuroSeisTest requires smaller values between 1.4 and 3.1. Treasure Island requires the smallest D_{min} multipliers,

Table 3.4: D_{min} multipliers derived from time domain ground motion parameters

	D_{min} Multiplier		
Site	PGA	PGV	Ia
GV	3.1	2.8	3.1
EST	1.5	1.4	1.9
TI	0.9	0.5	1.5
DP	4.4	2.6	6.2

and for PGA and PGV the D_{min} multipliers are actually less than 1.0 although the D_{min} multiplier for Arias Intensity is 1.5. The D_{min} multipliers less than 1.0 for PGA and PGV are not realistic and are caused by trying to match ground motion parameters that represent only one instant in the time history rather than a broad measure of the motion over a range of frequencies and range of times. PGA and PGV of a single motion may be influenced by a high frequency spike that results in large PGA and PGV that requires a small D_{min} multiplier to be matched. However, the same motion may require a larger D_{min} multiplier to match the Ia.

3.5.2 High Frequency Spectral Decay Parameter

In engineering seismology, the high-frequency spectral decay parameter (κ) has been used to describe the high-frequency shape of the Fourier Amplitude Spectrum. This parameter can also be related to the shear wave velocity and damping ratio profile at a site (e.g., Campbell 2009), and this can be used to evaluate the appropriate damping characteristics for site response analysis (e.g., Cabas *et al.*, 2018).

Anderson and Hough (1984) proposed the following relationship to describe the shape of the FAS decay at high frequencies using κ:

$$A(f) = A_0 \exp(-\pi\kappa f) \tag{3.4}$$

where A_0 is the amplitude associated with source properties and propagation distances. Equation (3.4) implies an acceleration spectrum that decreases linearly in log (*A*) – *f* space. Anderson and Hough (1984) also observed that κ increases with distance due to regional attenuation but that a site-specific κ_0 could be derived by removing the distance dependence.

Many approaches have been developed to estimate κ_0 from ground motions recorded at a site, but the acceleration spectrum approach (AS) is most simple and requires the fewest assumptions (e.g., Ktenidou *et al.*, 2015). This approach measures κ of individual motions from the slope of the FAS and removes the distance dependence to estimate κ_0. For downhole array studies, the difference between the κ of the surface and borehole records (Δκ) represents the local attenuation characteristics between the surface and base

sensors. Note that the distance dependence can be ignored because the distance is the same for the surface and borehole sensors. The parameter Δκ can be related to the *Vs* and D_{min} profiles using (Campbell 2009):

$$\Delta\kappa = \int_0^z \frac{2D_{min}}{Vs} dz \tag{3.5}$$

The individual κ values at the surface and at the base were computed for each horizontal component for each event and used to compute Δκ. The average Δκ across all the components of motion was taken as the empirical Δκ. Then taking the ratio of the empirical Δκ from the recordings and the theoretical Δκ from equation (3.5) using the original D_{min} profile, D_{min} multipliers were derived for each site.

The average empirical Δκ for each site is plotted *Vs*. the theoretical Δκ in Figure 3.7. Across these sites the Δκ values imply a D_{min} multiplier of 3.1 and the individual sites

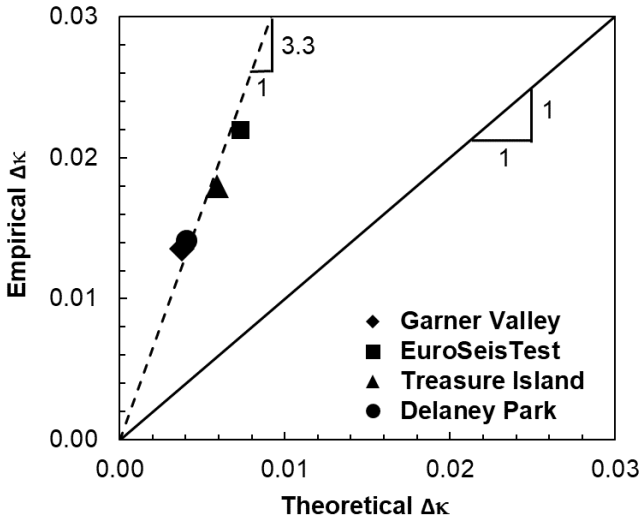

Figure 3.7: Average empirical Δκ and theoretical Δκ for the four sites.

indicate D_{min} multipliers of 3.6, 3.2, 2.7 and 2.9 for Garner Valley, EuroSeisTest, Treasure Island, and Delaney Park, respectively. Using the $\Delta\kappa$ approach results in more similar D_{min} multipliers across the sites as compared with the other measures of site response.

3.5.3 Shear Wave Velocity Randomization

As noted earlier, another approach to account for the effects of lateral variabilities at a site is to randomize the shear wave velocity profiles based on statistical models while maintaining the damping ratio equal to D_{min}. Then, the average response from the randomized *Vs* profiles are compared with the empirical site response. For this study, the Toro (1995) statistical framework for developing randomized *Vs* profiles was used. The shear wave velocity in each layer is assumed to be lognormal distributed with a mean defined from the baseline *Vs* model (i.e., Figure 3.3) and a specified standard deviation (σ_{lnVs}). Generally, σ_{lnVs} is assumed to be larger near the surface because soil properties are most variable near the surface due to variations in depositional and weathering processes. The Toro (1995) model incorporates an interlayer correlation coefficient (ρ) between the *Vs* in adjacent layers and recommends a set of parameters to predict ρ as a function of depth and layer thickness. These parameters are a function of site class. From our experience, the Toro (1995) model predicts excessively variable *Vs* profiles because the predicted ρ are too small (less than 0.3 to 0.4), particularly at the ground surface. Rodriguez-Marek *et al*. (2014) found a depth-independent correlation coefficient of 0.5 for a site consisting of weathered quartzitic sandstone. Based on the fact that the sites analyzed in this study are

alluvial soil sites, a constant value of ρ equal to 0.8 was used. For each layer the *Vs* is limited by $\pm 2\sigma_{lnVs}$ to avoid the generation of unrealistic shear wave velocity profiles. Note that Toro (1995) layer thickness randomization was not incorporated in this study.

Profiles of σ_{lnVs} were generated through trial and error for each site to best match the empirical TF with the average theoretical TF that incorporates *Vs* variability. Figure 3.8 shows the resulting σ_{lnVs} profiles that provide the best match. The near surface σ_{lnVs} for Delaney Park is the largest among the sites, followed by EuroSeisTest, Garner Valley, and Treasure Island. It is important to note that an exhaustive search of σ_{lnVs} profiles was not performed and the variability in layer thickness and inter-layer correlation coefficient were not considered. Therefore other σ_{lnVs} profiles may provide matches as good as those in Figure 3.8.

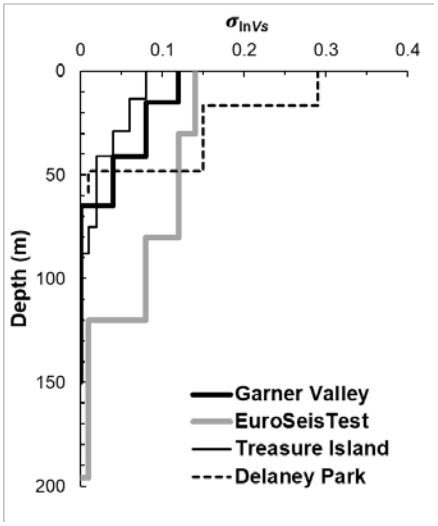

Figure 3.8: Profiles of σ_{lnVs} *Vs*. depth that provide the best-match with the empirical transfer function.

The average theoretical TF and AF from analyses of 50 *Vs* profiles generated by the site response program Strata (Kottke and Rathje 2008) using the σ_{lnVs} profiles from Figure 3.8 are shown in Figure 3.9 along with the empirical data. Also shown are the results with no randomization and the D_{min} profile. Including *Vs* randomization decreases the amplitude of the peaks, in a manner similar to the D_{min} multipliers, but also makes the TF smoother around the peak. These changes are a result of the averaging of individual peaks that occur at different frequencies due to the different *Vs* profiles. At higher frequencies, the averaging effect can significantly smooth out, or even remove, the higher mode peaks. The effect of *Vs* randomization is more significant on the TF than on the AF.

To quantify the improvement of the goodness-of-fit with the empirical data when using *Vs* randomization, the parameters *r*, d_1 and *RMSE* for each site are computed and listed in Table 3.5. The *r* values derived from randomization are similar to those from

Table 3.5 Goodness of fit parameters for theoretical TF and AF using *Vs* randomization

		Transfer Function			**Amplification Factor**		
Site	Frequency range, Hz	*r*	*d1*	*RMSE*	*r*	*d1*	*RMSE*
GV	1.95 - 9.02	0.60	0.49	0.57	0.40	0.29	0.31
EST	0.71 - 3.88	0.68	0.53	0.61	0.88	0.68	0.19
TI	0.81 - 4.77	0.90	0.70	0.51	0.95	0.64	0.19
DP	1.39 - 9.45	0.59	0.62	0.42	0.85	0.33	0.46

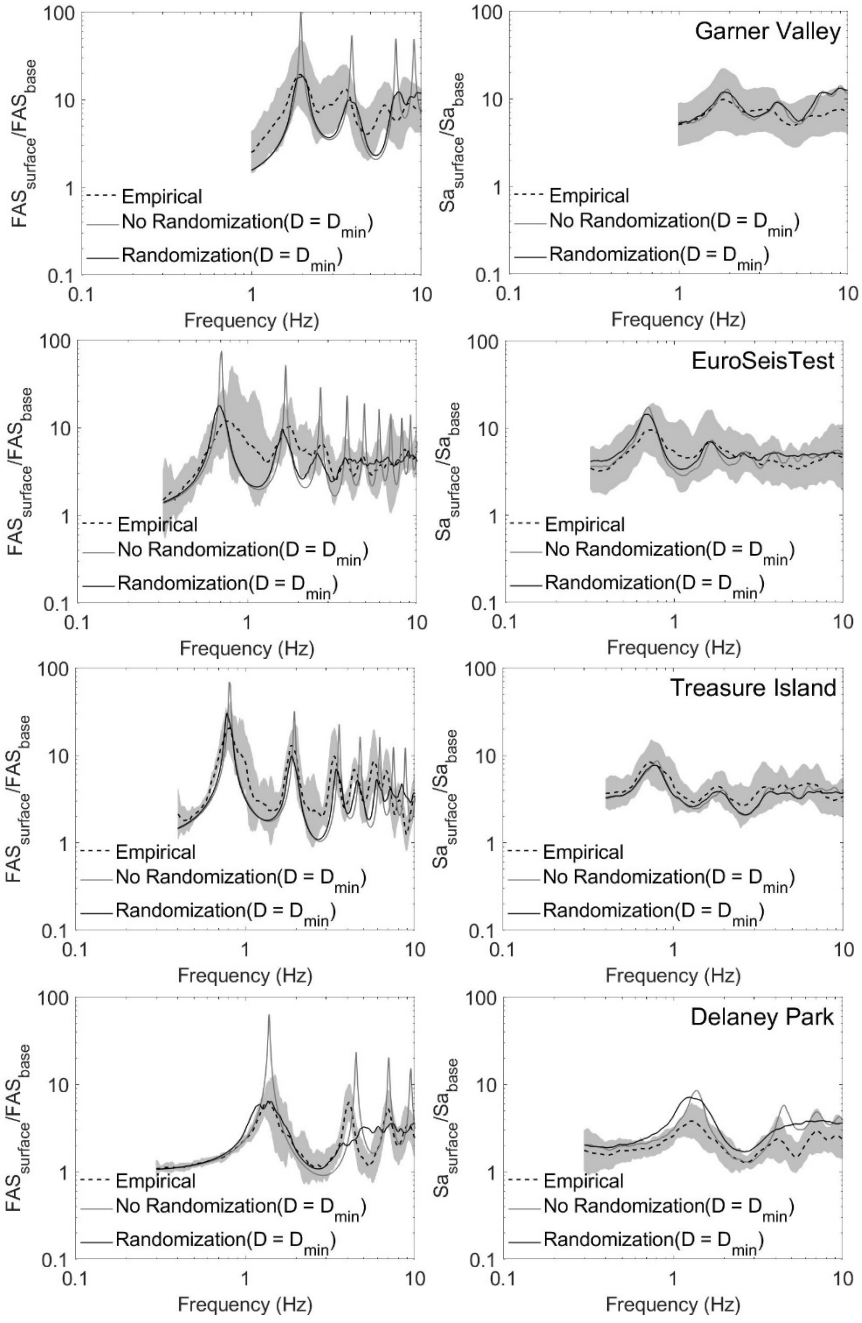

Figure 3.9: Empirical TF and AF compared with theoretical TF and AF computed for Monte Carlo simulations using *Vs* randomization and D_{min}. Median empirical values are shown in dash and the +/-$2\sigma_{ln}$ range of the data is shown in gray.

scaled D_{min} profiles as the location of peaks are not affected by the randomization. *Vs* randomization provides a better match with the empirical TF than using a D_{min} multiplier, as indicated by the larger d_1 and smaller *RMSE* in Table 3.5 as compared with Table 3.2. This result occurs because the TFs from the *Vs* randomization are smoother and thus closer in shape with the empirical TFs. However, the randomization method does not lead to more improvement for the AF, and for EuroSeisTest and Delaney Park the smaller d_1 and larger *RMSE* indicate poorer performance with *Vs* randomization than with the D_{min} multipliers.

It is important to note that while *Vs* randomization mimics the effects of the D_{min} multipliers at the site natural frequencies, it does not modify the shape of the FAS at high frequencies and thus does not modify κ. The *Vs* randomization mimics the effects of damping at the site natural frequencies because the variations in *Vs* lead to different site frequencies for each realization and averaging across the different realizations results in a smaller peak amplitude. However, the *Vs* randomizations do not change the site response at the higher frequencies associated with κ, and thus κ remains unchanged.

3.6 DISCUSSION

As presented above, the D_{min} multipliers required to best-fit the downhole array data vary considerably depending on the ground response characteristic being considered and the site under consideration. This may not be surprising given that different response characteristics measure different aspects of ground shaking and different sites have different levels of lateral variability and associated wave scattering.

Figure 3.10 summarizes the D_{min} multipliers computed for the different response characteristics (i.e., TF, AF, PGA, PGV, Ia, and $\Delta\kappa$) for the four sites. For each site, the D_{min} multipliers are generally largest for the TF. The large D_{min} multipliers for the TF are due to the fact that significant damping is required to reduce the large peaks in the theoretical TF to match the empirical data. Given that these D_{min} multipliers are selected to fit only a narrow frequency range around the peaks, they may overestimate the required damping to best match the overall site response. The D_{min} multipliers for AF and for the time domain characteristics (PGA, PGV, and Ia) at each site are generally similar to one another and they are smaller than for the TF. As these ground response characteristics represent a broader range of frequencies and capture the overall response of the site, these smaller D_{min} multipliers may be more appropriate. In fact, one could argue that the D_{min} multipliers for Ia are most appropriate because Ia represents the most complete measure of response than other parameters as noted before. Although the D_{min} multipliers for Ia will not provide the best-fit values of parameters *r*, d_1 and *RMSE* reported in Table 3.2, the values of these goodness of fit parameters are not sacrificed significantly. The *r* values generally decrease by less than 0.1 (max 15% change), the d_1 values decrease by less than 0.06 (max 10% change), and the *RMSE* increase by less than 0.04 (max 20% change).

Delaney Park is the one site that appears to have a different trend in the D_{min} multipliers for the different ground response characteristics. The D_{min} multipliers for Delaney Park span a larger range than for the other sites, with the D_{min} multiplier for PGV equal to

2.6 and the D_{min} multiplier for Ia equal to 6.2. The large D_{min} multiplier for Ia is similar to the D_{min} multiplier for the TF for this site, which was not observed for the other sites. It is not clear why Delaney Park has such a large variation in the D_{min} multipliers for the different ground response characteristics.

Across the four sites, the D_{min} multipliers indicated by $\Delta\kappa$ are consistently around 3.3 although the other parameters indicate different D_{min} multipliers for the different sites. The consistency in the D_{min} multipliers for $\Delta\kappa$ for the different sites is surprising, as other studies have shown vastly different D_{min} multipliers for different sites (Cabas *et al.*, 2018; Xu *et al.*, 2018). The D_{min} multipliers for $\Delta\kappa$ may be different than the others because $\Delta\kappa$ represents the higher frequency components of motion (generally above 5 Hz).

The data in Figure 3.10 allow for a comparison of the D_{min} multipliers across the different sites. The smallest D_{min} multipliers are required for Treasure Island (average ~1.5) and the largest for Delaney Park (average ~5.0). The alpine valleys of Garner Valley and EuroSeisTest have intermediate D_{min} multipliers with averages between 2.0 and 3.5. In terms of the level of shear wave velocity variability (σ_{lnVs}) required to fit the empirical TF and AF (Figure 3.7), Treasure Island required the least and Delaney Park required the most. This trend is similar to the trend for the relative values of D_{min} multipliers for these sites (i.e., smallest D_{min} multiplier for Treasure Island, largest for Delaney Park). For the other two sites (EusoSeisTest and Garner Valley) the trends are not consistent between σ_{lnVs} and the D_{min} multipliers: EusoSeisTest required larger σ_{lnVs}, yet Garner Valley

required the larger D_{min} multiplier. Nonetheless, these values were still intermediate to those required for Treasure Island and Delaney Park.

The relative values of the D_{min} multipliers and σ_{lnVs} across the sites may be interpreted within the context of the local geology (Figure 3.2) and the potential for shear wave velocity variability given the depositional environment. Treasure Island is an island of

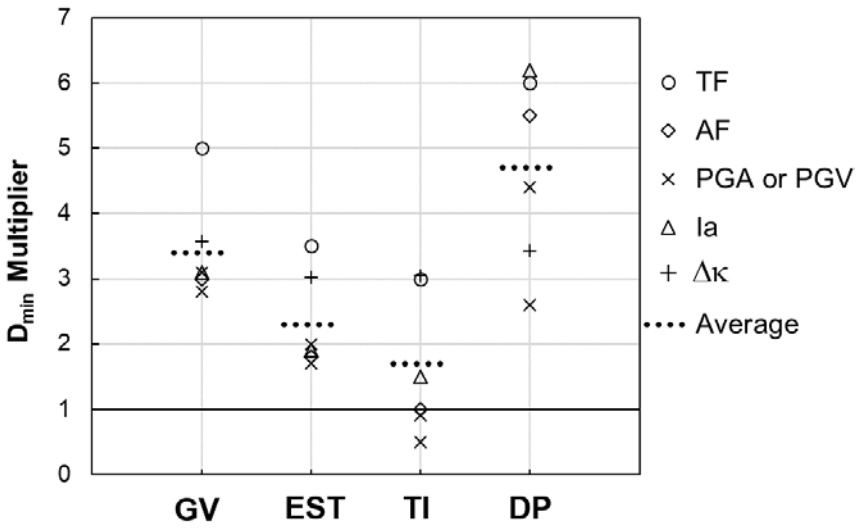

Figure 3.10: Comparison of D_{min} multipliers considered for different ground response characteristics for each site.

artificial fill located in the middle of a vast estuary environment, and therefore the subsurface conditions are likely the least variable, particularly at depths below the artificial fill. Delaney Park is located in a triangular lowland that has been shaped by glacial movements and the scale of changes in the geologic features is on the order of tens to hundreds of

meters, and thus the subsurface conditions are considered the most variable. Garner Valley and EuroSeisTest are both sediment-filled alpine valleys and the transition from alluvium deposits to surrounding rock formations occur at distances on the order of a kilometer or more. The depositional processes at work in alpine, alluvial valleys likely result in more variability subsurface conditions than Treasure Island but less variable subsurface conditions than Delaney Park. Thus, the size of the D_{min} multipliers appears to reflect the potential shear wave velocity variability and associated wave scattering, at least as inferred from the geologic environment. However, this hypothesis requires further investigation through detailed shear wave velocity characterization at these sites with significant focus on quantifying the variability across the sites and more sites need to be studied in this manner.

Finally, it is important to note the two and three-dimensional (2D/3D) aspects of wave propagation that are not captured by a 1D site response analysis. The presence of surface waves will introduce low frequency oscillations that occur later in an earthquake record (Baise *et al*., 2003a) and these cannot be modeled in 1D analysis. It is not likely that surface wave effects influenced the TF and AF results over the frequency range investigated in this study (e.g., frequencies greater than about 0.3 to 0.5 Hz) but they could affect lower frequencies at some sites. Another issue is that the 1D *Vs* randomization used in this study is a simplified way to approximate the complex effects associated with wave propagation through a 2D/3D heterogeneous domain. Thompson *et al*. (2009) showed that incorporating 2D/3D variability in a full wave field analysis more thoroughly captures wave

scattering, although it requires more computational resources and uncertainty is associated with the characterization of the 2D/3D variability. Despite these limitations, 1D site response analysis often captures the most important aspects of wave propagation and provides an acceptable estimate of ground response.

3.7 CONCLUSIONS

Previous studies have demonstrated that using small-strain damping from laboratory measurements in site response will lead to an over-predication of the site response. These studies recommend increasing the laboratory based D_{min}, although there is no accepted approach to assign an appropriate level of additional D_{min}.

This study uses earthquake motions from four well characterized downhole array sites to identify the required increase in D_{min}, as quantified by the D_{min} multiplier, to match the site response. Different ground response characteristics are used to characterize the site response: TF, AF, PGA, PGV, Ia and $\Delta\kappa$. Across the four sites analyzed, the required D_{min} multiplier varies from 1.5 to 5.0. Treasure Island requires the smallest D_{min} multiplier, Delaney Park requires the largest, and Garner Valley and EuroSeisTest require intermediate values.

This study distinguishes itself from previous studies in two important ways: (1) the comparison of the D_{min} multipliers required to fit different ground response characteristics at a site and (2) the interpretation of the different D_{min} multipliers for the four sites within the context of the local geology, the depositional environment, and the potential for spatial

variability in shear wave velocity that results in wave scattering. At a given site, the required D_{min} multiplier varies considerably depending on the ground response characteristic considered. We argue that the D_{min} multiplier required to best-fit the surface Ia is most appropriate for site response analysis. In terms of interpreting the D_{min} multipliers across sites, we hypothesize that the required D_{min} multiplier may be related to the shear wave velocity variability and associated wave scattering at a site. It is important to point out that this hypothesis requires further investigation through detailed shear wave velocity characterization at downhole array sites with a significant focus on quantifying the variability in shear wave velocity across sites.

3.8 Acknowledgements

This study was supported by the U.S. Nuclear Regulatory Commission (NRC) under grant NRC-HQ-60-15-C-0005. This support is gratefully acknowledged.

3.9 References

Agbabian Associates. (1993). "Suspension P and SH wave velocity measurements at the Treasure Island Firehouse, Borehole USN-1." <https://www.strongmotioncenter.org/NCESMD/photos/CGS/splayouts/sp58642.pdf> (Feb. 21, 2018).

Agbabian Associates. (1994, 1996). "Shallow (1994) and Deep (1996) PS Suspension log." <http://nees.ucsb.edu/facilities/GVDA> (Feb. 21, 2018).

Anderson, J. G., Hough, S. E. (1984). “A model for the shape of the Fourier amplitude spectrum of acceleration at high frequencies.” *Bulletin of the Seismological Society of America*, 74(5), 1969-1993.

Badal, J., Dutta, U., Serón, F., and Biswas, N. (2004). “Three-dimensional imaging of shear wave velocity in the uppermost 30 m of the soil column in Anchorage, Alaska.” *Geophysical Journal International*, 158(3), 983-997.

Baise, L. G., Glaser, S. D., and Dreger, D. (2003). “Site response at Treasure and Yerba Buena Islands, California.” *Journal of Geotechnical and Geoenvironmental Engineering*, 129(5), 415-426.

Baise, L. G., Dreger, D. S., & Glaser, S. D. (2003a). “The Effect of shallow San Francisco Bay Sediments on Waveforms Recorded during the Mw 4.6 Bolinas, California, Earthquake.” *Bulletin of the Seismological Society of America*, 93(1), 465-479.

Bard P-Y, Duval AM, Lebrun B, Lachet C, Riepl J, Hatzfeld D. (1997). “Reliability of the H/V technique for site effect measurement: an experimental assessment.” *Proc.,17th International conference on soil dynamics and earthquake engineering*, Istanbul, 19–24 July 1997

Bard, P. Y., SESAME-Team, (2005). “Guidelines for the implementation of the H/V spectral ratio technique on ambient vibrations measurements, processing and interpretation.” *SESAME European Research Project EVG1-CT-2000-00026*.

Bedrossian, T. L., Roffers, P., Hayhurst, C. A., Lancaster, J. T., and Short, W. R. (2012). Geologic compilation of Quaternary surficial deposits in southern California. *California Geol. Surv. Spec. Rept. 217.*

Bonilla, L. F., Steidl, J. H., Gariel, J. C., and Archuleta, R. J. (2002). "Borehole response studies at the Garner Valley downhole array, southern California." *Bulletin of the Seismological Society of America*, 92(8), 3165-3179.

Bora, S.S., Scherbaum, F., Kuehn, N., and Stafford, P. (2016). "On the Relationship between Fourier and Response Spectra: Implications for the Adjustment of Empirical Ground-Motion Prediction Equations (GMPEs)." *Bulletin of the Seismological Society of America*, 106 (3), pp. 1235–1253.

Cabas, A., Rodriguez-Marek, A., & Bonilla, L. F. (2017). "Estimation of Site-Specific Kappa (κ0)-Consistent Damping Values at KiK-Net Sites to Assess the Discrepancy between Laboratory-Based Damping Models and Observed Attenuation (of Seismic Waves) in the Field." *Bulletin of the Seismological Society of America*, 107(5), 2258-2271.

Campbell, K. W. (2009). "Estimates of shear-wave Q and κ0 for unconsolidated and semiconsolidated sediments in eastern North America." *Bulletin of the Seismological Society of America*, 99(4), 2365-2392.

Combellick, R. (1999). Simplified geological map of central and east Anchorage, Alaska, scale 1: 25000, *Alaska Div. Geol. Geophys. Surv., Fairbanks, Alaska.*

Darendeli, M. B. (2001). "Development of a new family of normalized modulus reduction and material damping curves." *Ph.D. Dissertation, University of Texas at Austin*, 296-298.

Elgamal A., Lai T., Yang Z., He L. (2001). "Dynamic Soil Properties, Seismic Downhole Arrays and Applications in Practice." *Proc., 4th International Conference on Recent Advances in Geotechnical Earthquake Engineering and Soil Dynamics,* S. Prakash, ed., San Diego, CA.

Gibbs, J. F. (1989). "Near-surface P-and S-wave velocities from borehole measurements near Lake Hemet, California." *US Geological Survey Open-File Report*, 89, 630.

Gibbs, J. F., Fumal, T. E., and Powers, T. J. (1992). " Seismic velocities and geologic logs from borehole measurements at seven strong-motion stations that recorded the 1989 Loma Prieta, California, earthquake (No. 94-222)," *US Geological Survey*.

Goulet, C. A., C. H. Cramer, R. B. Darragh, W. J. Silva, Y. M. A. Hashash, J. Harmon, J. P. Stewart, K. E. Wooddell, and R. R. Youngs. (2014). "PEER NGA-East database." *PEER Report* 2014, 17.

Graizer, V. (2011). “Treasure Island Geotechnical Array – Case Study for Site Response Analysis” *4th IASPEI/IAEE International Symposium: Effects of Surface Geology on Seismic Motion*, University of California Santa Barbara, August 23-26, 2011

Griffiths, S. C., Cox, B. R., Rathje, E. M., & Teague, D. P. (2016). “Surface-wave dispersion approach for evaluating statistical models that account for shear-wave velocity uncertainty.” *Journal of Geotechnical and Geoenvironmental Engineering*, 142(11), 04016061.

Haghshenas, E., Bard, P. Y., Theodulidis, N., and SESAME WP04 Team. (2008). “Empirical evaluation of microtremor H/V spectral ratio.” *Bulletin of Earthquake Engineering*, 6(1), 75-108.

Hill, R. I. (1981). “Field, petrologic, and isotopic studies of the intrusive complex of San Jacinto Mountain. Geology of the San Jacinto Mountains: Santa Ana, California.” *South Coast Geological Society, Annual Field Trip Guidebook*, 9, 76-89.

Kalkan, E., Ulusoy, H. S., Wen, W., Fletcher, J. P., Wang, F., and Nakata, N. (2017). “Sites properties inferred from Delaney Park Downhole Array in Anchorage, Alaska.” *Bulletin of Seismological Society of America*, in press.

Kaklamanos, J., Baise, L. G., Thompson, E. M., and Dorfmann, L. (2015). “Comparison of 1D linear, equivalent-linear, and nonlinear site response models at six KiK-net validation sites.” *Soil Dynamics and Earthquake Engineering*, 69, 207-219.

Kottke, A., and Rathje, E. (2008). “Technical manual for Strata.” *PEER Report* 2008, 10.

Kramer, S. L. (1996). *Geotechnical Earthquake Engineering*, Prentice-Hall, New Jersey, pp. 255

Ktenidou, O.-J., Norman A.A., S. Drouet and F. Cotton (2015). “Understanding the physics of kappa (κ): insights from a downhole array.” *Geophysical Journal international*, 203, 678-691.

Lee, C. H. (1969). “Treasure Island fill.” *Bay mud developments case histories*, C. Lee and U. Praszker, eds., California Division of Mines and Geology, 69–72.

Legates, D. R., and McCabe, G. J. (1999). “Evaluating the use of “goodness-of-fit” measures in hydrologic and hydroclimatic model validation.” *Water resources research*, 35(1), 233-241.

Lermo, J., and Chávez-García, F. J. (1994). “Are microtremors useful in site response evaluation?” *Bulletin of the Seismological Society of America*, 84(5), 1350-1364.

Manakou, M. V., Raptakis, D. G., Chávez-García, F. J., Apostolidis, P. I., and Pitilakis, K. D. (2010). “3D soil structure of the Mygdonian basin for site response analysis.” *Soil Dynamics and Earthquake Engineering*, 30(11), 1198-1211.

McCrea S., Myers M., Utley S. (2012). Preliminary Geologic Map of Quaternary Surficial Deposits in Southern California Palm Springs 30'x60' Quadrangle. *Project for Dept. Water Resources, Cali. Geol. Surv.*

Nakamura, Y. (1989). “A method for dynamic characteristics estimation of subsurface using microtremor on the ground surface.” *Railway Technical Research Institute, Quarterly Reports*, 30(1).

Nakamura, Y. (2000). “Clear identification of fundamental idea of Nakamura’s technique and its applications.” *Proc., XII World Conf. Earthquake Engineering*, New Zealand, Paper no 2656.

Nath, S. K., Chatterjee, D., Biswas, N. N., Dravinski, M., Cole, D. A., Papageorgiou, A., ... and Poran, C. J. (1997). “Correlation study of shear wave velocity in near surface geological formations in Anchorage, Alaska.” *Earthquake Spectra*, 13(1), 55-75.

Nogoshi, M., and T. Igarashi. (1971). “On the amplitude characteristics of microtremor (part 2).” *J. Seism. Soc. Japan*, no. 24, 26–40 (in Japanese with English abstract).

Nour, A., Slimani, A., Laouami, N., and Afra, H. (2003). “Finite element model for the probabilistic seismic response of heterogeneous soil profile.” *Soil Dynamics and Earthquake Engineering*, 23(5), 331-348.

Papadopulos, S., Eliahu, U. (2009). “Geotechnical Conceptual Design Report – Treasure Island, San Francisco, CA.” *ENGEO Incorporated Report.*

Pina Flores, J., García-Jerez, A., Luzón, F., Perton, M., and Sánchez-Sesma, F. J. (2014). “Inversion of H/V ratio in layered systems.” *American Geophysical Union, Fall Meeting 2014*, San Francisco, CA, abstract id. S12A-07.

Raptakis, D., Chávez-Garcıa, F. J., Makra, K., and Pitilakis, K. (2000). “Site effects at Euroseistest—I. Determination of the valley structure and confrontation of observations with 1D analysis.” *Soil Dynamics and Earthquake Engineering*, 19(1), 1-22.

Rodriguez, V. H., and Midorikawa, S. (2002). “Applicability of the H/V spectral ratio of microtremors in assessing site effects on seismic motion.” *Earthquake Engineering and Structural Dynamics*, 31(2), 261-279.

Rodriguez-Marek, A., Rathje, E.M., Bommer, J.J., Stafford, P.J., and Scherbaum, F. 2014. “Application of Single-Station Sigma and Site Response Characterization in a Probabilistic Seismic Hazard Analysis for a New Nuclear Site,” *Bulletin of the Seismological Society of America*, 104(4), 1601–1619, doi:10.1785/0120130196

Rollins, K. M., Hryciw, R. D., Shewbridge, S. E., McHood, M. D., and Homolka, M. (1994). “Ground response on Treasure Island.” *US Geol. Surv. Prof. Pap*, 1551.

Sánchez-Sesma, Francisco J., *et al*. (2011). “A theory for microtremor H/V spectral ratio: application for a layered medium.” *Geophysical Journal International*, 186.1: 221-225.

Seekins, L. C., Wennerberg, L., Margheriti, L., and Liu, H. P. (1996). “Site amplification at five locations in San Francisco, California: A comparison of S waves, codas, and microtremors.” *Bulletin of the Seismological Society of America*, 86(3), 627-635.

Stein, S., and Wysession, M. (2003). *An Introduction to Seismology, Earthquakes, and Earth Structure*. Blackwell Publishing, Massachusetts, pp. 185-191.

Stewart, J. P., Afshari, K., and Hashash, Y. M. (2014). "Guidelines for performing hazard-consistent one-dimensional ground response analysis for ground motion prediction." *PEER Rep*ort, 2014, 16.

Stokoe, K. H., Jennie, C., Milton, T., Asli Kurtulus, M. S., and Menq, F. Y. (2004). "SASW measurements at the NEES garner valley test site, California." *Data report*, College of Engineering, University of Texas at Austin, Austin, TX.

Teague, D., Cox B., Rathje, E.M. (2018). "Measured *Vs.* Predicted Site Response at the Garner Valley Downhole Array Considering Shear Wave Velocity Uncertainty from Borehole and Surface Wave Methods." *Soil Dynamics and Earthquake Engineering*, submitted.

Thompson, E., L. Baise, R. Kayen, and B. Guzina. (2009). "Impediments to Predicting Site Response: Seismic Property Estimation and Modeling Simplifications," *Bulleting of Seismological Society of America*, 99(5), 2927-2949

Thompson, E., L. Baise, Y. Tanaka, and R. Kayen. (2012). "A Taxonomy of Site Response Complexity." *Soil Dynamics and Earthquake Engineering*, 41, 32-43

Toro, G. R. (1995). “Probabilistic models of the site velocity profiles for generic and site-specific ground motion amplification studies.” *Technical Report*, No. 779574, Brookhaven National Laboratory, Upton, N.Y., pp. 147

Toro, G. R., Silva, W. J., McGuire, R. K., and Herrmann, R. B. (1992). “Probabilistic seismic hazard mapping of the Mississippi Embayment.” *Seismological Research Letters*, 63(3), 449-475.

Tsai C.C., and Hashash Y.M.A. (2009). “Learning of Dynamic Soil Behavior from Downhole Arrays,” *Journal of Geotechnical and Geoenvironmental Engineering*, 135(6): 745–757.

Updike, R. G., Olsen, H. W., and Schmoll, H. R. (1988). “Geologic and geotechnical conditions adjacent to the Turnagain Heights landslide, Anchorage, Alaska.” *U.S. Geological Survey Bulletin 1817*.

Wagner D. L., Bortugno E. J., McJunkin R. D. (1991). Geologic Map of the San Francisco – San Jose Quadrangle. *Cali. Geol. Surv.*, Regional Geologic Map No. 5A.

Willmott, C. J. (1981). “On the validation of models.” *Physical geography*, 2(2), 184-194.

Xu, B., Rathje, E. M., Hashash, Y., Stewart, J., Campbell, K., Silva, W. (2018). “$\boldsymbol{\kappa_0}$ for Soil Sites: Observations from Kik-net Sites and Their Use in Constraining Small-Strain Damping Profiles for Site Response Analysis.” *Earthquake Spectra*, submitted.

Yee E., Stewart J.P., Tokimatsu K. (2013). “Elastic and Large-Strain Nonlinear Seismic Site Response from Analysis of Vertical Array Recordings.” *Journal of Geotechnical and Geoenvironmental Engineering*, 139(10): 1789-1801.

Zalachoris, G., and Rathje, E. M. (2015). “Evaluation of one-dimensional site response techniques using borehole arrays.” *Journal of Geotechnical and Geoenvironmental Engineering*, 141(12), 04015053.

Chapter 4: Taxonomy for Evaluating the Site-Specific Applicability of One-Dimensional Ground Response Analysis

Yumeng Tao[6], and Ellen Rathje[7]

ABSTRACT

Because one-dimensional (1D) ground response analysis remains the state-of-practice for geotechnical earthquake engineering, one crucial task is to identify whether the response of a site can be modeled well by 1D analysis. Previous studies have used downhole array data for this evaluation and came to the troubling conclusion that only a small fraction of sites are suitable for 1D analysis. In this study, ground response analyses incorporating 1D transfer functions (*TF*) and the H/V Spectral Ratio (*HVSR*) technique are carried out for 34 downhole array sites and used to develop a taxonomy that assesses the suitability of 1D analysis for a site. The *HVSR* is used to identify the first-mode resonant frequency of the site, and the within and outcrop *TF* are used to distinguish true-resonances from pseudo-resonances. The taxonomy is focused on identifying sites in which true-resonances are captured by the 1D analysis because pseudo-resonances are only present in downhole array sites and sites analyzed in practice are generally not downhole array sites. Using the proposed taxonomy, an increased portion of sites are considered suitable for 1D

[6] Graduate Research Assistant, Department of Civil, Architectural, and Environmental Engineering, University of Texas, Austin, TX 78712

[7] Janet S. Cockrell Centennial Chair in Engineering, Department of Civil, Architectural, and Environmental Engineering, University of Texas, Austin, TX 78712

analysis. This more favorable result is a direct result of considering only true-resonances, as indicated by the *HVSR* and theoretical transfer functions, in the assessment of 1D applicability. This taxonomy system is developed using downhole array data but it can be applied to any site (even non-downhole array sites) in which the *HVSR* curve and shear wave velocity profile are measured, making it easily applied in engineering practice.

Key words: Site response, taxonomy, pseudo-resonance, forward analysis

4.1 INTRODUCTION

An important task in geotechnical earthquake engineering is to predict the ground response caused by earthquake shaking. One-dimensional (1D) ground response analysis is the most common tool for this task and it involves a model in which the site response is assumed to be controlled by the vertically propagating, horizontally polarized SH shear waves (SH1D) through layers that are assumed to extend infinitely in the horizontal direction (Kramer 1996). It is necessary for this 1D computational model to be validated by using experimental data and to evaluate if a realistic site can be represented by this simplified model (Bradley, 2011). The seismic downhole array, which consists of accelerometers located at the surface and at one or more depths in the ground, has been widely used to assess and calibrate the 1D site response model. Downhole arrays are used because they have the advantage of separating the local site effects from other seismic processes such as

earthquake source and path effects (Satoh *et al*., 1995; Thompson *et al*., 2012). Also, by specifying the input motion of the recorded motion at the downhole sensor, this approach eliminates the uncertainty associated with assigning an input motion from a nearby rock site (Steidl *et al*., 1996). Thus downhole arrays provide the most direct observations of how the seismic waves are modified by the properties of the geological material between a location in the ground and the surface.

Downhole arrays have been used to evaluate the applicability of SH1D assumption by many research groups (Bonilla *et al*., 2002; Thompson *et al*., 2009; Thompson *et al*., 2012; Zalachoris and Rathje, 2015). Bonilla *et al*., (2002) evaluated the site response predictions for the Garner Valley Downhole Array using two types of boundary conditions: borehole (i.e., within) and outcrop. They found that the borehole boundary condition provided the best match with the empirical data for the downhole sensors at shallow depth (less than about 50 m) but that the outcrop boundary condition performed better for the deeper sensors. Thompson *et al*., (2009) also utilized the two types of boundary conditions to assess the SH1D applicability for 13 downhole array sites from the KiK-Net database (Aoi *et al*., 2004) in Japan. They concluded that few sites were accurately modeled by the 1D analysis and they showed an example of an improved fit to the empirical data when using full wavefield modeling with spatially correlated seismic properties across a three-dimensional domain.

Thompson *et al*. (2012) represents the most thorough attempt at developing a taxonomy to identify sites that are modeled well by 1D analysis. Using low intensity motions from 100 Kik-Net downhole array sites, the taxonomy aims at distinguishing sites where the 1D analysis is adequate from the sites that require more sophisticated analysis. The taxonomy classification is based on two parameters: (1) the inter-event variability (σ_i) of the computed empirical transfer function and (2) the Pearson correlation coefficient (r) between the empirical and theoretical transfer functions. The parameter σ_i quantifies the variability in the recorded empirical transfer functions at a site and Thompson *et al*. (2012) proposed a threshold of 0.35 to distinguish low (L) and high (H) variability sites. The parameter r is a measure of the goodness-of-fit between the empirical and theoretical transfer functions and Thompson *et al*. (2012) proposed a threshold of $r > 0.6$ to distinguish good fit (G) and poor fit (P) sites. The study stated that only LG sites (i.e., $\sigma_i < 0.35$, $r > 0.6$) should be considered suitable for 1D analysis.

Figure 4.1 shows three examples of downhole array sites evaluated using the Thompson *et al*. (2012) criteria. IBRH13 is an LG site ($\sigma_i = 0.32$, $r = 0.75$) with the transfer function peaks well-aligned and small variability in the empirical transfer function data. IWTH12 is an LP site ($\sigma_i = 0.26$, $r = -0.10$) with the empirical transfer function showing amplification over a broad range of frequencies that do not align with the theoretical transfer function peaks. KSRH05 is an LP site ($\sigma_i = 0.34$, $r = 0.37$) where the transfer function peaks are generally aligned but the differences in the amplitudes of the peaks result in a

value of *r* smaller than the threshold of 0.6. Of the 100 sites analyzed by Thompson *et al*. (2012), only 16% were classified as LG and considered suitable for 1D analysis.

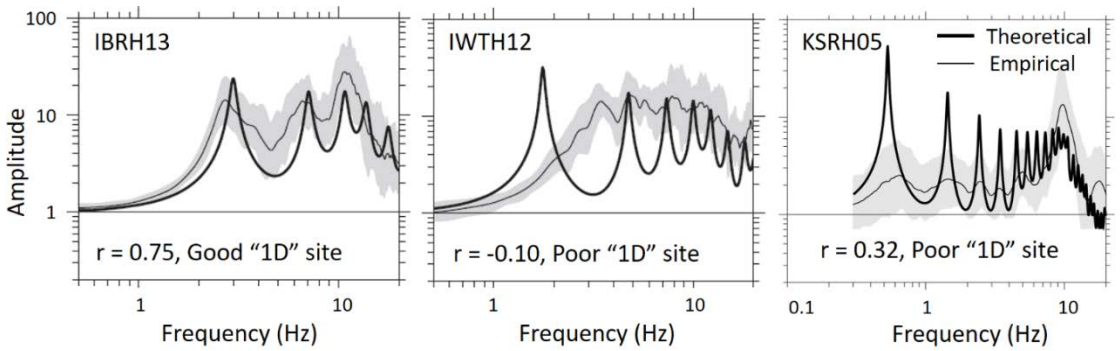

Figure 4.1. Example Sites for Evaluation of SH1D Assumption: IBRH13 and IWTH12 are adapted from Thompson *et al*., (2012); KSRH05 is adapted from Tao and Rathje (2019b).

More recently, the strict use of the Pearson correlation coefficient (*r*) to evaluate the alignment of peaks and goodness-of-fit of the empirical and theoretical transfer functions has been examined. Tao and Rathje (2019a) analyzed in detail four downhole array sites in an effort to evaluate the level of small-straining damping required to best match the empirical recordings. Qualitatively, these four sites displayed theoretical transfer functions whose peaks aligned well with the empirical transfer functions, yet the computed values of *r* were small for some sites due to the fact that this parameter is significantly affected by peaks in the data (Legates and McCabe 1999). Although increasing the damping in the

soil resulted in larger values of *r*, it would be difficult to determine apriori how much damping would be required to achieve an appropriate *r*.

Zalachoris and Rathje (2015) evaluated 1D ground response analysis using 11 downhole array sites and attempted to understand the subsurface characteristics that were associated with the best fit to the 1D analysis. They found that the best fit occurred at sites with an impedance contrast within the shear wave velocity (*Vs*) profile, and a slightly poorer fit occurred for sites that did not have an impedance contrast but only if the base sensor was at a depth less than about 100 m. A poor fit was observed for sites with no impedance contrast and a deep (> 200 m) base sensor.

These previous studies have indicated that, perhaps, relatively few downhole array sites are modeled well by 1D ground response analysis. However, the use of strict quantitative measures of analysis may result in an underestimation of the number of sites modeled well by 1D analysis. Additionally, the previous studies have focused on taxonomies that can only be applied to downhole array sites, and thus these taxonomies cannot be applied to non-downhole array sites which represent almost all the sites analyzed in engineering practice. In an effort to improve the evaluation of the applicability of 1D ground response analysis, this study develops a taxonomy that uses the theoretical transfer functions for a site and the H/V Spectral Ratio (*HVSR*, Nakamura 1989) to classify sites into groups that represent different characteristics of ground response. Importantly, this taxonomy takes into the account the difference in boundary conditions for a downhole array (i.e., within

boundary condition) and for a typical site analyzed in practice (i.e., outcrop boundary condition). This taxonomy is developed through analysis of downhole array data but is applicable to non-downhole array sites that are encountered in practice.

4.2 DISTINGUISHING PSEUDO-RESONANCES FROM TRUE-RESONANCES

An important issue not considered in previous studies that used downhole array data to evaluate 1D response is the effect of the assumed boundary condition at the base, downhole sensor. Traditionally, a within boundary condition is assumed at the downhole depth, which accounts for the down-going wave effect and pseudo-resonances associated with the material above the downhole sensor. However, forward analyses performed in practice for non-downhole array sites use outcrop motions as the input motions and thus use an outcrop boundary condition at the base of the soil column.

At any point in a downhole wavefield there generally exist both up-going (incident) and down-going (reflected) waves, and the within boundary condition accounts for both of these waves. The outcrop boundary condition assumes that only the up-going wave is present at the base sensor, and this boundary condition is used in forward site response analyses because the input motions applied at the base of the soil column represent recorded rock motions at the ground surface.

Tao and Rathje (2019b) investigated the effect of the assumed boundary condition on the predicted theoretical transfer functions for hypothetical sites with different velocity

profiles. They showed that for sites with a deeper velocity impedance contrast the effect of the boundary condition was simply to change the amplitudes of the peaks in the transfer function. However, sites with no impedance contrast or a shallow velocity impedance contrast displayed drastically different responses for the within and outcrop boundary conditions. For example, Figure 4.2 shows the within (TF_{within}) and outcrop ($TF_{outcrop}$) transfer functions for two hypothetical sites with a velocity impedance contrasts (IC) of 5 and two depths to the velocity contrast for a 100 m downhole array. For the site with the large IC at a very shallow depth of 5 m, $TF_{outcrop}$ has a single peak at 10 Hz associated with the 5-m thick layer near the surface, while TF_{within} has multiple peaks and the lowest frequency peak is at 2.5 Hz. The lower frequency peaks are pseudo-resonances that simply due to the down-going wave effect, while the 10 Hz peak is the true resonance of the site. For a deeper IC, the peaks align better such that both the within and outcrop transfer functions predict similar frequencies of amplification. Tao and Rathje (2019b) showed that the f_1 ratio, defined as the ratio of the first resonant peak frequency ratio in the $TF_{outcrop}$ and TF_{within} (i.e., $f_{1,outcrop} / f_{1,within}$), can be used to identify pseudo-resonances for a site. Additionally, they showed that the size of the IC and the depth of the IC control the f_1 ratio (Figure 4.2).

Another tool that can be used to identify true resonances from pseudo-resonances is the H/V Spectral Ratio (*HVSR*). The *HVSR*, defined as the ratio between the horizontal and vertical *FAS* of surface recordings, was first introduced by Nogshi and Igarashi (1971)

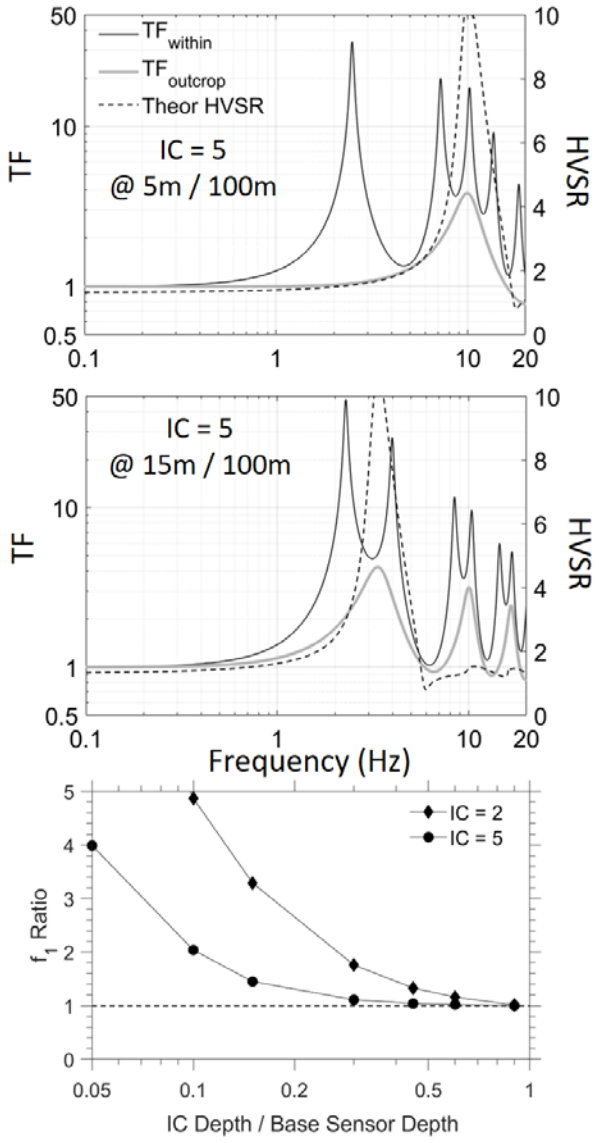

Figure 4.2. The Influences of Size and Depth of Impedance Contrast (IC) on Pseudo-resonances.

and was further developed by Nakamura (1989, 2000). A large number of studies have successfully linked the peak frequency in the *HVSR* to the fundamental resonant frequency of a soil deposit (e.g., Lermo and Chávez-García, 1994; Field and Jacob, 1995; Seekins *et al.*, 1996; Bard *et al*., 1997; Bard *et al*, 2005; Haghshenas *et al*., 2008). Theoretical *HVSR* curves can be computed from a *Vs* profile using the Diffuse Field Approach (DFA) developed by Sánchez-Sesma *et al.* (2008, 2011) and implemented in the program HV-INV (García-Jerez *et al*. 2016). Tao and Rathje (2019b) used the HV-INV to compute the theoretical *HVSR* for hypothetical *Vs* profiles and showed that the peak in the theoretical *HVSR* corresponds with the peak in the outcrop transfer function. These theoretical *HVSR* spectra are shown in Figure 4.2 for the hypothetical *Vs* profiles, and the *HVSR* peaks clearly align with the peak in the outcrop *TF*.

Based on the above observations, Tao and Rathje (2019b) proposed that only frequencies associated with true resonances be taken into account when using downhole arrays to evaluate 1D site response analysis. They recommended that the frequencies associated with true resonances be identified from the outcrop *TF* for the measured *Vs* profile and the empirical *HVSR* spectra. Additionally, they proposed that the fit between the theoretical *TF* and empirical *TF* be assessed, qualitatively, rather than quantitatively using *r*.

4.3 Data Selection and Analysis

In this study a total of 34 downhole array sites are analyzed, including 28 sites in Japan, 5 sites in the United States and 1 site in Greece (Table 4.1). The Japanese sites were

Table 4.1 Summary of Sites Studied

Site Code	**Depth of Base Sensor (m)**	Vs_{30} **(m/s)**	Vs_{base} **(m/s)**	**No. events**	**Group** This study	**Group** Thompson *et al* criteria
Delaney Park	61	265.9	944.9	6	A_1	LG
EuroSeisTest	200	225.6	2300	7	A_1	HG
Garner Valley	150	283.2	3000	50	A_1	LP
HYGH10	100	223.9	1341	60	A_1	LP
Treasure Island	122	176.4	2500	5	A_1	LG
FKSH16	300	531.6	1680	22	A_2	HG
IBRH17*	510	302.9	2300	31	A_2	LG
FKSH14	147	236.6	1210	33	A_3	HG
FKSH19	100	338.1	3060	18	A_3	LP
IBRH11	103	220.1	2371	39	A_3	HP
IBRH13	100	335.4	3000	72	A_3	LG
IWTH04	106	455.9	2300	21	A_3	HG
KSRH10	255	212.9	1700	54	A_3	HP
IBRH18*	504	461.5	2200	58	B_1	HP
KSRH05	330	470.1	800	86	B_1	LP
KSRH07	222	204.1	510	100	B_1	LP
MYGH05	337	302.6	690	42	B_1	LP
SZOH39*	103	559.5	1500	33	B_1	HP
TKCH05*	100	396.9	640	30	B_1	LP
EHMH02*	110	990.5	2195	125	B_2	LP
IWTH27*	100	595.9	2790	62	B_2	HP
KOCH05*	100	758.7	2040	18	B_2	HP
OKYH07*	100	933.3	2100	37	B_2	LP
OKYH14	100	709.9	2250	24	B_2	LP
El Centro - Meloland	240	176.2	615	5	C	LG
La Cienega (100m)	100	265.2	583.3	14	C	LG
La Cienega (252m)	252	265.2	666.7	6	C	LP
NMRH04	216	168.1	410	86	C	HP
HRSH03	200	486.8	2600	32	D_1	HP
IWTH12	100	367.9	1130	12	D_2	LP
SMNH02	101	502.7	1200	23	D_2	HP
KSRH06	237	294.8	660	76	D_3	LP
NIGH14	387	437.6	1330	58	D_3	HP
NGNH18	100	379.5	1300	35	D_3	HP
IWTH24	150	486.4	540	35	D_3	LP

Note: Sites marked with asterisk have *Vs* profiles modified.

selected from the KiK-Net (Kiban Kyoshin Network) strong-motion database, which is maintained by the National Research Institute for Earth Science and Disaster Prevention (NIED). The KiK-Net database provides abundant recordings of surface-downhole station pairs deployed at approximately 700 locations across Japan and most sites are characterized by downhole P-wave and S-wave measurements (Aoi *et al*., 2004). Three of the Californian downhole array sites (i.e., La Cienega, El Centro – Meloland, and Treasure Island) were selected from the Center for Engineering Strong Motion Data (CESMD, https://www.strongmotioncenter.org/), which collects and disseminates the records of ground and structural responses to earthquake motions of engineering interest (Haddadi *et al*. 2012). Two other US downhole array sites (Garner Valley, CA and Delaney Park, AK) were selected from the arrays currently maintained by the Earthquake Engineering Group at University of California at San Barbara (http://nees.ucsb.edu/).

Finally, the northern Greek downhole array site (i.e., EuroSeisTest) is part of a permanent accelerometric network maintained by a joint effect of multiple European organizations (Pitilakis *et al*., 1999). The information for data access for the aforementioned databases can be found in Data and Resources.

4.3.1 Data Processing

The sites were selected to span a wide range of geological conditions in terms of Vs_{30} and *Vs* at the depth of the base sensor. We also purposely selected some sites that Thompson *et al*. (2012) reported as having a poor fit with 1D analysis. To focus on only

the evaluation of 1D analysis, this study only analyzes linear-elastic, small-strain earthquake motions so as not to be compounded by nonlinear soil effects. To conduct the linear-elastic analysis, low intensity earthquake events were selected: the selection of events for most sites is limited by PGA at surface from 0.001g – 0.01 g. For some sites, slightly larger values of PGA were included (i.e, 0.01 g – 0.05 g) due to noisy records and low signal-to-noise ratios (SNR) for the smaller intensity motions. To confirm the linearity of the motions, the shear strain index was calculated for the selected events (i.e., $I_r = PGVs_{urface} / Vs_{30}$, Idriss, 2011). The I_r values are generally smaller than 0.01%, so the linear-elastic analysis is appropriate (Kaklamanos *et al*., 2015).

For this study, the filter frequency range for each site is identified by ensuring that both the surface and base recordings have SNR greater than 3.0. Then, the following processing steps were applied: removal of mean, application of a fifth-order Butterworth, time-domain, acausal filter over the defined frequency range, and baseline correction. The empirical transfer functions (i.e., $TF = FAS_{surface} / FAS_{base}$) are smoothed in the frequency domain using a log-scale rectangular window as described by Goulet *et al.* (2014) and the data is represented by its median and the $+/-2\sigma_{ln}$ range of the data in the same manner as Thompson *et al.* (2009).

In this study, instead of noise data, we utilize low intensity earthquake recordings to compute the *HVSR*. For each site, the empirical *HVSR* is represented by the average *HVSR* curve computed from individual *HVSR* corresponding to each earthquake motion.

The empirical *HVSR* for each individual motion is plotted to allow for the observation of the inter-event variability in the *HVSR*.

4.3.2 Vs Profile Calibration using HVSR

The theoretical *TF* are computed for each site from the measured *Vs* profile and an assumed small-strain damping ratio (D_{min}). The *Vs* profiles for all our selected sites were obtained from their database websites (see Data and Resources) and the D_{min} profiles were derived from the Darendeli (2001) empirical relationship based upon the in-situ stress and plasticity index. The D_{min} profiles were multiplied by a factor of 3, based on the results of Tao and Rathje (2019a). However, the provided *Vs* profiles may not be accurate for some sites, particularly near the surface. Recently, researchers have proposed using the peak frequency measured from *HVSR* as a constraint and check on measured *Vs* profiles (Teague *et al*., 2018).

For example, Figure 4.3 shows the *HVSR* based on the reported *Vs* profiles for sites KSRH05 and TKCH05, along with the empirical *HVSR*. For KSRH05 the reported *Vs* profile clearly does not fit the empirical *HVSR* at the peak frequency of about 10 Hz.

This resonant frequency is quite strong and represents a shallow, thin layer, which is difficult to characterize with borehole *Vs* methods (Stolte and Cox, 2019). The fit is improved by increasing the *Vs* of the top 4-m thick layer from 100 m/s to 150 m/s, which shifts the theoretical *HVSR* peak from 6.0 Hz to 9.3 Hz to match the empirical *HVSR* peak

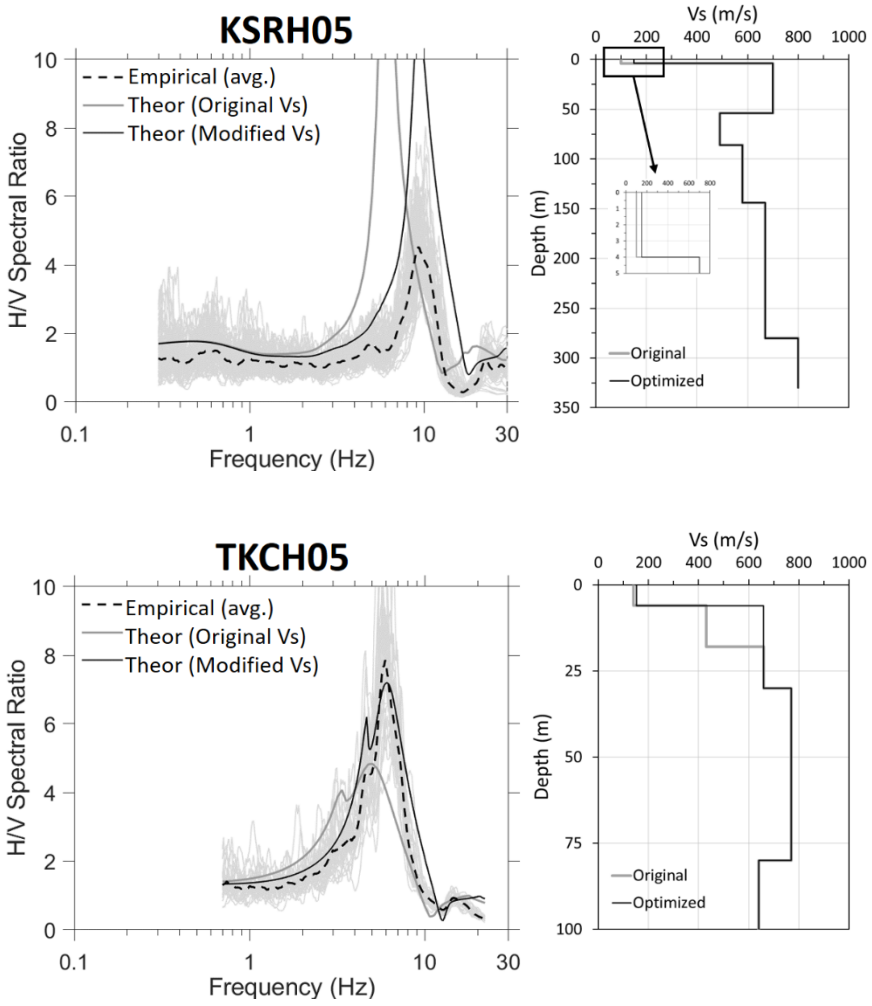

Figure 4.3. Example Sites for Vs Profile Calibration Using HVSR.

at 9.5 Hz. A slightly more extensive modification was required to better fit the data from site TKCH05, although the modifications were limited to the top 20 m.

For this study, empirical *HVSR* were computed for each site using recorded earthquake motions and for 8 of the 28 Kik-Net sites the *Vs* profile was modified to fit the peak in the *HVSR*. These modifications were generally limited to the top 20 m of the profiles,

with the reported profiles maintained at deeper depths. The reported *Vs* profiles and our modified *Vs* profiles are available in the electronic supplement accompanying this article.

4.4 PROPOSED SITE RESPONSE TAXONOMY

A site response taxonomy for downhole arrays is proposed that aims at differentiating sites based on the degree of pseudo-resonances and evaluating the fit of 1D site response analysis to the empirical site response over the frequencies associated with true resonances. The application of the proposed taxonomy is not limited to downhole array sites, but rather can be applied to any site with available wave velocity profiles (*Vp* and *Vs*) and empirical *HVSR* data. The taxonomy, summarized in Figure 4.4, assigns sites to one of four main groups:

- Group A: 1D sites dominated by true resonances
- Group B: 1D sites with both pseudo-resonances and true-resonances
- Group C: 1D sites dominated by pseudo-resonances
- Group D: Non-1D sites

The justification of the taxonomy is described below with examples for each taxonomy group. Although the justifications of the taxonomy utilize observations from downhole array data, the taxonomy criteria in Figure 4.4 utilize only information from *HVSR*, theoretical transfer functions, and details of the *Vs* profile. Thus, the taxonomy can be applied to non-downhole array sites.

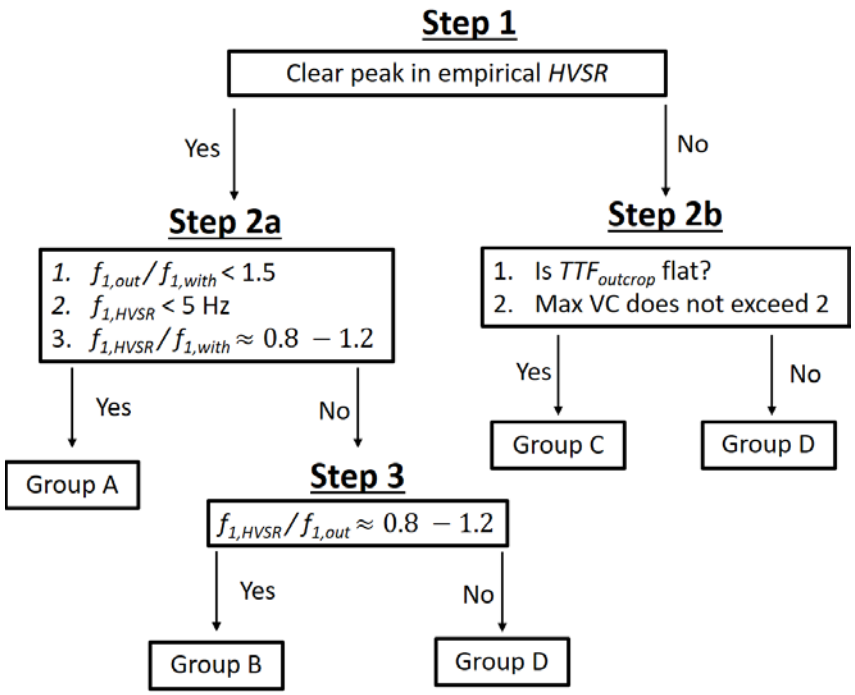

Figure 4.4. Flow Chart Showing the Steps for Site Response Taxonomy.

4.4.1 Group A: 1D Sites Dominated by True Resonances

The first step in the taxonomy (Figure 4.4) involves identifying a clear peak in the empirical *HVSR*. The peak in the averaged *HVSR* is defined by its frequency (f_{peak}) and its amplitude (A_{peak}). For a peak to qualify as a "clear" peak, it needs to be "strong" (i.e., A_{peak} greater than 3) and "distinguishable" (i.e., the *HVSR* curve falls below $0.5 \cdot A_{peak}$ within the frequency range from $0.5 \cdot f_{peak}$ to f_{peak} and the range from f_{peak} to $2 \cdot f_{peak}$). These criteria represent a revised and simplified version of the criteria defined by the SESAME guide-lines (Bard *et al*. 2005). Sites displaying a clear *HVSR* peak are usually associated with a strong impedance contrast, whereas sites without a clear *HVSR* peak are either flat or

contain multiple lower-amplitude peaks at similar frequencies. These sites are likely burdened with significant pseudo-resonances or contain non-1D effects.

If a clear *HVSR* peak is identified (Figure 4.4), the next step involves separating sites based on the presence of pseudo-resonances. This step involves three criteria: (1) an f_1 ratio < 1.5, which ensures that the first peak of the TF_{within} is mostly free from the down-going wave effect and associated pseudo-resonances; (2) the first resonant peak in the empirical *HVSR* (i.e., $f_{1,HVSR,}$) smaller than 5 Hz, which is used to exclude sites that are dominated by high frequency resonances controlled by shallow impedance contrasts; and (3) the ratio $f_{1,HVSR} / f_{1,within}$ in the range of 0.8 – 1.2, which ensures that the first peak in the TF_{within} is consistent with the empirical first mode resonant frequency indicated by the *HVSR*. If all criteria are fulfilled, the site is classified as Group A. These downhole array sites are well modeled by 1D analysis and are not significantly affected by pseudo-resonances. Of the 35 sites analyzed, a total of thirteen sites were assigned to Group A (Table 4.1).

Figure 4.5 shows three examples of sites categorized as Group A. For each site, Figure 4.5 shows plots of the transfer function responses, the *HVSR* responses, and the *Vs*

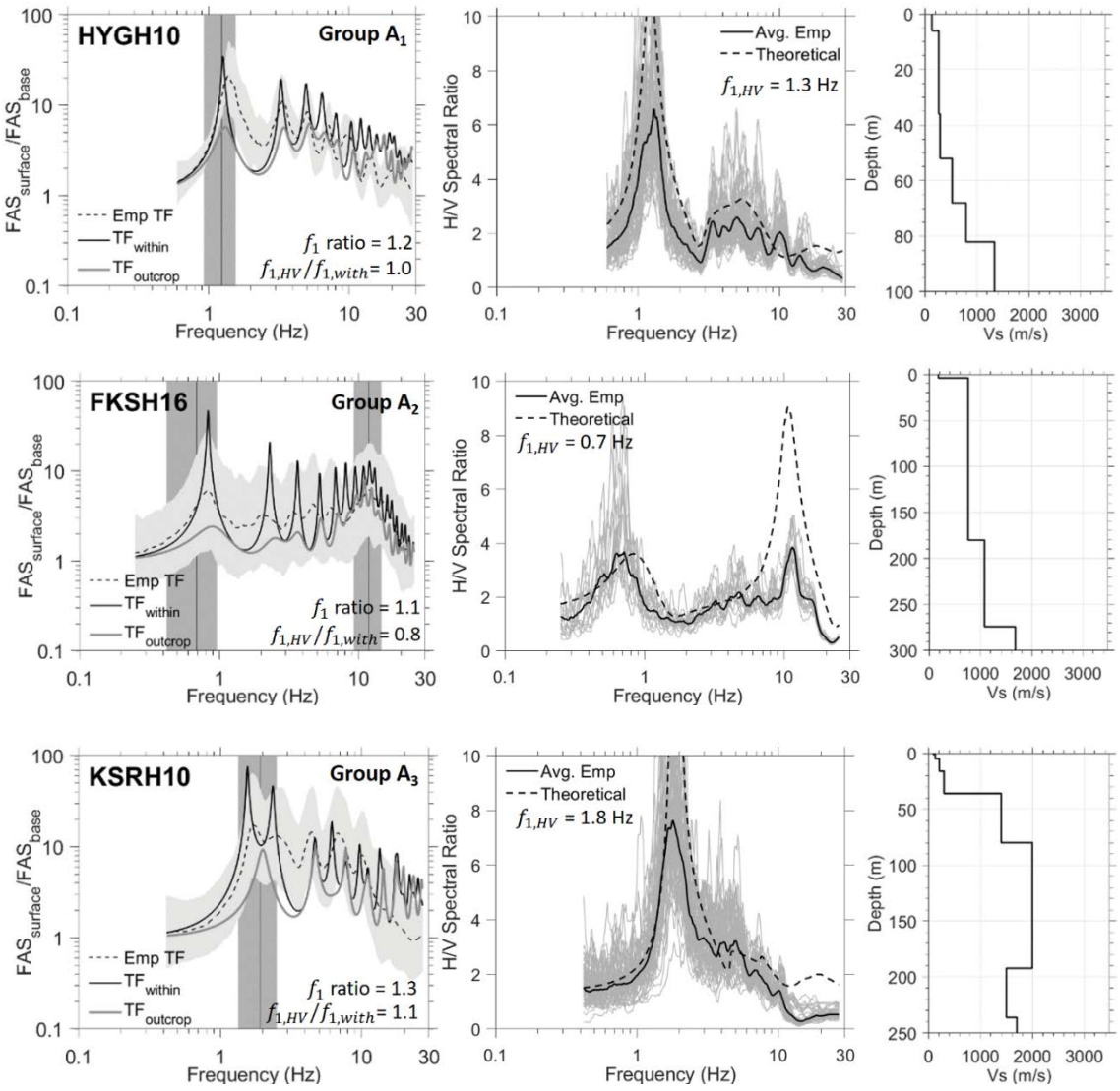

Figure 4.5. Transfer function responses, *HVSR* responses, and *Vs* profiles for three example sites from Group A.

profile used in the 1D model. To show the fit of the *HVSR* and *TF*, the vertical grey column in the *TF* plot represents the frequency range associated with the width of the *HVSR* peak, as measured by the frequencies associated with half of the maximum amplitude (i.e., $0.5 \cdot A_{peak}$) of the *HVSR* peak. For the three sites shown, the within and outcrop *TF* generally have similar peak frequencies with values of f_1 ratio less than 1.5, indicating that the *Vs* profile does not imply the presence of pseudo-resonances. The first mode peak frequencies from the *HVSR* and TF_{within} are similar (i.e., $f_{1,HVSR}$ / $f_{1,within}$ ratio of 0.8 – 1.2), indicating that $f_{1,within}$ captures the empirical *HVSR* fundamental site frequency. The empirical *TF* peaks align with the theoretical *TF* peaks and the empirical *HVSR*, indicating that 1D analysis models these sites well.

Across the three sites shown in Figure 4.5, there are some differences. For HYGH10, the empirical and theoretical *HVSR* show a single peak that corresponds with the first mode frequency in the *TF*. This site has a relatively deep impedance contrast that controls this first mode frequency. Four other sites that behave similarly and are considered Group A_1 are: Delaney Park (DP), EuroSeisTest (EST), Garner Valley (GV), and Treasure Island (TI). For FKSH16, Figure 4.5 shows two clear *HVSR* peaks at 0.7 Hz and 11.5 Hz, which are consistent with peaks in the empirical TF. The two peaks can be related to the deep impedance contrast at 274 m and the shallow impedance contrast at 4 m indicated by the *Vs* profile. Site IBRH17 displays a similar response and these two sites are considered Group A_2. Finally, the response of site KSRH10 is slightly more complex (Figure 4.5).

Although the f_1 ratio is less than 1.5, the outcrop *TF* shows a single peak around 2 Hz but the within *TF* has two peaks in this frequency range, indicating that the site is slightly affected by the down-going wave effect. This effect is due to the relatively shallow impedance contrasts as compared to the base of the downhole array. Nonetheless, the clear *HVSR* peak at 2 Hz is consistent with the empirical and theoretical *TF*, and thus this site is considered well-modeled by 1D analysis. Sites with a similar response are FKSH14, FKSH19, IBRH11, IBRH13 and IWTH04, and these are considered Group A_3.

Figure 4.6 summaries all the *Vs* profiles of the Group A sites. The A_1 sites all have the maximum velocity contrast (VC) at relatively deep locations as compared with

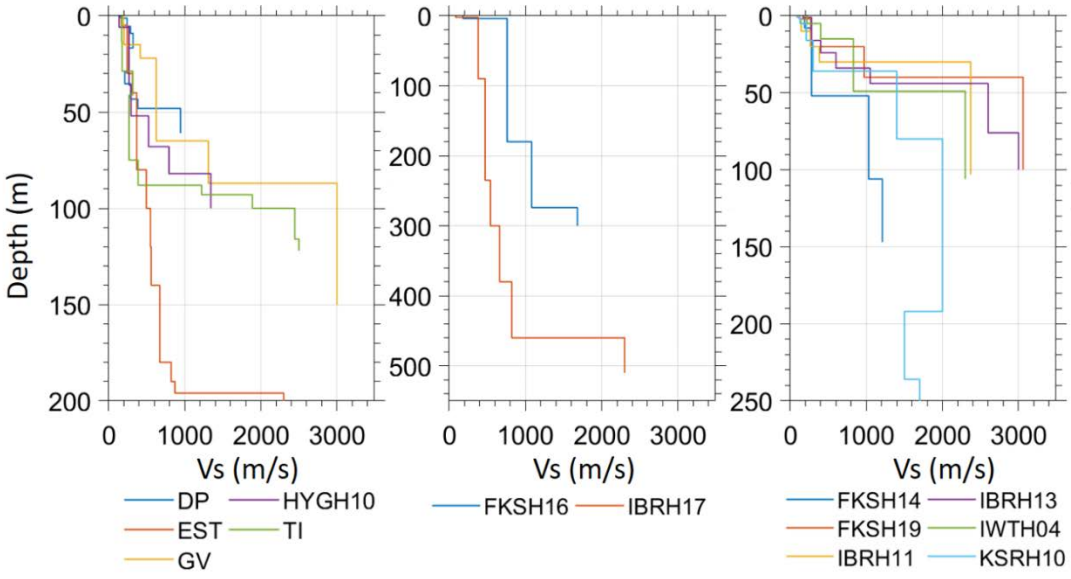

Figure 4.6. *Vs* Profiles for All Sites in Group A.

the depth of the base sensor, with the maximum VC occurring somewhere between 52% and 98% of the base sensor depth for these five sites. For the A_2 sites two VC are observed, one very close to the base sensor (VC depth ratio > 90%) and the other located at a VC depth ratio less than 2%. The A_3 sites have VCs generally in the shallow to the middle of the profiles, with VC depth ratio ranging from 14% to 46%.

4.4.2 Group B: 1D sites with Both Pseudo-Resonances and True-Resonances

Group B sites satisfy the initial criteria of having a clear *HVSR* peak, but they fail the criteria related to distinguishing the presence of pseudo-resonances (Step 2a in Figure 4.4). Although these sites may be influenced by pseudo-resonances, they may still be accurately modeled by 1D analysis. The potential for these sites to be modeled well by 1D analysis is evaluated using the first peak in the *HVSR* ($f_{1,HVSR}$) and first mode frequency in the outcrop *TF* ($f_{1,outcrop}$), which has been shown to represent a true resonance of a site (Tao and Rathje 2019b). If these frequencies are within about 20% (i.e., $f_{1,HVSR}$ / $f_{1,outcrop}$ ~ 0.8 to 1.2), the site is considered well modeled by 1D analysis in the frequency range associated with the true resonances of the site. A total of 11 sites were categorized as Group B.

Group B sites can be generally characterized as having moderate pseudo-resonances at lower frequencies and a clear higher frequency *HVSR* peak consistent with the response predicted by the outcrop transfer function. The Group B sites are distinguished into two subgroups based on distinct behaviors in the empirical *TF*. The 6 sites in Group

B_1 have consistent low-frequency pseudo-resonances in the empirical *TFs*, while the 5 sites in Group B_2 only display pseudo-resonances in the within *TF* but not in the empirical TF.

Examples from the B_1 and B_2 sites are shown in Figure 4.7. IBRH18 is a Group B_1 site and two low-frequency pseudo-resonances are observed in both the within and

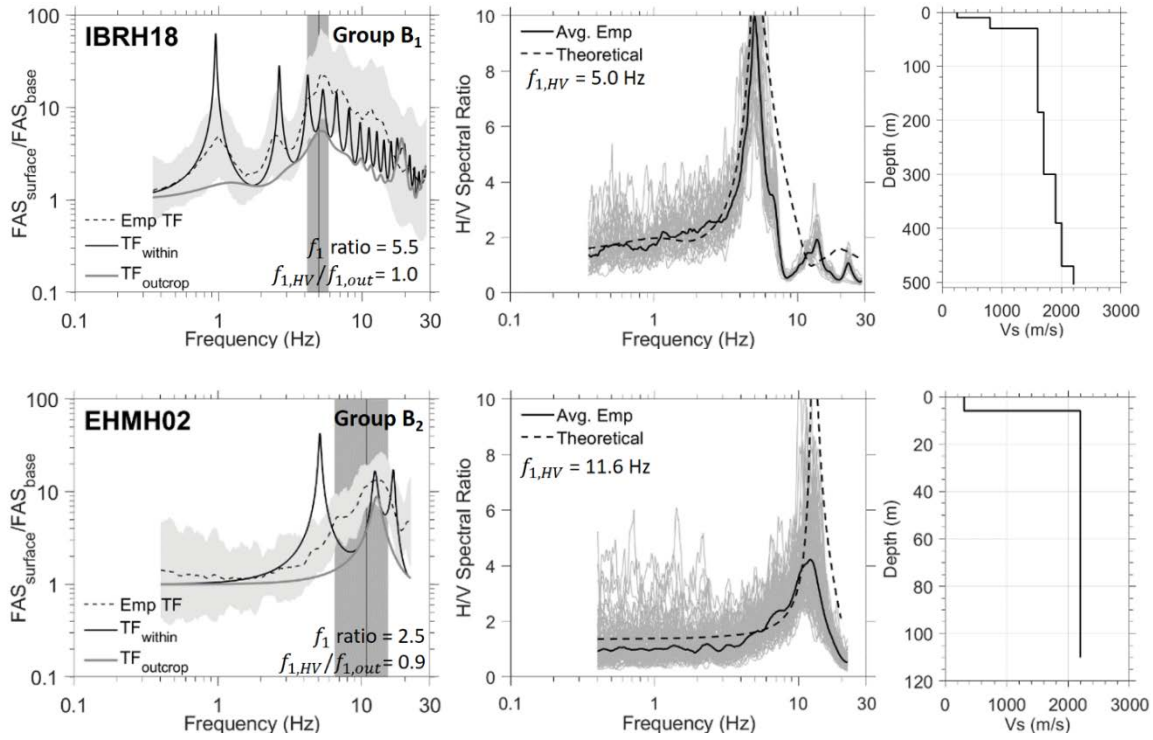

Figure 4.7. Transfer function responses, *HVSR* responses, and *Vs* profiles for two example sites from Groups B.

empirical *TFs*. These are considered pseudo-resonances because peaks are not observed in the outcrop *TF* at these frequencies. However, consistent peaks are observed in the

empirical, outcrop, and within *TFs* at about 5 Hz, and this frequency is also associated with a clear *HVSR* peak. This peak is controlled by the shallow impedance contrast in the *Vs* profile at 10 m. The other sites in Group B_1 are KSRH05, KSRH07, MYGH05, SZOH39, TKCH05.

The major difference that distinguishes Group B_2 from Group B_1 is the absence of pseudo-resonances in the empirical *TF*. For site EHMH02 (Figure 4.7) the empirical *TF* response is characterized by only a single peak at ~ 13 Hz, which is aligned with the outcrop *TF* and the clear *HVSR* peak at this frequency. However, the within *TF* exhibits a clear, lower frequency pseudo-resonance at 5.2 Hz, which is absent in the empirical *TF*. The other sites in Group B_2 are IWTH27, KOCH05, OKYH07, and OKYH14.

Figure 4.8 summaries the *Vs* profiles for Groups B_1 and B_2. All these sites generally share the common feature of having a shallow impedance contrast in the soil profile. The one difference is that Group B_1 sites are deeper and/or have a smaller *Vs* below the impedance contrast. The B_2 sites all reach a *Vs* of 2000 m/s within the top half of the profile.

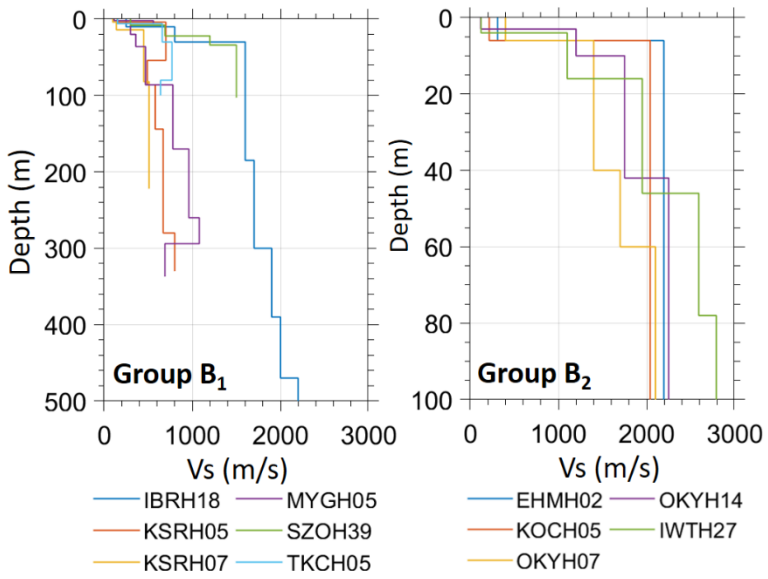

Figure 4.8. *Vs* Profiles for Sites in Groups B_1 and B_2.

4.4.3 Group C: 1D sites Dominated by Pseudo-Resonances

Group C sites fail the initial taxonomy criteria (Figure 4.4) because they do not have a clear *HVSR* peak. However, they also display a flat response in the outcrop *TF* (Step 2b, Figure 4.4), which is consistent with the *HVSR* data. Group C sites are deep soil sites with gradually increasing, yet generally smaller, *Vs* throughout the profile. The gradually increasing *Vs* is quantified by the maximum velocity contrast (VC) between adjacent layers in the profile, and sites with max VC less than 2 are classified as Site C (Step 2b, Figure 4.4). Interestingly, the empirical *TF* at these sites may be captured well by 1D analysis using the within boundary condition due to significant pseudo-resonances in both

the empirical and within *TF*. A total of 3 sites were categorized as Group C (La Cienega, El Centro - Meloland, and NMRH04).

Figure 4.9 shows the responses at Group C site La Cienega. The downhole sensors are located at multiple depths and the results from depths 100 m and 252 m are shown in Figure 4.9. For both depths, the within and empirical *TFs* agree very well indicated by the alignment of peaks. Because the outcrop *TFs* are almost flat in both cases, the peaks in the empirical *TF* are considered pseudo-resonances. Note that the peaks in the empirical *TF*

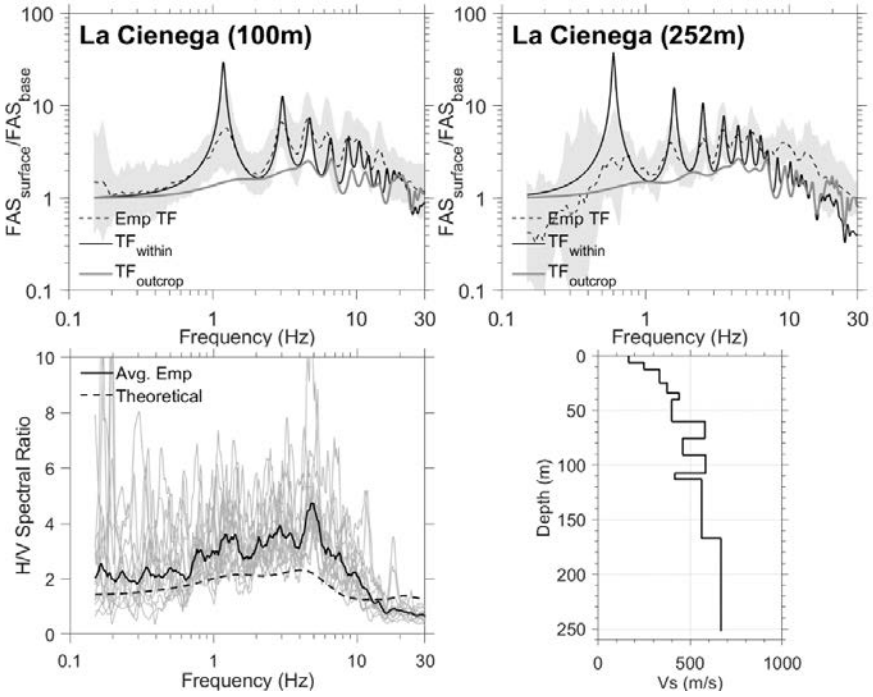

Figure 4.9. Transfer function responses, HVSR responses, and Vs profiles for one example site from Group C.

appear at different frequencies for the 100 m data (f_1 ~ 1.2 Hz) and the 252 m data (f_1 ~ 0.6 Hz). This observation is another indication that the downhole data are dominated by pseudo-resonances because the frequencies associated with pseudo-resonances will change with the depth of the downhole sensor. Note that there is no real velocity contrast in the

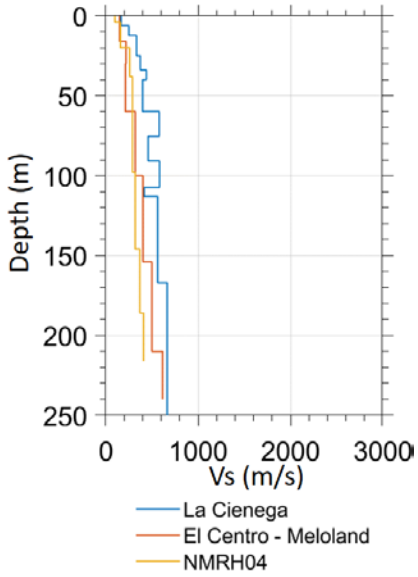

Figure 4.10. Vs profiles of Group C.

Vs profile at La Cienega and thus little information regarding the true-resonances of this site can be extracted from downhole array data, even if the empirical *TF* agrees well with the within TF. Figure 4.10 shows the *Vs* profiles for the three Group C sites and it is clear that they all exhibit a gradually increasing *Vs* throughout the profile. It is possible that these sites have a very deep velocity contrast and an associated very low site frequency

that could not be captured by the *HVSR* due to the low frequency limitations of the seismic station and the small magnitude earthquake signals analyzed.

4.4.4 Group D: Non-1D Sites

Group D sites are not modeled well by 1D analysis using either a within or outcrop TF. There are two paths through the taxonomy that may result in a site being classified as Group D. Group D_1 represents sites that have a clear *HVSR* peak but this peak does not correspond with either the peak in the within *TF* ($f_{1,within}$) or the peak in the outcrop *TF* ($f_{1,outcrop}$). Groups D_2 and D_3 represent sites that do not have a clear *HVSR* peak despite having velocity contrast above 2 within the profile.

Examples of the responses of the Group D sites are shown in Figure 4.11. Group D_1 only has one site, IWTH12. The empirical *TF* displays a very broad, plateau-like peak that spans from 3 to 12 Hz. The *HVSR* has a clear peak at 3.0 Hz but this frequency does not fall within ± 20% of either $f_{1,within}$ or $f_{1,outcrop}$, as indicated by both $f_{1,HVSR} / f_{1,within}$ and $f_{1,HVSR} / f_{1,outcrop}$ larger than 1.2. The theoretical *HVSR* for the *Vs* profile does show a peak at about 2 Hz, but the *Vs* profile would need significant modification to match the *HVSR* peak.

The responses of site HRSH03 from Group D_2 are shown in Figure 4.11. This site displays a single broad peak that spans from 6.7 to 11 Hz, with amplification as high as 40, yet the theoretical *TF* completely fail to capture this response. Despite the strong empirical

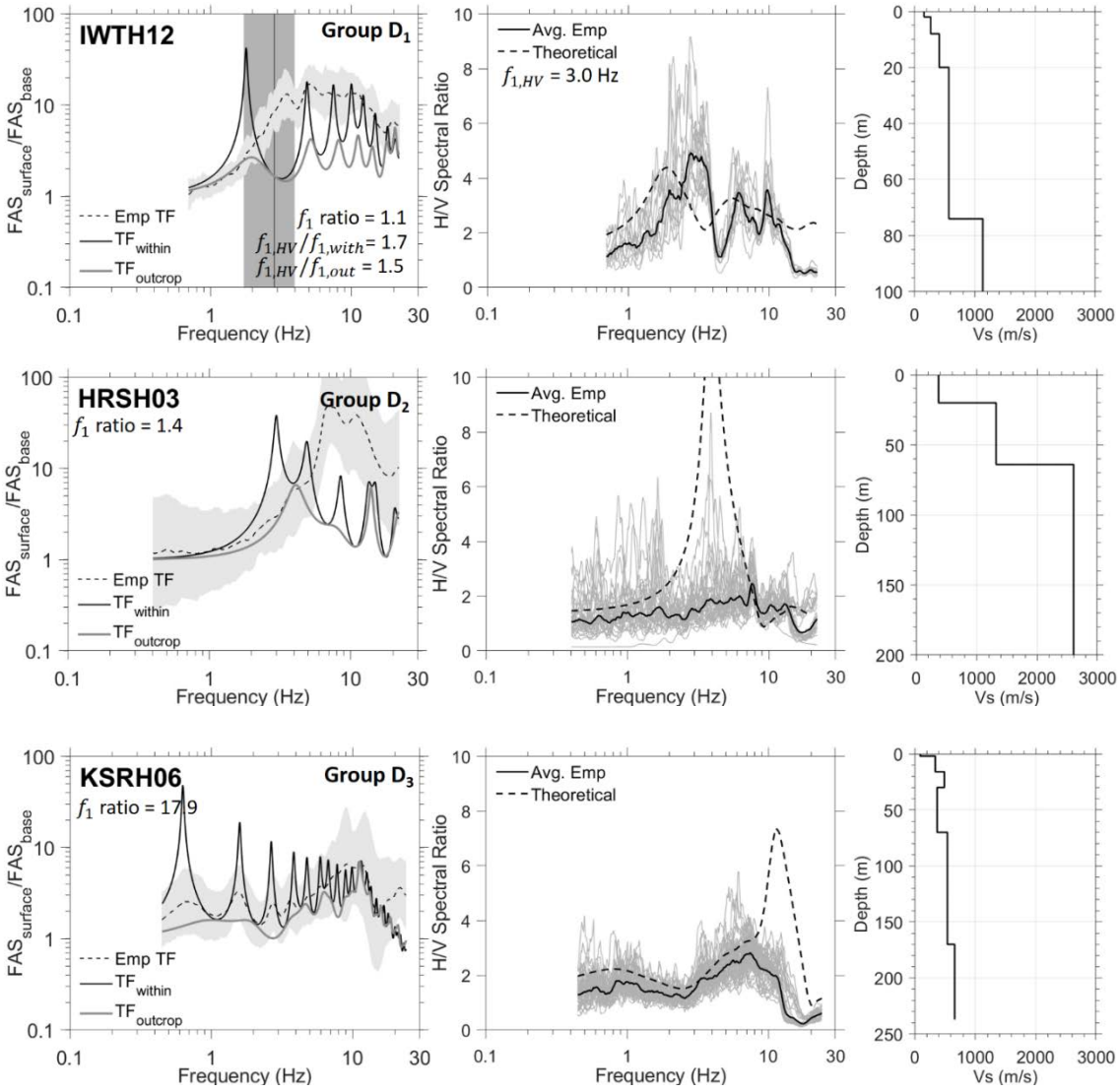

Figure 4.11. Transfer function responses, *HVSR* responses, and *Vs* profiles for three example sites from Group D.

TF, the empirical *HVSR* curve is almost flat and does not agree with the empirical response. Finally, the theoretical *HVSR* for this site does show a strong *HVSR* peak, but at a frequency that is not consistent with the empirical TF. This result may indicate errors in the measured *Vs* profile for this site. Three sites are categorized as Group D_2 (HRSH03, SMNH02 and NGNH18).

The responses of site KSRH06 from Group D_3 are shown in Figure 4.11. Judging from the *TF* responses, these four sites share some characteristics of Group B_1, weak low-frequency pseudo-resonances and a high-frequency true-resonance in the empirical *TF*. However, an important difference is that the high-frequency true-resonance is not verified by the empirical *HVSR*. Thus, Group D_3 sites are distinguished mainly by the lack of informative *HVSR* peaks. Group D_3 has three sites: KSRH06, NIGH14 and IWTH24.

Figure 4.12 shows all of the *Vs* profiles for Groups D sites. The *Vs* profiles for Groups D_1 and D_2 show little similarity, but the *Vs* profiles for the Group D_3 sites are similar to those from Group B_1 with a shallow velocity contrast.

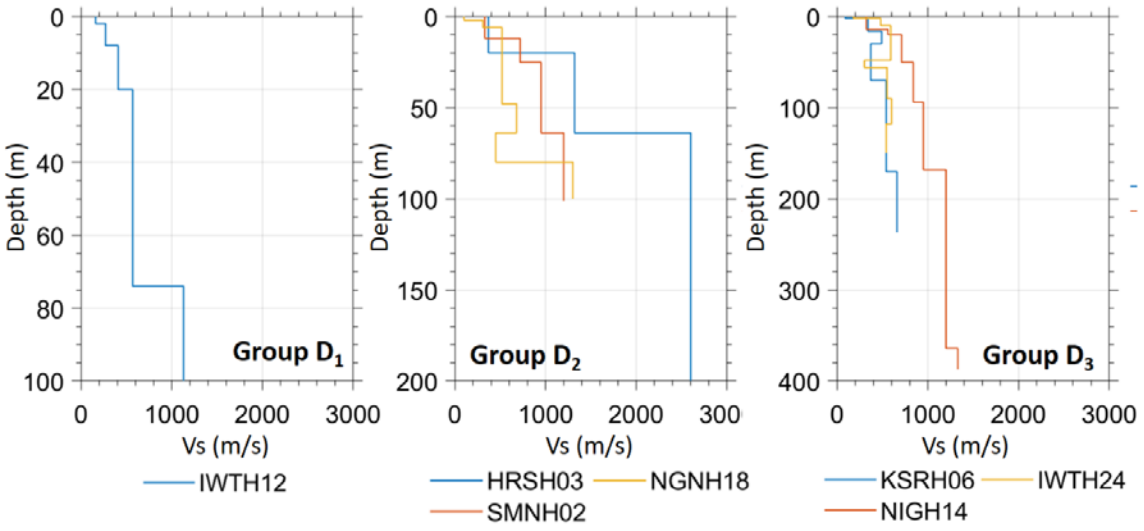

Figure 4.12. *Vs* Profiles Group D.

4.5 DISCUSSION

The features of the sites in each group defined above, along with their characterization via *HVSR*, are investigated to better understand what site characteristics lead to the difference responses associated with the different groups.

4.5.1 Frequencies of Site Amplification

Various indicators of the frequencies of site amplification have been discussed in this study: the first mode frequency of the empirical *HVSR* (denoted as $f_{1,HVSR}$), the first mode frequency of the empirical *TF* ($f_{1,ETF}$), the frequency of maximum amplification of the empirical *TF* ($f_{amp,max}$ (*ETF*)), the first mode frequency of the within *TF* (f_1 (TF_{within})),

and the first mode frequency of the outcrop *TF* (f_1 ($TF_{outcrop}$)). For the first mode frequencies, these always represent the lowest frequency peak in the transfer function.

Figure 4.13 compares these different frequencies with the $f_{1,HVSR}$ for Groups A, B_1, and B_2. Recall that Group A sites are modeled well by the ID analysis, while the Group B sites have moderate pseudo-resonances at lower frequencies and a clear higher frequency *HVSR* peak. The $f_{1,HVSR}$ is considered because it represents an empirical measure of the true resonant frequency of a site that can be measured at a non-downhole array site. It is important to consider first whether $f_{1,HVSR}$ is a good measure of the empirical site amplification. Figure 4.13 (a) compares $f_{1,HVSR}$ with $f_{1,ETF}$ and shows good agreement of these frequencies for both Groups A and B_2. The good agreement is a result of the first resonant peak in the empirical *TF* being free from the effects of pseudo-resonances. For Group B_1 sites, the data indicate $f_{1,ETF} < f_{1,HVSR}$ because the lower frequency peaks in the empirical *TF* are pseudo-resonances that do not show up in the *HVSR*. These lower frequency peaks in the empirical *TF* are commonly associated with smaller amplitudes (e.g., Figure 4.7) and thus $f_{amp,max}(ETF)$ may be a better measure of the true-resonant frequency. Figure 4.13 (b) shows that $f_{amp,max}(ETF)$ better agrees with $f_{1,HVSR}$ for most sites, although four sites show a poor match (Group A: FKSH16, IBRH13 and IBRH17, Group B_1: KSRH07). These sites showed a good match for $f_{1,ETF}$ but also have empirical *TF* with a strong high frequency peak due to a shallow impedance contrast.

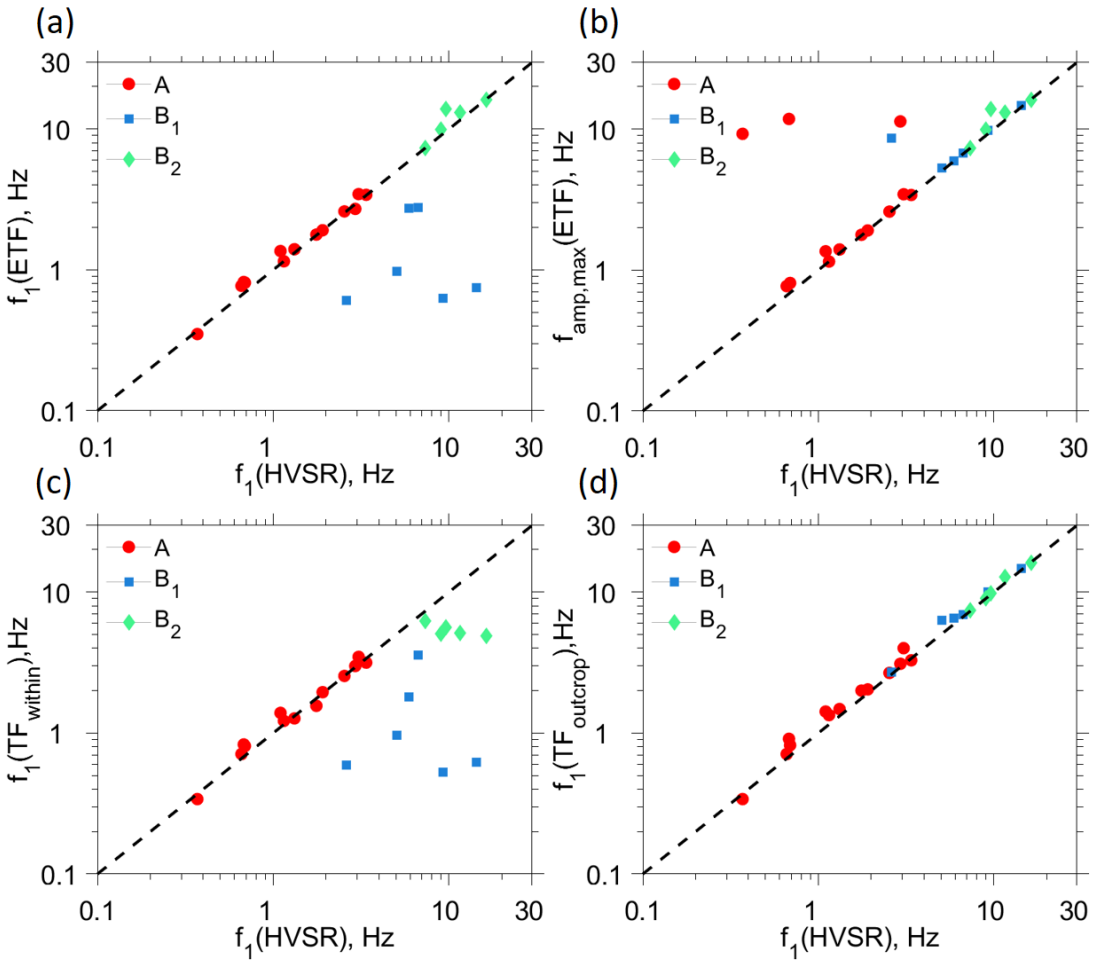

Figure 4.13. Comparison of frequencies of site amplification derived from *HVSR*, theoretical TF, and empirical *TF* for Groups A, B_1 and B_2.

Figures 4.13 (c) and (d) compare $f_{1,HVSR}$ with the first mode frequencies in the within and outcrop theoretical *TF*. For f_1 (TF_{within}), shown in Figure 4.13 (c), all the Group A sites show values close to $f_{1,HVSR}$ while Groups B_1 and B_2 show f_1 (TF_{within}) < $f_{1,HVSR}$. The

agreement in the frequencies for the Group A sites indicates that the first resonant mode is not affected by pseudo-resonances and these sites are suitable for 1D analysis. The predictions for Group B_1 and B_2 sites are subject to the influence of pseudo-resonances and thus f_1 (TF_{within}) does not match $f_{1,HVSR}$. However, when considering f_1 ($TF_{outcrop}$) in Figure 4.13 (d), the frequencies agree for these sites and all groups fall on the 1:1 line. Thus, the empirical *TF* for all sites in Groups A, B_1, and B_2 are modeled well by 1D analysis when using the outcrop boundary condition, which is the boundary condition appropriate for forward analysis.

Figure 4.13 also provides information regarding the frequency range of the true-resonances for the different sites. The first mode resonant frequencies for Group A are smallest, ranging from 0.2 to 4 Hz, while the Group B sites are larger with Group B_1 between 3 and 9 Hz, and Group B_2 between 7 and 16 Hz.

4.5.2 Comparison of Vs Profile Characteristics

The empirical ground response characteristics are driven by features in the subsurface layering at a site and the most important element is the presence of velocity contrast (VC) in the soil profile, as defined as the ratio between *Vs* in adjacent layers. Figure 4.14 compiles the max VC, depth of the max VC, and the *Vs* below the VC for all

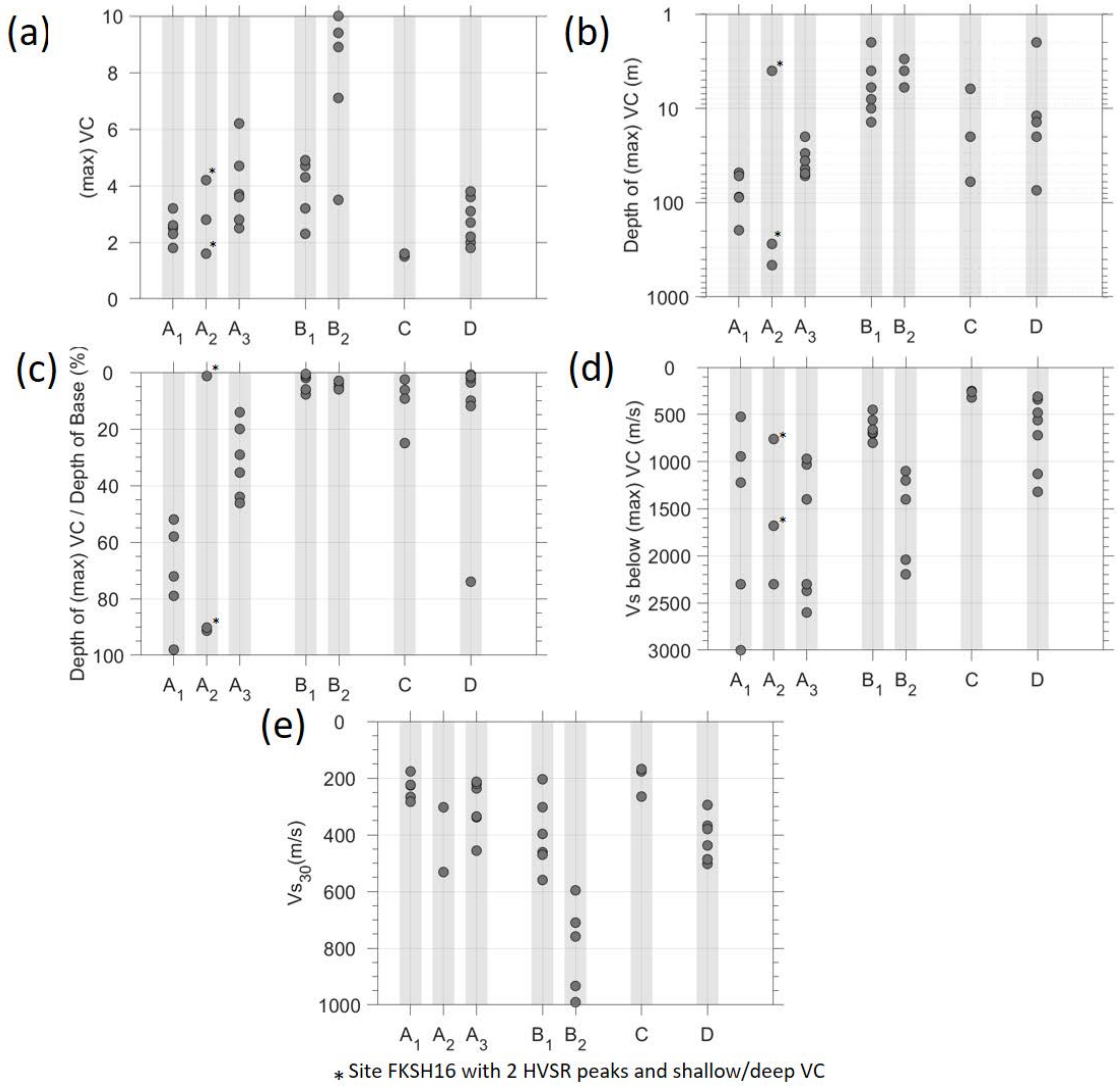

Figure 4.14. Comparison of Features of Shear Wave Velocity Profile across different taxonomy groups.

of the different groups, along with Vs_{30}. The Group A sites have a max VC in the range of 2 to 6, the max VC occurs at a depth greater than about 20 m, and the material below the

max VC is generally soft or hard rock with *Vs* greater than 1000 m/s. The Group A_1 and A_2 sites have the max VC generally in the bottom half of the profile, while the Group A_3 sites have the max VC in the top half. The Vs_{30} of these sites generally range from 180 to 300 m/s. The Group B_1 sites have a similar max VC as the Group A sites but the max VC occurs at a shallower depth (less than 10 m and within the top 10% of the profile) and the *Vs* of the material below the max VC is smaller. The Group B_2 sites have larger values of max VC of mostly between 7 and 10 at similarly shallow depths, but with a much larger *Vs* below the max VC. The shallower depth of the max VC for the Group B sites is what controls the presence of the pseudo-resonances in the theoretical within *TF* at these sites (see Figure 4.2), and the larger *V*s below the max VC appears to contribute to the absence of pseudo-resonances in the empirical *TF* for Group B_2 sites. The Vs_{30} of the Group B_2 (600-1000 m/s) sites are larger than for the Group B_1 sites (200-600 m/s).

The Group C sites have max VC less than 2 with very small *Vs* below the max VC (~300-400 m/s), indicative of the gradually increasing *Vs* at these sites with no significant VC above the base sensor depth. The Group D sites generally have max VC between 2 and 4 and the max VC occurs at a range of depths, although most are in the top 10% of the profile The Vs_{30} of the Group D sites range from 300 to 500 m/s.

4.5.3 Taxonomy Results Compared to Previous Studies

Thompson *et al*. (2012) used two metrics (i.e., inter-event variability, σ_i and Pearson correlation coefficient, *r*) in their taxonomy study. We applied their classification

criteria to the analysis of the sites in this study and the results for each site are listed in Table 4.1. Table 4.2 compares the results from the two taxonomy criteria. Note that the inter-event variability is not considered in this study and thus the comparison is focused on the level of match between the empirical and theoretical *TF* (i.e., G = Good (LG/HG) *Vs*. P = Poor (LP/HP)). For our study, Groups A, B, and C are considered sites well-modeled with 1D analysis and only Group D sites are considered non-1D sites.

Table 4.2 Comparison of Taxonomy with Thompson *et al*. (2012)

Group	LG/HG	LP/HP	Total
A	8	5	**13**
B	0	11	**11**
C	2	2	**4**
D	0	7	**7**
Total	**10**	**25**	**35**

Eight of the 13 Group A sites are classified as G, but five are classified as P. Based on this study, Group A sites are the most suitable for 1D analysis so the large number of P sites is surprising. For these sites, visual judgement in this study indicated good alignment of resonant peaks between the empirical and theoretical *TF* although the *r* values were still less than 0.6. As noted by Tao and Rathje (2019a), the *r* values are sensitive to the peaks in the *TF* and thus the level of damping modeled. It is for this reason that in this study we used visual judgement to assess the alignment of peaks, which results in more sites being considered 1D sites.

All the Group B sites are considered P sites using the Thompson *et al*. (2012) criteria. This result is mainly because these sites are affected by pseudo-resonances, which tend to be stronger in the theoretical within *TF* than the empirical *TF* and lead to small values of *r*. We consider the Group B sites as 1D sites because they capture accurately the true resonance of each sites, as defined by the *HVSR*, when using the outcrop boundary condition. When using the outcrop *TF*, the computed *r* values are significantly increased with most above 0.8. One site of particular interest is TKCH05, which was categorized as LP in Thompson *et al*., (2012). They concluded that the poor fit to the 1D theoretical within *TF* was due to spatial variability across the site that scatters the down-going wave and minimize the pseudo-resonance in the empirical *TF*. This may, in fact, be the cause of the diminished pseudo-resonance at lower frequencies, but we argue that this site can still be modeled as 1D without consideration of spatial variability because the outcrop *TF* accurately captures the true resonance of the site at higher frequencies.

For Group C, two sites are considered P sites (i.e., NMRH04, La Cienega - 252m), while the other two sites are considered G sites (i.e., El Centro – Meloland, La Cienega – 100m). Group C sites are dominated by pseudo-resonances, and the strength of the pseudo-resonances in the empirical *TF* controls whether the computed values of *r* are large enough to classify a site as G. The within *TF* always has strong pseudo-resonances for Group C sites because they do not have a significant velocity contrast, so sites with weak pseudo-resonances in the empirical *TF* (e.g., La Cienega - 252m, Figure 4.9) will have smaller *r*

values and sites with stronger pseudo-resonances (e.g., La Cienega – 100m, Figure 4.9) will have larger *r* values.

As expected, all of the Group D sites are classified as P by the Thompson *et al*. (2012) criteria, which is consistent with the results of this study that found that these sites are not modeled well by 1D analysis.

4.6 CONCLUSIONS

In this study, we analyze the linear-elastic site response for 34 downhole array sites by comparing the empirical transfer functions with the theoretical transfer functions from SH1D analysis. The theoretical transfer functions consider two boundary condition assumptions at the depth of the base sensor of the downhole array and we also consider the site frequency implied by the *HVSR* technique. A taxonomy scheme is proposed that classifies the sites into different groups based on the similarity in their responses. The taxonomy distinguishes sites based on the presence of a clear *HVSR* peak, the presence of true-resonances *Vs*. pseudo-resonances at a site, characteristics of the theoretical *TF*, and features of the *Vs* profile. The primary goal of this classification scheme is to identify, apriori, sites that are suitable for 1D ground response analysis. The taxonomy proposed in this paper distinguishes itself from previous work in that it can be applied to any site (even non-

downhole array sites) in which the *HVSR* curve and *Vs* profile are measured, making it easily applicable to sites analyzed in engineering practice.

The taxonomy includes four major groups, Group A (1D sites dominated by true resonances), Group B (1D sites with both pseudo-resonances and true-resonances), Group C (1D sites dominated by pseudo-resonances), and Group D (Non-1D sites). Groups A through C are considered appropriate for 1D analysis. We have identified a total number of 24 sites (13 in Group A, 11 in Group B, and 4 in Group C) that can be modeled well by 1D analysis, which represents 71% of the total sites analyzed. Group A sites have a strong *HVSR* peak that tends to correspond with a strong velocity contrast within the profile and the true-resonance associated with the first mode frequency in the empirical transfer function. Group B sites also have a strong *HVSR* peak that is associated with a true-resonance of the site and this peak in captured by the 1D analysis, but these sites also have lower frequency pseudo-resonances in the theoretical within transfer functions that are not significant in the empirical transfer function. Because the outcrop transfer functions for the Group B sites capture the true-resonances and an outcrop transfer function is used in all forward analyses for sites in practice, we consider 1D analysis applicable to Group B sites. Group C sites are deeper, softer sites without a clear *HVSR* peak in which the response is dominated by pseudo-resonances. The empirical transfer functions at these sites generally were modeled well by the 1D within transfer function. Finally, Group D sites generally do not have a strong *HVSR* peak or have a strong *HVSR* peak that does not correspond with

any peaks in the theoretical or empirical transfer functions. This poor fit indicates that 1D analysis will not model the response of these sites well. More research is required to better understand the reason for the poor fit for these sites and to evaluate an appropriate analysis to estimate the ground response.

4.7 Data and Resources

Downhole array data (seismograms and boring log data) in Japan region used in this study were obtained from the KiK-net strong motion network (http://www.kyoshin.bosai.go.jp/, last accessed July, 2018). Downhole array data (seismograms and *Vs* measurement data) for the there Californian downhole arrays, La Cienega, El Centro – Meloland and Treasure Island were obtained from CESMD (https://www.strongmotioncenter.org/, last accessed August, 2018). Downhole array data (seismograms and *Vs* measurement data) for Garner Valley (CA), Delaney Park (AK) downhole arrays were obtained from NEES@UCSB (http://nees.ucsb.edu/, last accessed December, 2017). Downhole array data (seismograms and *Vs* profile data) for Euro-SeisTest site (Greece) was obtained from EUROSEISTEST Database (http://euroseisdb.civil.auth.gr/, last accessed December, 2017).

4.8 Acknowledgements

This study was supported by the U.S. Nuclear Regulatory Commission (NRC) under grant NRC-HQ-60-15-C-0005. This support is gratefully acknowledged.

4.9 REFERENCES

Aoi, S., Kunugi, T., & Fujiwara, H. (2004). Strong-motion seismograph network operated by NIED: K-NET and KiK-net. *Journal of Japan association for earthquake engineering*, 4(3), 65-74.

Bard P-Y, Duval AM, Lebrun B, Lachet C, Riepl J, Hatzfeld D. (1997). Reliability of the H/V technique for site effect measurement: an experimental assessment. *Proc.,17th International conference on soil dynamics and earthquake engineering*, Istanbul, 19–24 July 1997

Bard, P. Y., SESAME-Team, (2005). Guidelines for the implementation of the H/V spectral ratio technique on ambient vibrations measurements, processing and interpretation. *SESAME European Research Project* EVG1-CT-2000-00026.

Bonilla, L. F., Steidl, J. H., Gariel, J. C., & Archuleta, R. J. (2002). Borehole response studies at the Garner Valley downhole array, southern California. *Bull. Seism. Soc. Am.*, 92(8), 3165-3179.

Bradley, B. A. (2011). A framework for validation of seismic response analyses using seismometer array recordings. *Soil Dynamics and Earthquake Engineering*, 31(3), 512-520.

Darendeli, M. B. (2001). Development of a new family of normalized modulus reduction and material damping curves. *Ph.D. Dissertation, University of Texas at Austin*, 296-298.

Field, E. H., & Jacob, K. H. (1995). A comparison and test of various site-response estimation techniques, including three that are not reference-site dependent. *Bull. Seism. Soc. Am.*, 85(4), 1127-1143.

García-Jerez, A., Piña-Flores, J., Sánchez-Sesma, F. J., Luzón, F., & Perton, M. (2016). A computer code for forward calculation and inversion of the H/V spectral ratio under the diffuse field assumption. *Computers & Geosciences*, 97, 67-78.

Goulet, C. A., C. H. Cramer, R. B. Darragh, W. J. Silva, Y. M. A. Hashash, J. Harmon, J. P. Stewart, K. E. Wooddell, and R. R. Youngs. (2014). *PEER NGA-East database*. PEER Report 2014, 17.

Haddadi, H., Shakal, A., Huang, M., Parrish, J., Stephens, C., Savage, W., & Leith, W. (2012). *Report on progress at the center for engineering strong motion data (CESMD)*. In 15th World conference on earthquake engineering. Lisbon, Portugal (pp. 1-7).

Haghshenas, E., Bard, P. Y., Theodulidis, N., and SESAME WP04 Team. (2008). Empirical evaluation of microtremor H/V spectral ratio. *Bulletin of Earthquake Engineering*, 6(1), 75-108.

Idriss, I. M. (2011). Use of *Vs*30 to represent local site conditions. *In Proceedings of the 4th IASPEI/IAEE international symposium*. Effects of source geology on seismic motion, August (pp. 23-26).

Kaklamanos, J., Baise, L. G., Thompson, E. M., & Dorfmann, L. (2015). Comparison of 1D linear, equivalent-linear, and nonlinear site response models at six KiK-net validation sites. *Soil Dynamics and Earthquake Engineering*, 69, 207-219.

Kramer, S. L. (1996). *Geotechnical Earthquake Engineering*, Prentice-Hall, New Jersey, pp. 255.

Legates, D. R., and McCabe, G. J. (1999). Evaluating the use of "goodness-of-fit" measures in hydrologic and hydroclimatic model validation. *Water resources research*, 35(1), 233-241.

Lermo, J., and Chávez-García, F. J. (1994). Are microtremors useful in site response evaluation? *Bull. Seism. Soc. Am.*, 84(5), 1350-1364.

Nakamura, Y. (1989). A method for dynamic characteristics estimation of subsurface using microtremor on the ground surface. *Railway Technical Research Institute, Quarterly Reports*, 30(1).

Nakamura, Y. (2000). Clear identification of fundamental idea of Nakamura's technique and its applications. *Proc., XII World Conf. Earthquake Engineering*, New Zealand, Paper no 2656.

Nogoshi, M., and T. Igarashi. (1971). On the amplitude characteristics of microtremor (part 2). *J. Seism. Soc. Japan*, no. 24, 26–40 (in Japanese with English abstract).

Pitilakis, K., Raptakis, D., Lontzetidis, K., Tika-Vassilikou, T., & Jongmans, D. (1999). Geotechnical and geophysical description of EURO-SEISTEST, using field, laboratory tests and moderate strong motion recordings. *Journal of Earthquake Engineering*, 3(03), 381-409.

Sánchez-Sesma, F. J., Pérez-Ruiz, J. A., Luzón, F., Campillo, M., & Rodríguez-Castellanos, A. (2008). Diffuse fields in dynamic elasticity. *Wave motion*, 45(5), 641-654.

Sánchez-Sesma, F. J., Rodríguez, M., Iturrarán-Viveros, U., Luzón, F., Campillo, M., Margerin, L., ... & Rodríguez-Castellanos, A. (2011). A theory for microtremor H/V spectral ratio: application for a layered medium. *Geophysical Journal International*, 186(1), 221-225.

Satoh, T., Hayakawa, T., Oshima, M., Kawase, H., Matsushima, S., Nagashima, F., & Tobita, K. (2014). Site Effects on Large Ground Motions at KiK-net Iwase Station IBRH11 during the 2011 Tohoku Earthquake. *Bull. Seism. Soc. Am.*, 104(2), 653-668.

Satoh, T., Kawase, H., & Sato, T. (1995). Evaluation of local site effects and their removal from borehole records observed in the Sendai region, Japan. *Bull. Seism. Soc. Am.*, 85(6), 1770-1789.

Seekins, L. C., Wennerberg, L., Margheriti, L., and Liu, H. P. (1996). Site amplification at five locations in San Francisco, California: A comparison of S waves, codas, and microtremors. *Bull. Seism. Soc. Am.*, 86(3), 627-635.

Steidl, J. H., Tumarkin, A. G., & Archuleta, R. J. (1996). What is a reference site?. *Bull. Seism. Soc. Am*, 86(6), 1733-1748.

Stolte. A. C. and Cox. B. R. (2019). Towards consideration of epistemic uncertainty in shear wave velocity measurements obtained via SCPT. *Canadian Geotechnical Journal.* (submitted)

Tao, Y., Rathje, E. M. (2019a). Insights into Modeling Small-Strain Site Response Derived from Downhole Array Data. *J. Geotech. Geoenv. Eng*. (accepted).

Tao, Y., Rathje, E. M. (2019b). The Influence of the Down-going Wave and Pseudo-resonances on Downhole Array Data. *Bull. Seism. Soc. Am.*. (submiteed).

Teague, D. P., Cox, B. R., & Rathje, E. M. (2018). Measured *Vs*. predicted site response at the garner valley downhole array considering shear wave velocity uncertainty from borehole and surface wave methods. *Soil Dynamics and Earthquake Engineering*, 113, 339-355.

Thompson, E. M., Baise, L. G., Kayen, R. E., & Guzina, B. B. (2009). Impediments to predicting site response: Seismic property estimation and modeling simplifications. *Bull. Seism. Soc. Am.*, 99(5), 2927-2949.

Thompson, E. M., Baise, L. G., Tanaka, Y., & Kayen, R. E. (2012). A taxonomy of site response complexity. *Soil Dynamics and Earthquake Engineering*, 41, 32-43.

Zalachoris, G., and Rathje, E. M. (2015). Evaluation of one-dimensional site response techniques using borehole arrays. *J. Geotech. Geoenv. Eng.*, 141(12), 04015053.

Chapter 5: Summary, Conclusions and Recommendations

5.1 Summary and Conclusions

This research was focused on using downhole arrays to investigate the accuracy of one-dimensional (1D) seismic site response analysis. This type of analysis remains the state-of-the-practice in geotechnical earthquake engineering despite the fact that previous studies using downhole arrays have concluded that few sites are modeled well by the 1D approach, and even when sites are well-modeled by 1D analysis, the small strain damping (D_{min}) obtained from laboratory tests tends to over-predict the site response.

Towards addressing these issues, three main research efforts were undertaken: (1) an investigation into the phenomenon of pseudo-resonances and their impact on the interpretation of site response from downhole arrays (Chapter 2); (2) an assessment of the appropriate level of small-strain damping (D_{min}) needed to model the effects of seismic energy dissipation from wave scattering and to better match empirical site response (Chapter 3); and (3) development of a new taxonomy that can identify sites that are modeled well by 1D analysis, takes into account the complexities associated with pseudo-resonances in downhole array data, and can be applied to non-downhole array sites encountered in engineering practice (Chapter 4). The conclusions from each chapter are given below.

Chapter 2. Downhole arrays include sensors at the ground surface and at varying depth within the ground. The destructive interference between the up-going and down-going waves at locations within the ground results in diminished wave amplitudes at the

downhole sensor at frequencies related to the two-way travel time between the downhole and surface sensors. These diminished wave amplitudes can either increase the amplitude of the transfer function at the true resonant frequencies of a site or they can generate pseudo-resonances that are associated only with the depth of the base sensor. These pseudo-resonances do not reflect the true resonant frequencies of amplification that would be predicted in a forward site response analysis using an outcrop boundary condition. Pseudo-resonances occur for downhole array sites with little to no impedance contrast or for sites with an impedance contrast that is closer to the surface.

The within boundary condition used to analyze downhole array data incorporates the effects of the down-going wave. However, most site response analyses performed in engineering practice utilize the outcrop boundary condition because a downhole sensor is not available. Thus, when using downhole array data to assess the accuracy of 1D site response analysis it is important to focus on the true-resonances of the site that would be modeled by the outcrop transfer function (TF). To distinguish true-resonances from pseudo-resonances, it is recommended to consider the within TF, the outcrop TF, and the empirical horizontal to vertical spectral ratio (HVSR) spectra. All peaks in the outcrop TF are true-resonances, while peaks that are present in the within TF but not present in the outcrop TF are considered pseudo-resonances. The peaks in the empirical HVSR spectra represent true resonances and these peaks should align with the true-resonances present in the within and outcrop TFs. After identifying the true-resonances for a site, the comparison

of the empirical and theoretical TFs for a downhole array site should be focused over the frequencies associated with the true-resonances.

Chapter 3. Four well-characterized downhole array sites that are modeled well by 1D analysis were selected to identify the required increase in D_{min}, as quantified by the D_{min} multiplier, to match the empirical site response. This study is significant in three aspects: (1) the D_{min} multipliers were developed considering different ground response parameters that represent various aspects of ground shaking; (2) the D_{min} multipliers were compared across the different sites and the comparison was interpreted within the context of the local geology, depositional environment, and the potential for quantifying spatial variability in the shear wave velocity profile; and (3) approaches that take into account wave scattering by incorporating the *Vs* randomization were also considered.

The ground response characteristics that were used to characterize the site response were the transfer function (TF), response spectral amplification factors (AF), peak ground acceleration (PGA), peak ground velocity (PGV), Arias Intensity (Ia) and the change in the high-frequency spectra decay parameter ($\Delta\kappa$). The D_{min} multiplier varies from 1.5 to 5.0, depending on the characteristics considered. Across the four sites analyzed, the required D_{min} multipliers for the AF and for the time domain characteristics (PGA, PGV, and Ia) at each site were generally similar to one another and they are smaller than for the TF. For $\Delta\kappa$, the D_{min} multipliers were consistently around 3 for all sites. Across the four sites, Treasure Island required the smallest D_{min} multiplier, Delaney Park required the largest,

and Garner Valley and EuroSeisTest required intermediate values. Similarly, in terms of the shear wave velocity variability required to fit the response, Treasure Island needed the least, Delaney Park the most, and the other two sites were in between. It is hypothesized that the magnitude of the D_{min} multiplier may be related to the geologic depositional environment of the site, with larger D_{min} multipliers associated with more spatially variable geologic conditions. Treasure Island is located in the middle of a vast estuary environment with little variability, Delaney Park is located in a highly variable glacial environment, and Garner Valley and EuroSeisTest are both sediment-filled alpine valleys with moderate variability.

Chapter 4. A total of 34 downhole array sites were analyzed to compare the empirical transfer functions with the theoretical transfer functions from SH1D analysis. A taxonomy scheme was proposed that classifies the sites into different groups based on the similarity in their responses in terms of being modeled well by 1D analysis. The taxonomy distinguishes sites based on the presence of a clear HVSR peak, the presence of true-resonances vs. pseudo-resonances at a site, characteristics of the theoretical TF, and features of the *Vs* profile. The primary goal of this classification scheme was to provide a mechanism to identify, apriori, sites that are suitable for 1D ground response analysis. The proposed taxonomy distinguishes itself from previous work in that it can be applied to any site (even non-downhole array sites) in which the HVSR curve and *Vs* profile are measured, making it easily applicable to sites analyzed in engineering practice.

The taxonomy includes four major groups, Group A (1D sites dominated by true resonances), Group B (1D sites with both pseudo-resonances and true-resonances), Group C (1D sites dominated by pseudo-resonances), and Group D (Non-1D sites). Groups A through C are considered appropriate for 1D analysis. We identified a total number of 24 sites (13 in Group A, 11 in Group B, and 4 in Group C) that can be modeled well by 1D analysis, which represents 71% of the total sites analyzed. Group A sites have a strong HVSR peak that tends to correspond with a strong velocity contrast within the profile and the true-resonance associated with the first mode frequency in the empirical transfer function. Group B sites also have a strong HVSR peak that is associated with a true-resonance of the site and this peak in captured by the 1D analysis, but these sites also have lower frequency pseudo-resonances in the theoretical within transfer functions that are not significant in the empirical transfer function. Because the outcrop transfer functions for the Group B sites capture the true-resonances and an outcrop transfer function is used in all forward analyses for sites in practice, we consider 1D analysis applicable to Group B sites. Group C sites are deeper, softer sites without a clear HVSR peak in which the response is dominated by pseudo-resonances. The empirical transfer functions at these sites generally were modeled well by the 1D within transfer function. Finally, Group D sites generally do not have a strong HVSR peak or have a strong HVSR peak that does not correspond with any peaks in the theoretical or empirical transfer functions. This poor fit indicates that 1D analysis will not model the response of these sites well. More research is required to better

understand the reason for the poor fit for these sites and to evaluate an appropriate analysis to estimate the ground response.

5.2 Recommendations for Future Work

Based on the research presented in this dissertation, there remain several issues related to evaluating the accuracy of 1D site response analysis that still need investigation. These issues are discussed below.

The hypothesis proposed in Chapter 3 relating the D_{min} multipliers to the spatial variability of shear wave velocity given the local geologic conditions needs more investigation. The shear wave velocity variability can be quantified by conducting *Vs* measurements at multiple locations across a site and these investigations need to be performed at several different sites. With the subsurface *Vs* profile mapped spatially across a site, a better site-specific relatinoship between the *Vs* variability and required additional D_{min} may be established to benefit predicting site response more accurately.

In Chapter 3, 1D *Vs* randomization was utilized to model the site response due to spatially variable materials. Note that this approach is a simplified way to approximate the complexities associated with wave propagation through a multiple dimensional heterogeneous domain. Thompson *et al*. (2009) demonstrated that performing a 3D full wavefield analysis incorporating spatially correlated heterogeneity achieved a better match to the empirical site response. With proper characterization of 2D/3D seismic properties at a site and

available computational resources, this approach may improve the precision of site response estimates and gain more insights on the sites.

The HVSR technique has proven to be a useful tool for capturing important aspects of true site response. Many studies have been performed on implementing and interpreting HVSR measured from ambient vibrations (e.g., Lermo and Chávez-García, 1994; Seekins *et al.*, 1996; Bard *et al*., 1997; Bard *et al*, 2005; Haghshenas *et al*., 2008). This research demonstrated the application of HVSR using earthquake recordings. There are certainly similarities between the HVSR obtained from both sources; yet, in order for the earthquake HVSR to be more applicable, more work needs to be done in how to best interpret the HVSR data and define the clear peak.

Appendix

Yumeng Tao and Ellen M. Rathje

Summary and Results for 34 sites Analyzed

This appendix serves a supplement to Chapter 4 and it includes the computed empirical site responses (TF, HVSR) and theoretical estimates (TF_{within}, $TF_{outcrop}$, theoretical HVSR), Vs profiles used for the soil model for all the 34 sites. The supplement also includes tables that display the modified Vs profiles for 8 sites, Vs profile from another source for one site (IBRH13), integrated and modified profiles for 4 sites (Table 10 – 13, details in Tao and Rathje, 2019a). For the rest of sites in this study, the soil profile information is available in KiK-Net database (see 4.7 Data and Resources).

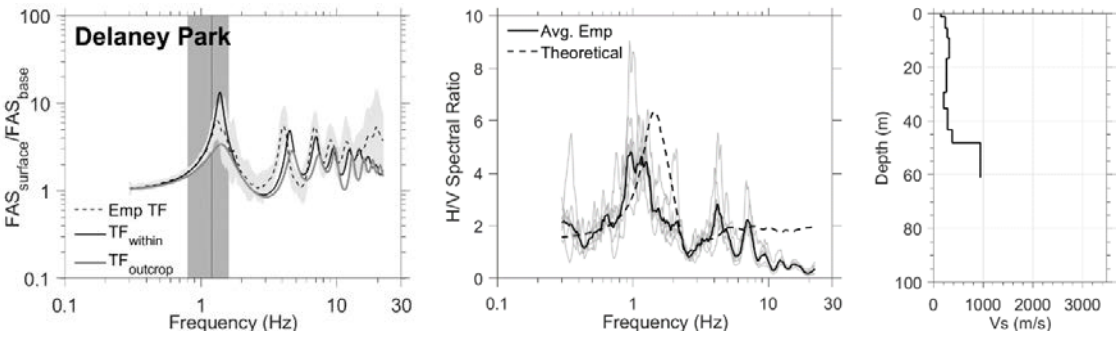

Figure A1. Group A_1: Plots for Delaney Park Downhole Array

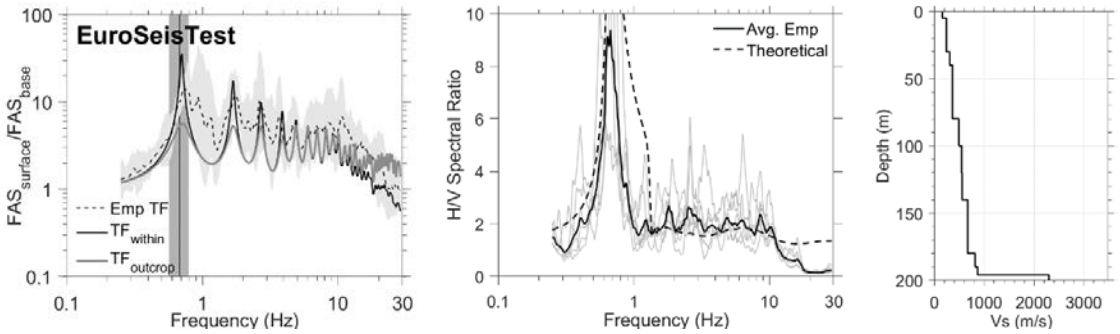

Figure A2. Group A_1: Plots for EuroSeisTest Downhole Array

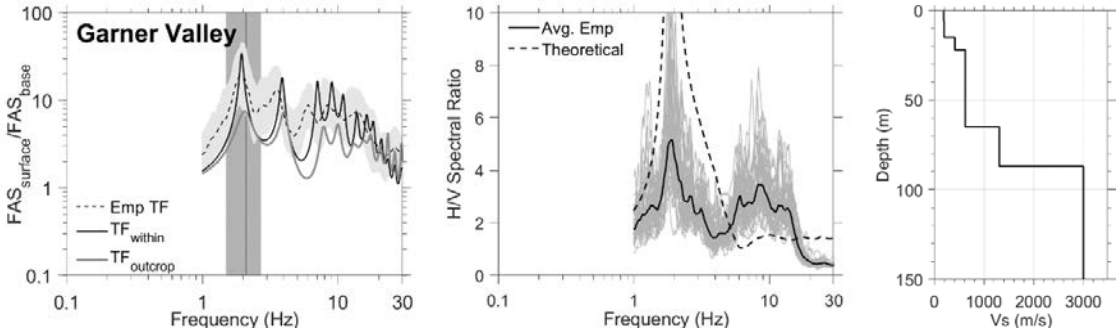

Figure A3. Group A_1: Plots for Garner Valley Downhole Array

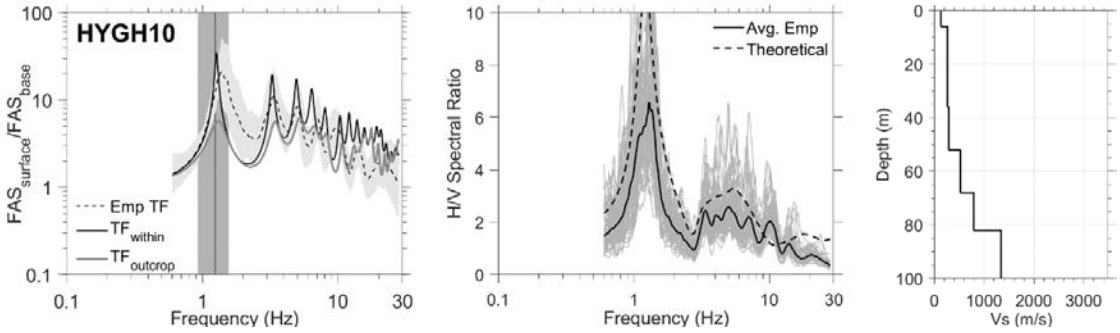

Figure A4. Group A_1: Plots for HYGH10

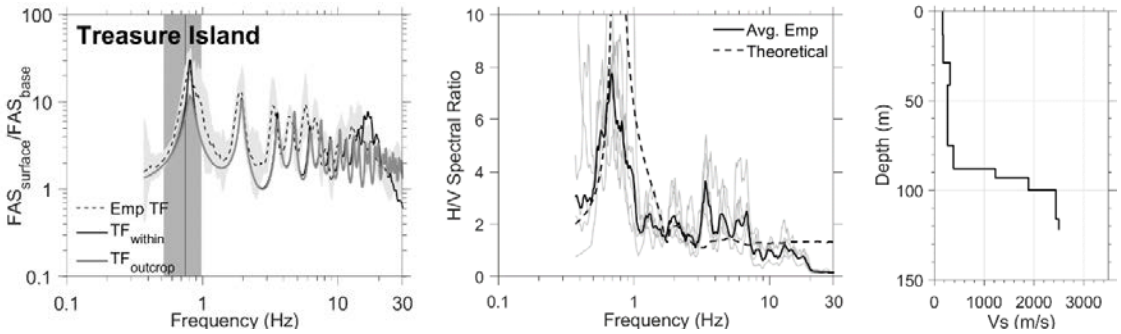

Figure A5. Group A_1: Plots for Treasure Island Downhole Array

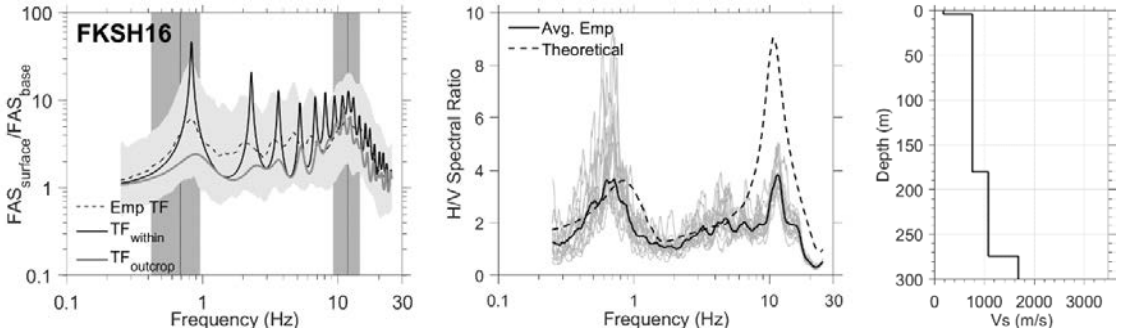

Figure A6. Group A_2: Plots for FKSH16

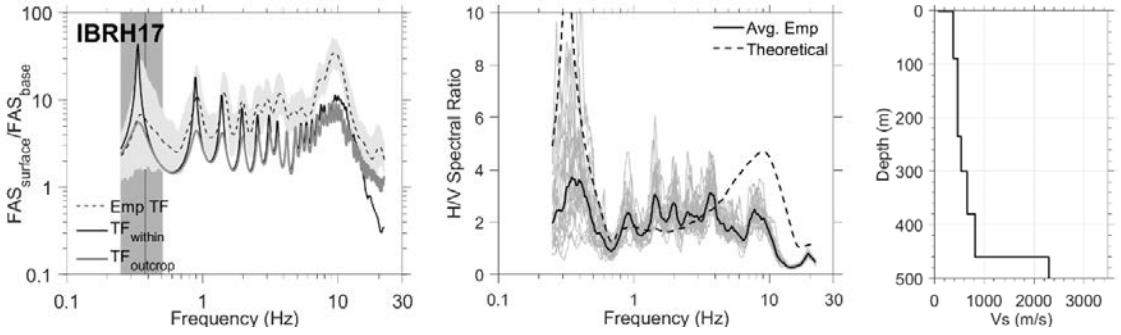

Figure A7. Group A_2: Plots for IBRH17

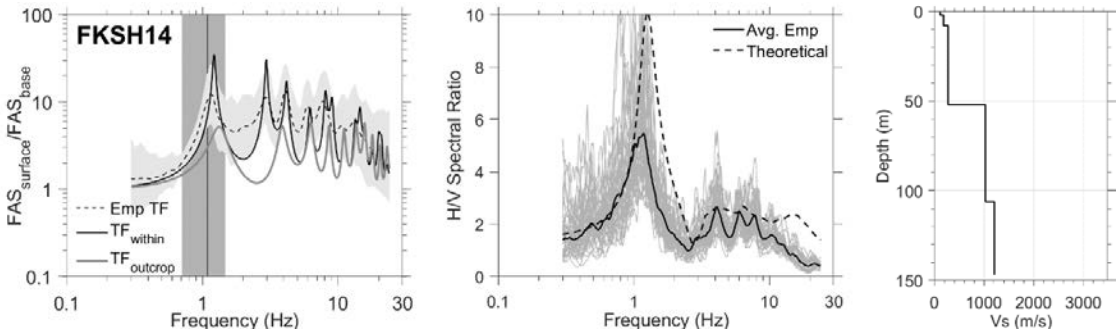

Figure A8. Group A_3: Plots for FKSH14

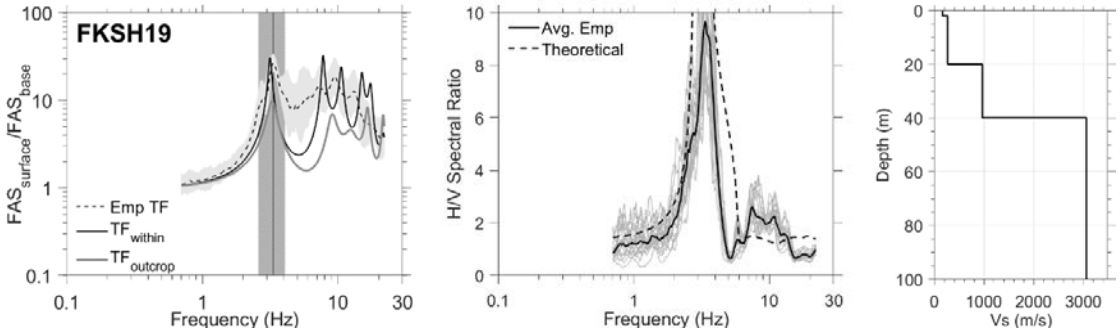

Figure A9. Group A_3: Plots for FKSH19

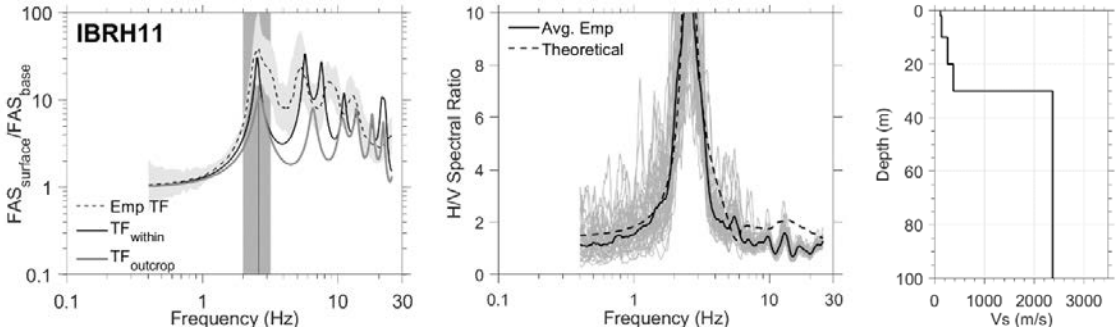

Figure A10. Group A_3: Plots for IBRH11

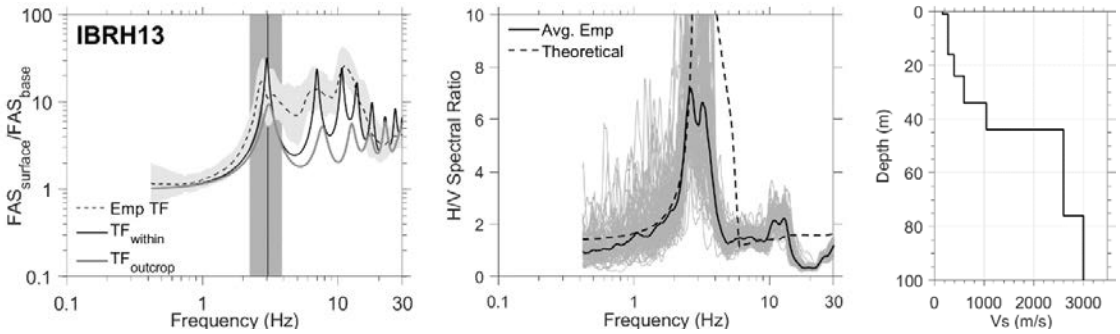

Figure A11. Group A_3: Plots for IBRH13

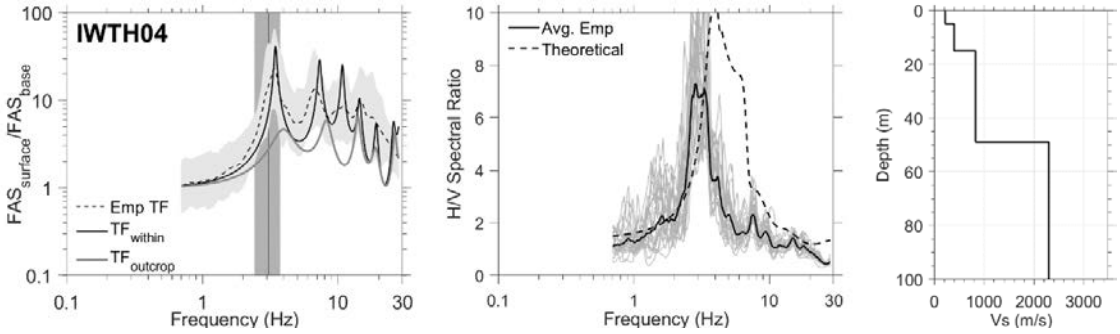

Figure A12. Group A_3: Plots for IWTH04

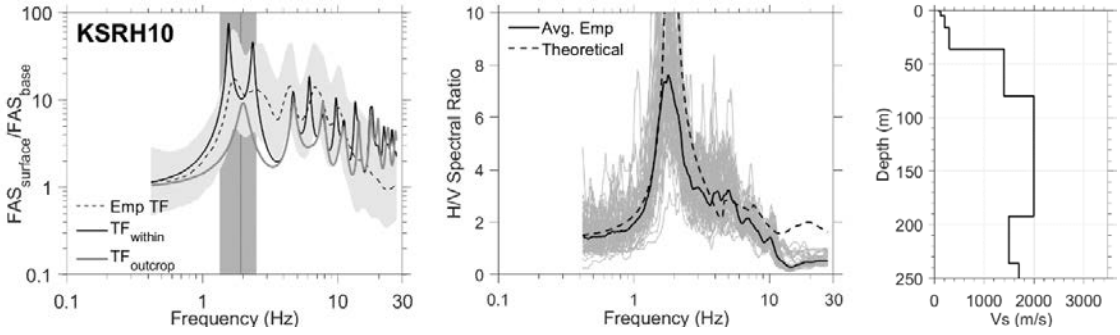

Figure A13. Group A_3: Plots for KSRH10

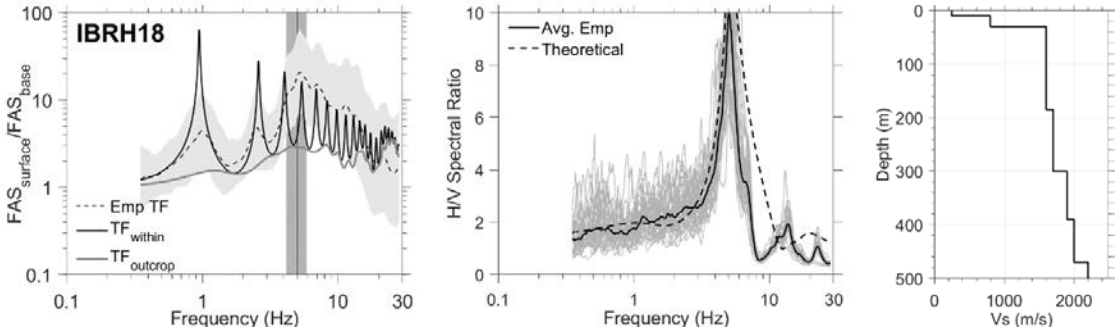

Figure A14. Group B_1: Plots for IBRH18

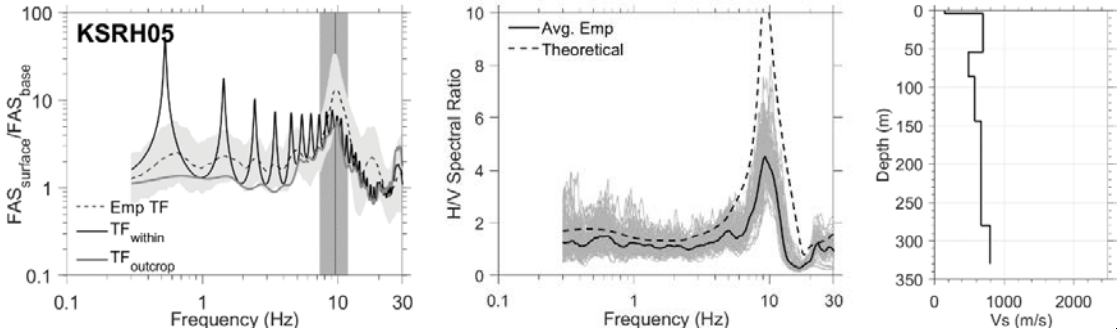

Figure A15. Group B_1: Plots for KSRH05

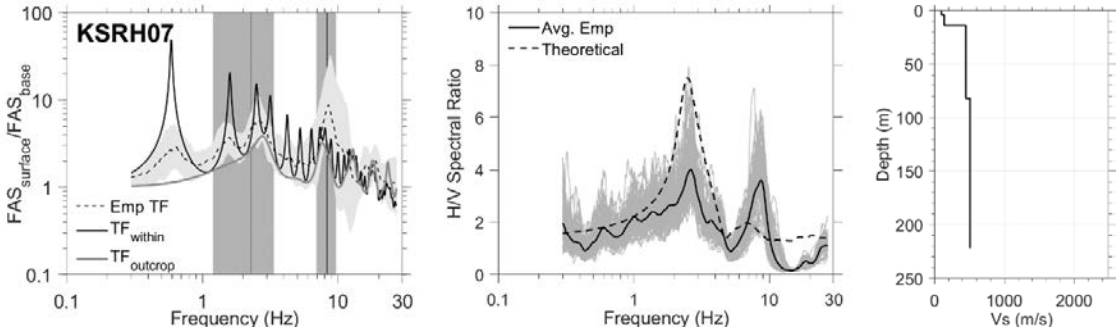

Figure A16. Group B_1: Plots for KSRH07

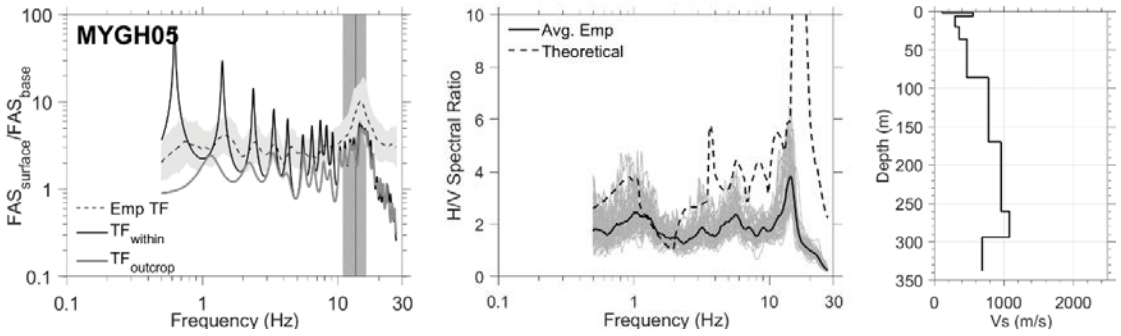

Figure A17. Group B_1: Plots for MYGH05

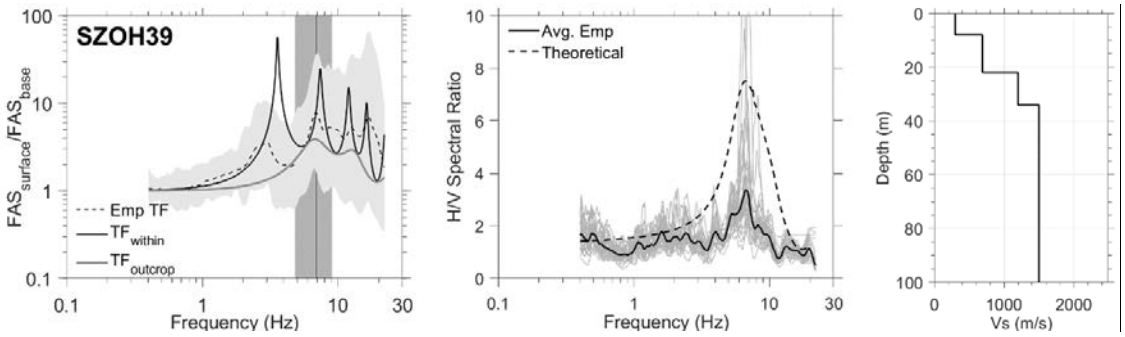

Figure A18. Group B_1: Plots for SZOH39

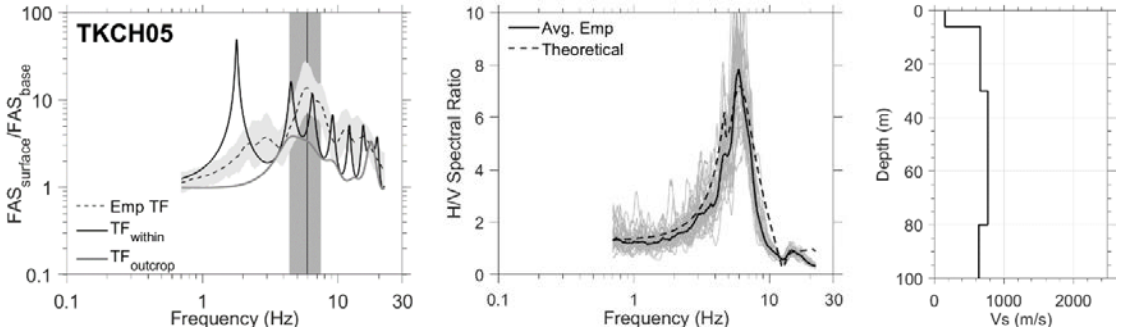

Figure A19. Group B_1: Plots for TKCH05

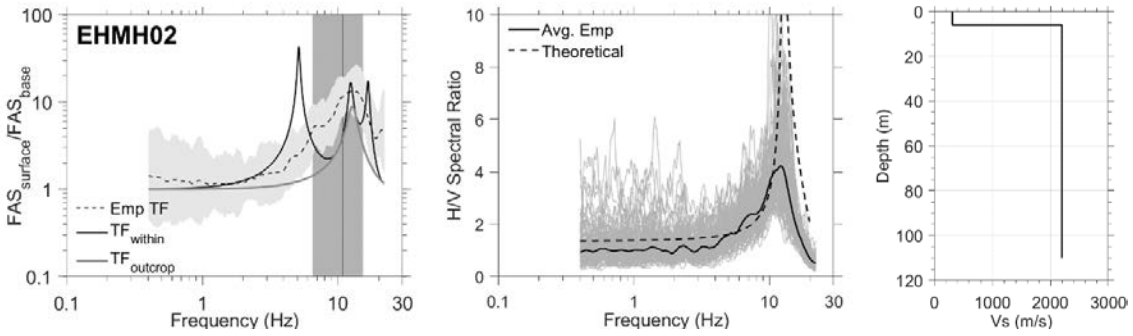

Figure A20. Group B_2: Plots for EHMH02

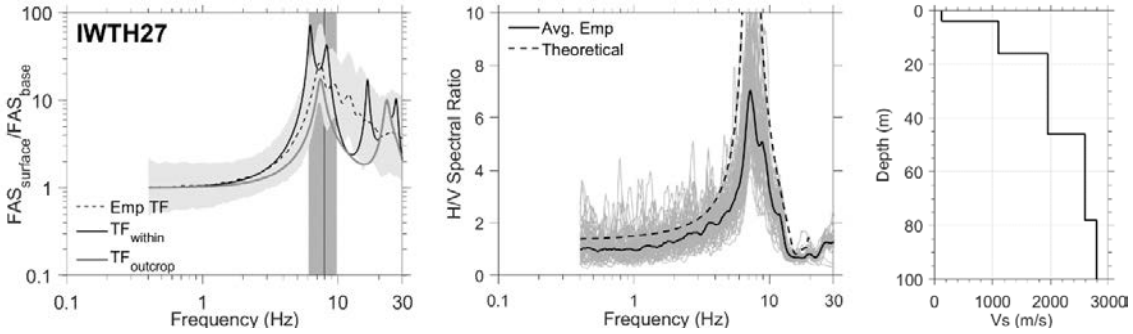

Figure A21. Group B_2: Plots for IWTH27

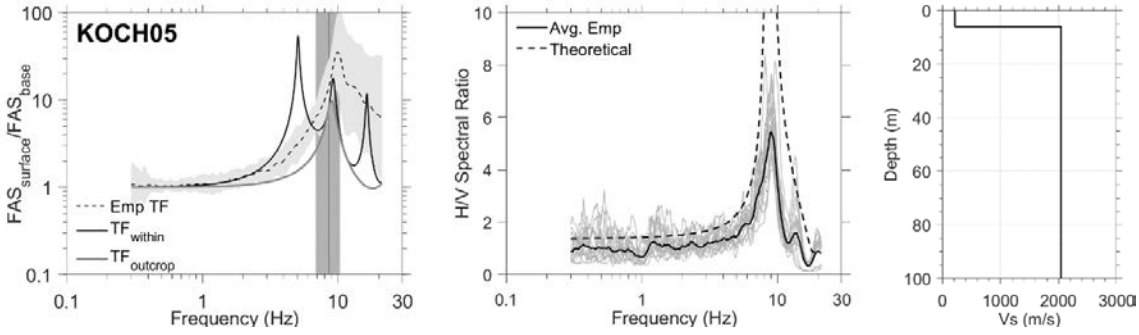

Figure A22. Group B_2: Plots for KOCH05

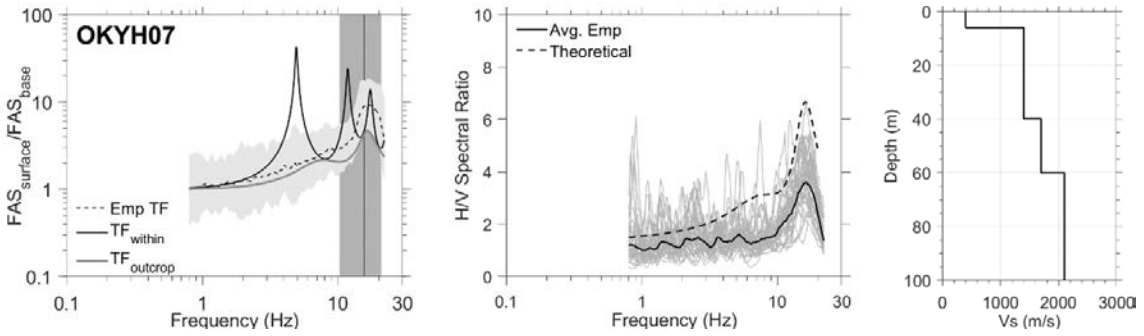

Figure A23. Group B_2: Plots for OKYH07

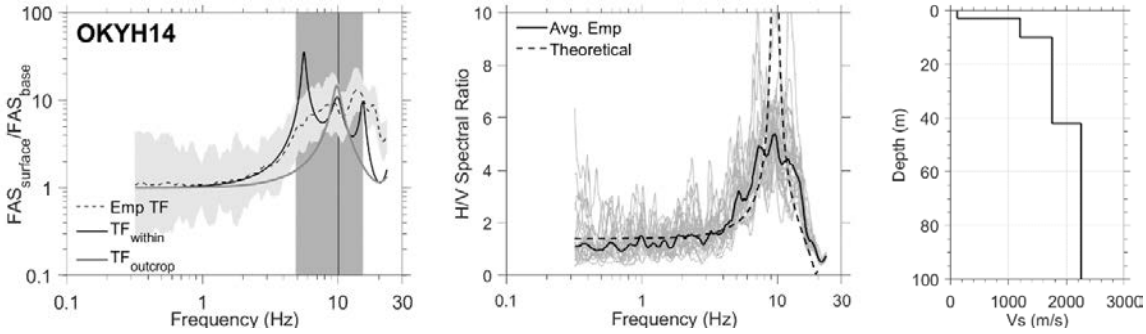

Figure A24. Group B_2: Plots for OKYH14

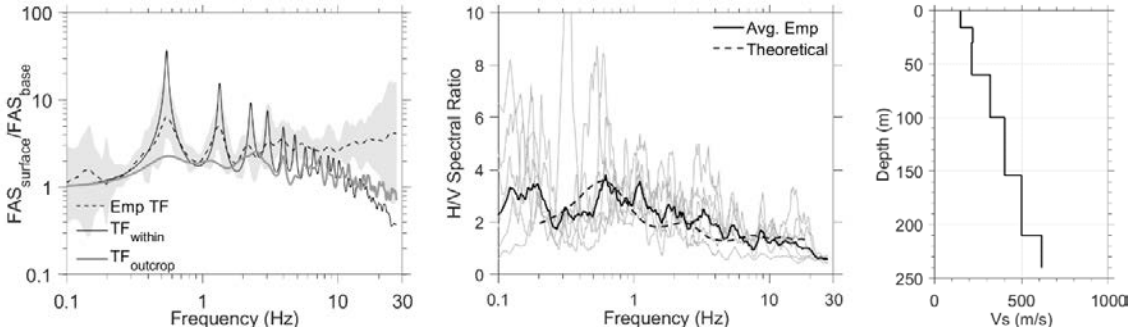

Figure A25. Group C: Plots for El Centro – Meloland Downhole Array

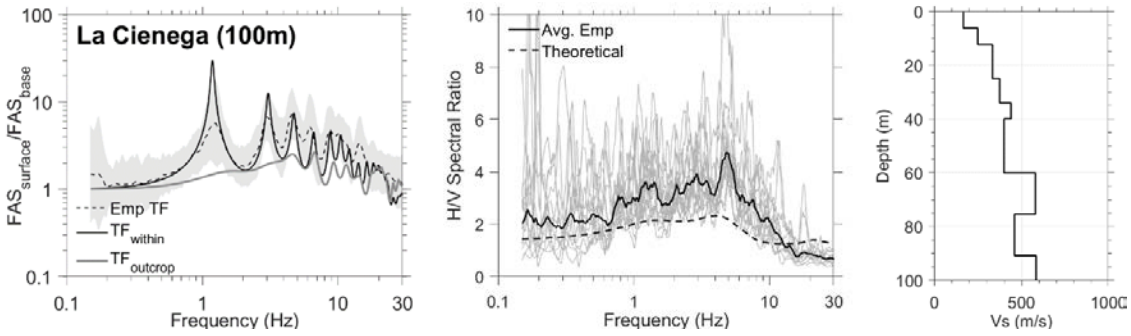

Figure A26. Group C: Plots for La Cienega Downhole Array (100m)

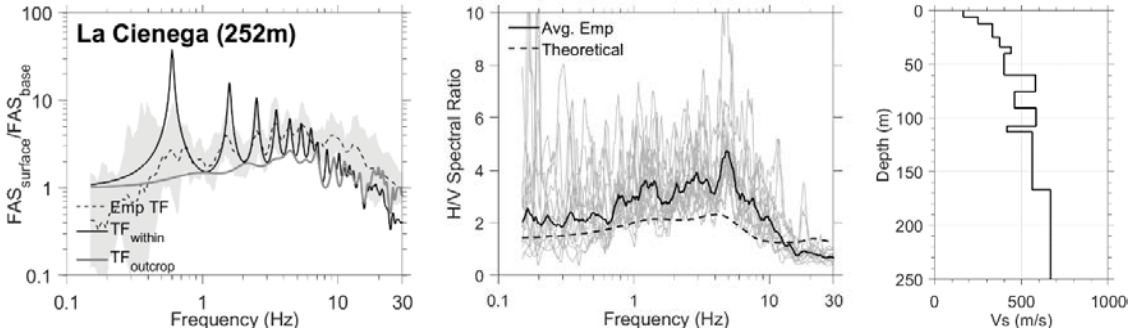

Figure A27. Group C: Plots for La Cienega Downhole Array (252m)

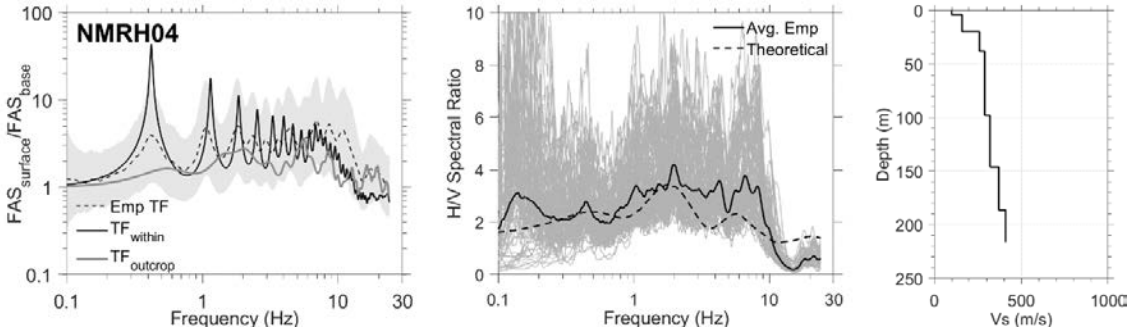

Figure A28. Group C: Plots for NMRH04

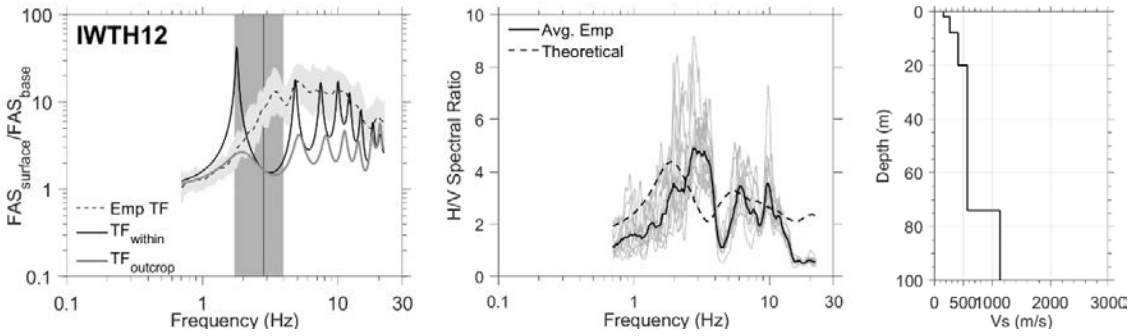

Figure A29. Group D_1: Plots for IWTH12

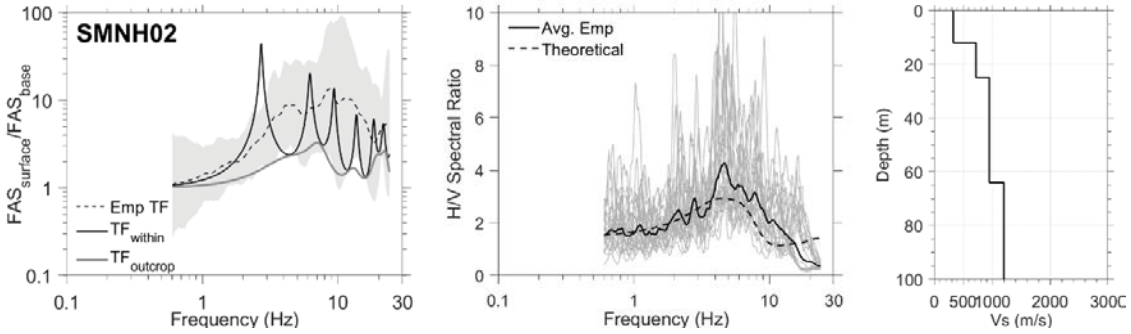

Figure A30. Group D_2: Plots for SMNH02

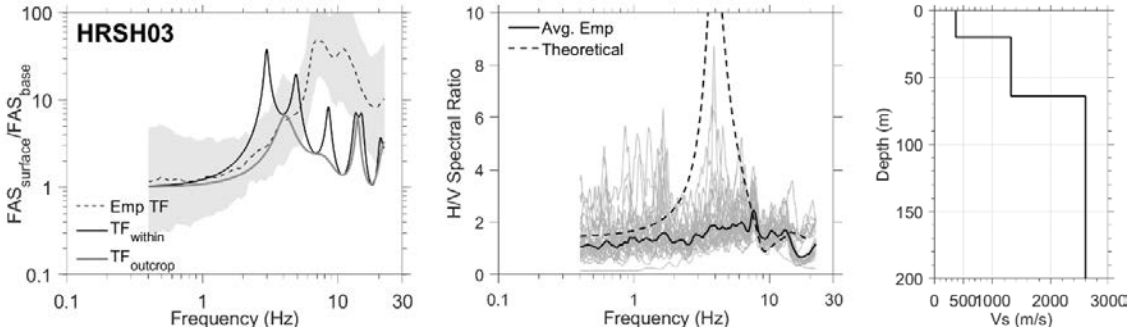

Figure A31. Group D_2: Plots for HRSH03

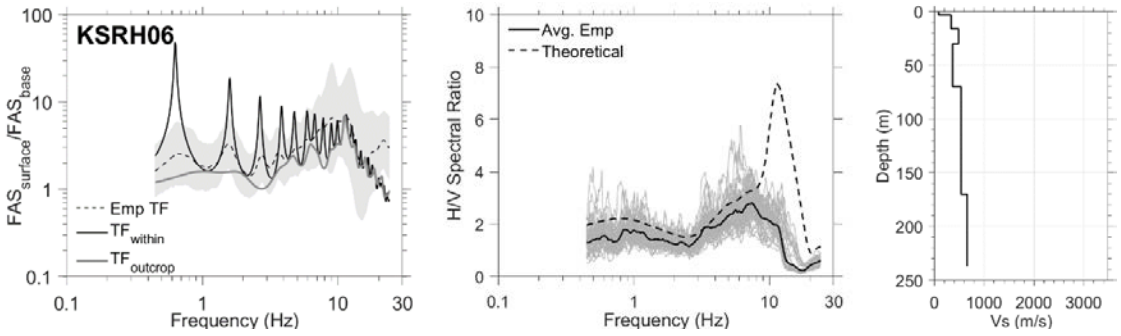

Figure A32. Group D_3: Plots for KSRH06

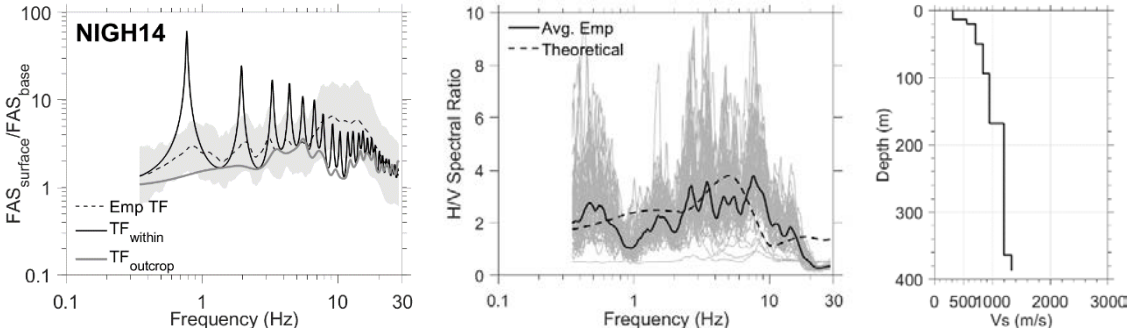

Figure A33. Group D_3: Plots for NIGH14

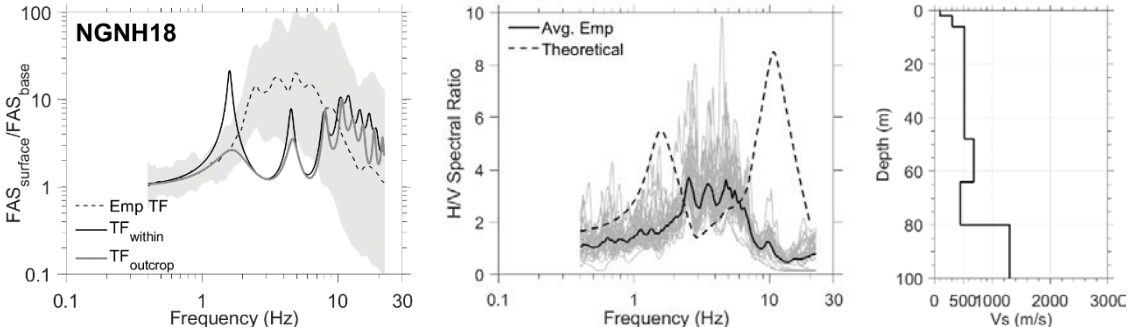

Figure A34. Group D_3: Plots for NGNH18

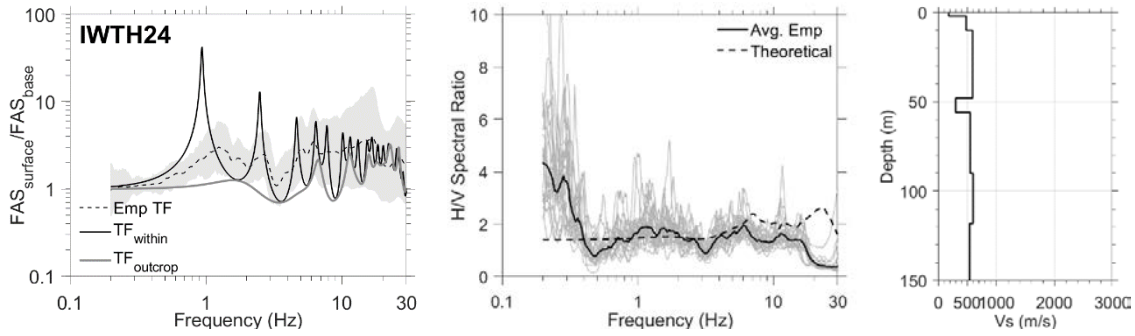

Figure A35. Group D_3: Plots for IWTH24

Table A1 Vs profile for IBRH13 (Satoh *et al*., 2014)

Thickness (m)	Vs (m/s)
2	123
8	143
10	264
10	381
73	2371

Table A2 Modified Vs profile for IBRH17

Thickness (m)	Vs (m/s)
2.2	85
7.8	380
80	380
145	470
65	540
80	660
80	820
50	2300

Table A3 Modified Vs profile for IBRH18

Thickness (m)	Vs (m/s)
10	250
20	800
35	1600
120	1600
115	1700
90	1900
80	2000
34	2200

Table A4 Modified Vs profile for SZOH39

Thickness (m)	Vs (m/s)
8	300
14	690
12	1200
69	1500
8	300

Table A5 Modified Vs profile for TKCH05

Thickness (m)	Vs (m/s)
4	153
2	153
12	660
12	660
50	770
20	640

Table A6 Modified Vs profile for EHMH02

Thickness (m)	Vs (m/s)
6	310
10	2195
94	2195

Table A7 Modified Vs profile for IWTH27

Thickness (m)	Vs (m/s)
4	124
12	1100
30	1950
32	2590
22	2790

Table A8 Modified Vs profile for KOCH05

Thickness (m)	Vs (m/s)
6	216
94	2040

Table A9 Modified Vs profile for OKYH07

Thickness (m)	Vs (m/s)
6	400
8	1400
26	1400
20	1700
40	2100

Table A10 Integrated and Modified Vs profile for Delaney Park Downhole Array

Thickness (m)	Vs (m/s)
1.22	155.4
4.27	241.5
3.65	285.0
7.62	320.7
12.5	264.8
6.1	210.3
7.92	289.0
4.88	381.0
12.84	944.9

Table A11 Integrated and Modified Vs profile for EuroSeisTest Downhole Array

Thickness (m)	Vs (m/s)
5	165
25	243.5
10	310.5
40	367.5
20	495
20	549
20	558
40	671
10	820
6	870
0	2300

Table A12 Integrated and Modified Vs profile for Garner Valley Downhole Array

Thickness (m)	Vs (m/s)
6	192
9	200
7	415
19	625
24	625
22	1310
63	3000

Table A13 Integrated and Modified Vs profile for Treasure Island Downhole Array

Thickness (m)	Vs (m/s)
13.3	170
15.5	176
12.4	350
33.8	267
13	386
5	1222
7	1888
14	2444
2	2444
6	2500

References

Vidale, J. E., & Helmberger, D. V. (1988). Elastic finite-difference modeling of the 1971 San Fernando, California earthquake. *Bulletin of the Seismological Society of America*, *78*(1), 122-141.

Frankel, A., & Vidale, J. (1992). A three-dimensional simulation of seismic waves in the Santa Clara Valley, California, from a Loma Prieta aftershock. *Bulletin of the Seismological Society of America*, 82(5), 2045-2074.

Li, Y. G., & Vidale, J. E. (1996). Low-velocity fault-zone guided waves: numerical investigations of trapping efficiency. *Bulletin of the Seismological Society of America*, *86*(2), 371-378.

Baise, L. G., Dreger, D. S., & Glaser, S. D. (2003). The effect of shallow San Francisco Bay sediments on waveforms recorded during the Mw 4.6 Bolinas, California, earthquake. *Bulletin of the Seismological Society of America*, *93*(1), 465-479.

Thompson, E., L. Baise, R. Kayen, and B. Guzina. (2009). Impediments to Predicting Site Response: Seismic Property Estimation and Modeling Simplifications. *Bulleting of Seismological Society of America*, 99(5), 2927-2949.

Lermo, J., and Chávez-García, F. J. (1994). Are microtremors useful in site response evaluation? *Bulletin of the Seismological Society of America*, 84(5), 1350-1364.

Seekins, L. C., Wennerberg, L., Margheriti, L., and Liu, H. P. (1996). Site amplification at five locations in San Francisco, California: A comparison of S waves, codas, and microtremors. *Bulletin of the Seismological Society of America*, 86(3), 627-635.

Bard P-Y, Duval AM, Lebrun B, Lachet C, Riepl J, Hatzfeld D. (1997). Reliability of the H/V technique for site effect measurement: an experimental assessment. *Proc.,17th International conference on soil dynamics and earthquake engineering*, Istanbul, 19–24 July 1997

Bard, P. Y., SESAME-Team, (2005). Guidelines for the implementation of the H/V spectral ratio technique on ambient vibrations measurements, processing and interpretation. *SESAME European Research Project EVG1-CT-2000-00026*.

Haghshenas, E., Bard, P. Y., Theodulidis, N., and SESAME WP04 Team. (2008). Empirical evaluation of microtremor H/V spectral ratio. *Bulletin of Earthquake Engineering*, 6(1), 75-108.